Progress in Surface Science 90 (2015) 85–143

Contents lists available at ScienceDirect

Progress in Surface Science

journal homepage: www.elsevier.com/locate/progsurf

Review

Action spectroscopy for single-molecule reactions – Experiments and theory

Y. Kim [a], K. Motobayashi [a,b,c], T. Frederiksen [d,e], H. Ueba [c,1], M. Kawai [c,*]

[a] Surface and Interface Science Laboratory, RIKEN, Wako 351-0198, Japan
[b] Catalysis Research Center, Hokkaido University, Sapporo 001-0021, Japan
[c] Department of Advanced Materials Science, Graduate School of Frontier Science, The University of Tokyo, 5-1-5, Kashiwa, Chiba 277-8561, Japan
[d] Donostia International Physics Center (DIPC), 20018 San Sebastián, Spain
[e] IKERBASQUE, Basque Foundation for Science, E-48011 Bilbao, Spain

ARTICLE INFO

Commissioning Editor: H. Petek

Keywords:
Action spectroscopy
Scanning tunneling microscope
Inelastic electron tunneling spectroscopy
Vibrational excitation
Vibrational relaxation
Anharmonic coupling
Electron–phonon interaction
Single molecule
Surface reaction
Reaction dynamics
Surface diffusion
Dissociation
Chemical reaction
Density of states
Chemisorption
Metal surfaces
Acetylene
Carbon monoxide
Dimethyl disulfide
Butene
Water dimer

ABSTRACT

We review several representative experimental results of action spectroscopy (AS) of single molecules on metal surfaces using a scanning tunneling microscope (STM) by M. Kawai's group over last decade. The experimental procedures to observe STM-AS are described. A brief description of a low-temperature STM and experimental setup are followed by key experimental techniques of how to determine an onset bias voltage of a reaction and how to measure a current change associated with reactions and finally how to observe AS for single molecule reactions. The experimental results are presented for vibrationally mediated chemical transformation of *trans*-2-butene to 1.3-butadiene molecule and rotational motion of a single *cis*-2-butene molecule among four equivalent orientations on Pd(1 1 0). The AS obtained from the motion clearly detects more vibrational modes than inelastic electron tunneling spectroscopy with an STM. AS is demonstrated as a useful and novel single molecule vibrational spectroscopy. The AS for a lateral hopping of water dimer on Pt(1 1 1) is presented as an example of novelty. Several distinct vibrational modes are detected as the thresholds in the AS. The assignment of the vibrational modes determined from the analysis of the AS is made from a view of the adsorption geometry of hydrogen-bond donor or acceptor molecules in water dimer.

* Corresponding author.
E-mail address: maki@k.u-tokyo.ac.jp (M. Kawai).
[1] Present address: Division of Nano and New Functional Materials Science, Graduate School of Science and Engineering, University of Toyama, Toyama 930-855, Japan.

http://dx.doi.org/10.1016/j.progsurf.2014.12.001

A generic theory of STM-AS, i.e., a reaction rate or yield as a function of bias voltage, is presented using a single adsorbate resonance model for single molecule reactions induced by the inelastic tunneling current. Formulas for the reaction rate $R(V)$ and $Y(V)$, i.e., reaction yield per electron $Y(V) = eR(V)/I$ are derived. It provides a versatile framework to analyze any vibrationally mediated reactions of single adsorbates on metal surfaces. Numerical examples are presented to demonstrate generic features of the vibrational generation rate and $Y(V)$ at different levels of approximations and to show how the effective broadening of the vibrational density of states (as described by Gaussian or Lorentzian functions) manifest themselves in $Y(V)$ near the threshold bias voltage corresponding to a vibrational excitation responsible for reactions. A prefactor of $Y(V)$ is explicitly derived for various types of elementary processes. Our generic formula of $Y(V)$ also underlines the need to observe $Y(V)$ at both bias voltage polarities, which can provide additional insight into the adsorbate projected density of states near the Fermi level within a span of the vibrational energy.

The theory is applied to analysis of some highlights of the experimental results: Xe transfer, hopping of a single CO molecule on Pd(1 1 0), a dissociation of a single dimethyl disulfide $(CH_3S)_2$ and a hopping of a dissociated product, i.e., single methyl thiolate CH_3S on Cu(1 1 1). It underlines that an observation of $Y(V)$ at both bias polarities permits us to certain insight into the molecular alignment with respect to the Fermi level.

Contents

Contents

1. Introduction

In a concluding remark of a pioneering work of a single atom switch realized by a reversible shuttling of a Xe atom between the tungsten tip of a scanning tunneling microscope (STM) and nickel (110) surface, Eigler et al. delivered a message: –*"It is clear that serious obstacles lies between what we have demonstrated and the realization of a genuinely useful atomic scale device. The prospect of atomic scale logic and memory devices is nonetheless a little bit closer. We are intrigued by the idea that atom switches might*

already exist in the form of single cage-like molecules which derive their switching function from an atom that is trapped in the cage" [1]. Since then, amazing and exciting progresses have been achieved in an STM control of motions and reactions of single atoms and molecules induced by electronic [2] and vibrational [3–5] excitation by tunneling electrons. Beyond simple motions and reactions of single molecule such as lateral hopping [6,7], rotation [8,9], dissociation [10], desorption [7] and single-bond formation [11] on metal surfaces at around 2000s, recent highlights include

- Electrically driven motion of a four-wheeled molecule [12]
- Four-level conductance switch based on a single proton transfer [13]
- Molecular switch of an encapsulated cluster within a fullerene cage [14]
- Hydrogen-atom relay reaction in a real space [15].

Adsorbate motions on surfaces constitute the most fundamental step for many surface chemical reactions. The observation of adsorbates moving, making and breaking the bonds on surfaces provides indispensable information of the microscopic mechanisms of surface chemical reactions. In general, chemical reactions are thermally driven and the relative rate of diffusion, reaction and dissociation of molecules at surfaces under a certain temperature is determined by thermodynamic coefficients. Thermal excitation homogeneously shifts the Boltzmann distribution of the system while electronic or vibrational excitation can transfer its energy at specific states to other vibrational states lying along the reaction coordinate.

Frontier orbitals are known to play an important role in chemical reactions. While individual electronic states can be excited for free molecules, discrete levels of the molecule couple with the continuous level of the substrate for molecules at surfaces. And as a result projected density of states (PDOS) of frontier orbitals lies close to the Fermi level [16]. Tunneling electrons from a tip of STM can be used for imaging as well as an atomic size source of electrons for electronic and vibrational excitations and to manipulate single atoms and molecules in a controlled manner on a surface. We can non-destructively apply a reasonable bias voltage of a few V by using STM, and thus PDOS within an energy range of few eV can be probed with the electrons from the STM tip. An STM thus provides a unique way to achieve mode-selective chemistry of single molecules by its electronic or vibrational excitations associated with the nuclear motions of constituent atoms of the adsorbed molecules on a surface.

The past twenty years have witnessed amazing and exciting progress of reactions of single atoms and molecules induced by electronic and vibrational excitation by tunneling electrons in an STM configuration. A pioneering effort to manipulate individual small molecules adsorbed on metal surfaces in a controlled manner with STM have been successfully demonstrated for lateral positioning of CO on Cu(2 1 1) by Meyer et al. [17]. They used typical tunneling parameters, 0.2 V of V_s and 100–200 nA of I_t, to reduce tunneling resistance for the manipulation at rather a high temperature (30 K) that provides higher mobility of the target CO molecule. Vertical manipulation of CO on Cu(1 1 1) by controlling gap distance was also demonstrated by Bartels et al. [18].

In 1998 Stipe, Rezaei and Ho opened new avenue of single molecule vibrational spectroscopy and microscopy using STM [8]. They observed the vibrational spectra of a single acetylene molecule on a Cu(1 0 0) surface which is defined as the second derivative of tunneling current I with respect to the applied bias V, i.e., d^2I/dV^2, and is named as inelastic electron tunneling spectroscopy (IETS). It showed an increase in the tunneling conductance at 358 meV, resulting from excitation of the C–H stretch mode and clearly exhibited the evidence of vibrational excitation by the isotope shift in C–D stretch mode.

Immediately after this pioneering work of "STM-IETS", they completed the first comprehensive and systematic experiments for a rotational motion of single $C_2H(D)_2$ molecule on Cu(1 0 0) controlled by applying a bias voltage pulse [9]. This achievement is the first realization of a single molecule switch. Almost all the experimental data methods reported there have now been established as indispensable in order to gain insights into the vibrationally mediated motions and reactions of single molecules with STM. The dependence of rotation rate per electron on applied bias V at a fixed current I shows a strong increase near $V = 358$ mV for C_2H_2 and 266 mV for C_2D_2. These voltages correspond to the peak position of the C–H(D) stretch mode observed in the STM-IETS, thereby clearly indicating that the excitation of the C–H(D) stretch mode triggers the rotation of a acetylene molecule. Since excita-

tion of the C–H stretch mode is different from the reaction coordinate (RC) of the rotational motion of the molecule, they proposed that the C–H stretch mode may relax by exciting a combination of bending and frustrated rotational modes, including overtones via anharmonic mode coupling. The relaxation of the bending modes can lead to further energy transfer to the hindered rotational mode. Rotation occurs if enough energy is transferred to the RC mode from the initial relaxation of the C–H mode excited by tunneling electrons.

A state-of-the-art experiment of single-molecule manipulation by vibrational excitation was also first reported by Stipe et al. [10] for dissociation of a single O_2 molecule on Pt(1 1 1). It is noteworthy that the power-law dependence of the dissociation rate, R_d, on the tunneling current, I, $R_d \propto I^n$, was precisely measured and revealed the bond cleavage by exciting O–O stretch mode (87 meV) in a manner of "vibrational ladder climbing" with inelastically tunneled electrons according to the value of n. They also estimated the dissociation barrier lying between 0.35 and 0.38 eV based on the model of multiple excitation of vibrational mode (5 quanta of O–O stretch mode). This is a pioneering work that the model for explaining ultrafast laser-induced bond dissociation [19] by multiple vibrational excitation can also be applied to single-molecule chemistry with STM.

As described above, a reaction rate $R(I)$ as a function of tunneling current I tells us how many electrons are required to induce a reaction. Another important information is obtained by measuring the reaction rate $R(V)$ or yield $Y(V) = eR(V)/I$ per electron as a function of V at a fixed I, which exhibits a noticeable increase near the bias voltage corresponding to the excitation of the vibrational mode (or electronic state into which tunneling electron or hole is injected [2]). The energy of the vibrational mode primarily responsible for a reaction has been determined from the peak position in $\Delta \log(Y)/\Delta V$ plot. Because of a small number of experimental points available, it has been desired to have a method that permits us to deduce as many important parameters directly from an analysis of $R(V)$ or $Y(V)$ as possible.

Kawai et al. [20] are the first who coined the term "Action Spectroscopy (AS)" for single molecule reactions. The term "Action spectroscopy" has been known as a technique in the fields of unimolecular reactions [21], electrochemistry and biology to measure the reaction rate as a function of the wavelength of irradiated light in UV–vis region for identifying the specific orbital or molecule that is active in the reaction induced by photons. In the field of STM, AS means to measure reaction yield $Y(V)$ as a function of sample bias voltage to identify the vibrational and/or electronic states responsible for the reaction. Kawai et al. have studied the response of vibrationally mediated molecular motion, i.e., hopping and rotational motion of *cis*-2-butene on Pd(1 1 0), to the applied bias voltage. The observed AS of the rotation yield showed several distinct thresholds indicating that an excitation of the particular vibrational mode is the trigger to the reaction. It is noted that not all the vibrational modes observed in the AS were detected in the IETS of a single *cis*-2-butene molecule on Pd(1 1 0) which shows only the strong C–H stretch mode [22]. It is now widely recognized that the vibrational signal in the STM-IETS is governed by the so-called propensity rule [24] and there is a competition between the negative elastic and positive inelastic current in the presence of the electron-vibration coupling [25,26]. In contrast to IETS, a vibrational fingerprint observed in AS is directly related to inelastic tunneling current as explicitly revealed in the theoretical section described below. The vibrational modes deduced from the AS are directly activated RC modes to above the reaction barrier or the modes indirectly excite the RC mode leading to reactions via inter-mode coupling. STM-IETS and -AS thus hold complementary aspect as vibrational spectroscopy of single molecules.

The vibrational modes appearing in STM-AS are resonantly excited through a temporal occupation of molecular orbitals (MOs) by the tunneling electrons and that the molecular vibrations are selectively excited depending on the spatial distribution and the population of the MOs near the Fermi level (ε_F) by hybridization with the substrate metal. STM-AS has revealed that excitation of C–H stretch mode and a combination of C–H stretch and S–S stretch modes is responsible for S–S bond dissociation of a $(CH_3S)_2$ (dimethyl disulfide, DMDS) and C–S stretch mode for lateral hopping of a CH_3S (methyl thiolate, MT) on Cu(1 1 1) [27]. Interestingly, the S–S bond dissociation of DMDS is induced by excitation of the C–H stretch mode, whereas lateral hopping of MT is not, although both molecules involve C–H bonds of the methyl (CH_3) group. Density functional theory (DFT) calculation of PDOS and the spatial distribution of the MO revealed that the MOs near the ε_F have significant component at C–H bond of DMDS, but not of MT. Since the temporal ionic state induced by transfer of electrons

perturbs a specific MO, vibration mode is considered to be resonantly excited. This explains why DMDS shows a C–H stretch signal in the STM-AS, whereas MT does not. This topic will be discussed in detail in Section 5.3.

The STM-AS detects all the vibrational modes responsible for single molecule motions and reactions induced by inelastic tunneling current I_{in}. Subsequently Ueba and Persson [28] proposed that the second derivative of I_{in} with respect to V is related to the vibrational density of states (DOS) $\rho_{ph}(V)$ which cannot be deduced from IETS composed of the elastic and inelastic tunneling current. The details of this topic will be presented in Section 2.3.

Motobayashi et al. [29] then proposed an empirical form of $I_{in}(V)$ by double integration of $\rho_{ph}(\omega)$. This gave an empirical formula which permits a fitting of the observed reaction yield $Y(V)$ over whole bias voltage using four parameters (vibrational energy, reaction order, effective rate constant, and broadening of the vibrational DOS and prefactor including a ratio of the elastic and inelastic conductance). They successfully applied the formula to reproduce the experimental $Y(V)$ for a lateral hopping of a single CO molecule on Pd(1 1 0) [6] and for a configuration change of *cis*-2-butene ($C_4H(D)_8$) on Pd(1 1 0) [22]. The best fitting to the experimental $Y(V)$ allows a more precise determination of the vibrational energy than that by a peak in $\Delta \log(Y)/\Delta V$-plot using small numbers of the data points. They applied this formula to reproduce the results of formate hopping on Ni(1 1 0) [30] and rotation/hopping of propene on Cu(2 1 1) [31] to demonstrate that this fitting gave us more precise assignment of vibrational modes even if two vibrational modes overlap each other in energy or if the modes exist in lower energy region than the actually observed spectral region [32]. This empirical formula has also been used to fit the switching yields of a single molecule switch utilizing rotation of a triangular Sc_3N cluster within an icosahedral C_{80} fullerene cage among three pairs of enantiomorphic configurations on Cu(1 1 0)–O surface [14]. Their finding will be a promising candidate for the integration of endohedral fullerene-based single molecule switches into multiple logic state molecular devices [33].

The STM-AS experiments have also been reported for many systems including rotation of a CCH(D) molecule on Cu(1 0 0) [34], hopping of a water molecule on Pd(1 1 1) [35], dehydrogenation of a methanol molecule on Cu(1 1 0) [36], helix inversion of the rotor unit of a four-wheeled molecule [12], isomerization of a chloronitrobenzene molecule on Cu(1 1 1) [37], hydrogen-bond exchange within a water dimer on Cu(1 1 0) [38], hopping of a Co atom on Cu(1 1 1) [39], chirality change of a chloronitrobenzene molecule on Au(1 1 1) [40], switching chirality of a propene molecule on Cu(2 1 1) [31], hydrogen atom relay reaction in water–hydroxyl linear complex on Cu(1 1 0) [15] and vibrationally induced tautomerization (intramolecular hydrogen atom transfer reaction) of a porphycene molecule on Cu(1 1 0) [41].

AS has thus established its firm position as the most indispensable experiment that allows us to gain deep insights into the microscopic elementary processes behind reactions of single molecules induced by vibrational [5] and electronic [2] excitation by tunneling currents. The first theoretical work to fit experimental AS [29] stimulated Frederiksen et al. to develop a general theory of AS using a single-adsorbate resonance model in order to reproduce the AS for a hydrogen atom relay reaction in real space for water–hydroxyl complex on a Cu(1 1 0) [15]. Recently more comprehensive theory of an STM-AS has been formulated by Frederiksen et al. [42]. In addition to the general features of AS at different levels of approximations, they underline an importance to observe AS at both polarities as have been usually done in STM-IETS in order to confirm vibrational signature superimposed on noisy background. Such an observation provides additional insight into the adsorbate density of states near the ε_F. In this sense STM-AS can be viewed as both electronic and vibrational spectroscopy of a single adsorbate. Table 1 provides a list of selected references of experimentally measured STM-AS for various dynamic behaviors of a single molecule by vibrational excitation with STM, since the first report of the dependence of Y on V for vibrationally-induced rotational motion of C_2H_2 on Cu(1 0 0) [9].

This review is organized as follows. A detailed description of the experimental procedures and techniques are presented in Section 2 together with the following experimental results among many works related to STM-AS [6,22,23,27,29,30,32,43–46,50–58] reported by M. Kawai group since 2002,

- Chemical transformation of *trans*-2-butene molecule on Pd(1 1 0) [43,52] is presented in Section 2.3 as an example of bond scission induced by the excitation of vibrational mode.

Table 1
selected references of STM-AS studies.

Ref.	Reaction	System	Threshold (meV)	Corresponding vibrational modes
[9]	Rotation	C_2H_2/Cu(100)	358	C–H stretching
[34]	Rotation	CCH/Cu(001)	65	C–H bending
[49]	Rotation	Dibutyl sulfide/Au(111)	375	C–H stretching
[22]	Rotation	*cis*-2-butene/Pd(110)	20	Pd–C stretching
			95	C–C stretching
			120	CH_3 rock
			365	C–H stretching
[7]	Desorption and hopping	NH_3/Cu(110)	410	N–H stretching
			280	1st overtone of N–H_3 umbrella
[6]	Hopping	CO/Pd(110)	240	C–O stretching
[47]	Hopping	C_2H_2/Cu(110)	230	C–H bending
			340	C–H stretching
[30]	Hopping	HCOO/Ni(110)	140	C–H bending
			360	C–H stretching
[51]	Hopping	H_2O/MgO/Ag(100)	448	O–H stretching
[48]	Hopping	H_2O hexamer/Cu(111)	210	Scissoring
			420	O–H stretching
[45,46]	Hopping	H_2O monomer/Pt(111)	104	HO–Pt libration
			134	HO–Pt libration
			192	Scissoring
		D_2O monomer/Pt(111)	141	Scissoring
			174	O–D Combination of two HO–Pt librations
		H_2O dimer/Pt(111)	208	Scissoring
			250	Scissoring + O–Pt stretching
			335	Scissoring + HO–Pt libration
			375	O–H stretching (doner, in HB)
		D_2O dimer/Pt(111)	272	O–D stretching (doner, in HB)
			313	O–D stretching (acceptor, in HB with Pt)
			332	O–D stretching (doner, free)
[43]	C–H breaking	*trans*-2-butene/Pd(110)	365	C–H stretching
[37]	Isomerization	Chloronitrobenzene/ Cu(111)	227	C–C stretching + C–Cl or C-NO_2 bending
[41]	tautomerization	porphycene/Cu(110)	279	N–D stretching
[14]	intramolecular rotation	$Sc_3N@C_{80}$	78	Sc–N stretching
[36]	Flip	CH_3O/Cu(110)	200	CH_3 rock and/or CH_3 bending
			360	sp^3 C–H stretching
[50,142]	Rotation O–H breaking	Formic acid(HCOOD)/ Ni(110)	140–160 260–280	C–O stretching O–D stretching
[27,44]	S–S breaking	DMDS/Cu(111)	410	C–H stretching
			357.5	C–H stretching + S–S stretching
	Hopping	MT/Cu(111)	85	C–S stretching
[31]	Rotation	Propene(C_3H_6)/Cu(211)	200	C=C stretching
			360	CH_3 stretching
	Hopping		375	sp^2 C–H stretching
	Interconversion		?	CH_3 stretching + sp^2 C–H stretching

- Motion of *cis*-2-butene molecule on Pd(110) [22,23,29] is in Section 2.3 to show a usefulness of AS as a vibrational spectroscopy of single molecule.
- Hopping of water dimer on Pt(111) [45,46] is in Section 2.3 as an example to characterize unknown species.

A general and comprehensive theory of STM-AS [42] (the brief formula has been described in a supporting information in Ref. [15]) is presented in Section 3. The fundamental theories for various elementary processes of vibrationally mediated reactions are presented in Section 4. In Section 5 the theory is applied to revisit the following systems:

- Single Xe atom transfer [1] in Section 5.1.
- Hopping of CO on Pd(1 1 0) [6,29,59] in Section 5.2
- Dissociation of DMDS and hopping of MT on Cu(1 1 1) [27,44,56–58] in Section 5.3

These examples demonstrate what we can learn from the analysis of STM-AS specified with the energy of the vibrational mode responsible for reactions and the prefactor characterized by the elementary processes of the vibrationally mediated motions and reactions of single molecules on metal surfaces. The concluding remarks and perspective for future developments are presented in Section 6.

2. Experimental procedure of STM-AS

Inelastic electron tunneling (IET) process at a single molecule confined in the tunnel junction of STM provides an effective pathway to excite molecular vibration leading to a variety of dynamic behaviors of the target molecule [3,4,43,61,62], such as lateral hopping [6,7,27,29–32,44–48,50,51,56,57,63–66], rotation [9,20,22,23,29,31,32,34,49,50,67,68], desorption [7] and even chemical reaction [10,27,37,41,43,51,52,56,58,69]. The IET process can also be utilized to detect vibrational signals of a single molecule by measuring bias voltage dependence of small change in the differential conductance for STM-IETS [20,22,30,43,53,54,70–85] in a static manner or of reaction yield (reaction rate per electron) for STM-AS [6,7,9,20,22,27,29–32,34,36,37,43–52,57,58,63,65] in a dynamic manner. In the case of STM-IETS, the technical difficulty lies in detecting tiny vibrational signal of d^2I/dV^2 resulting from only a few % of differential conductance change [86] against the background noise. Meanwhile, STM-AS provides much higher resolution in intensity of reaction yield for the detectable vibrational modes, mainly because the onset of reaction takes place in accordance with the appearance of vibrational DOS at the responsible vibrational energy for the reaction. However, the reaction induced by IET process shows a stochastic behavior, which requires accumulating a statistically-significant amount of data at every single bias voltage applied to induce the reaction. We describe here the experimental details for measuring STM-AS.

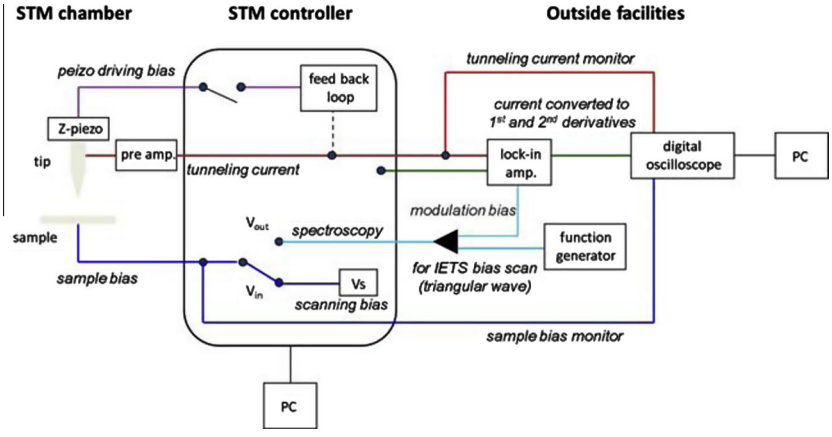

Fig. 1. Schematic diagram of STM setup for measurement of single-molecule spectroscopy.

2.1. Experimental setup

All experiments were performed using a low-temperature STM equipped in an ultrahigh-vacuum (UHV) chamber in which base pressure was maintained below 8.0×10^{-11} Torr at 4.7 K.

The LT-STM system mainly consists of three chambers: a load-lock chamber for loading the substrate, a preparation chamber for cleaning of the substrate and controlling molecular adsorption process, and a main chamber for STM measurements. Each chamber is equipped with one rotary pump and one turbo molecular pump to evacuate the system from atmospheric pressure. UHV conditions are maintained only in the preparation and main STM chambers, which are obtained by baking the chambers with evacuating the system for a few days at about 400 K. Since vibrations originating from the rotary and turbo molecular pumps result in interfering noise signals in the STM measurements, UHV conditions in the chambers are kept using only ion pumps and titanium sublimation pumps. Wobble sticks and magnetically coupled transfer-rods are used to move the sample inside the UHV chambers.

Low temperature can be achieved by filling an inner cryostat with liquid ^{4}He and an outer cryostat with liquid N_2. Since the STM stage equipped with a tip is cooled by touching the Cu block at the bottom of the inner cryostat, the STM stage can be kept at 4.7 K for about 25 h. To protect the STM stage from radiative heating, the STM stage is covered with two cylindrical Cu shields, which are movable for the insertion of the sample using the wobble stick. Temperature of the STM stage is monitored with a Si diode sensor.

To isolate the LT-STM system from mechanical vibrations, the whole system is located on a rigid bench fixed on four air-damping legs, and the STM stage is hung by three wires from the top of the chamber during the STM measurements. An eddy-current damper is installed inside the STM stage, and thus eddy currents induced by a conductor moving inside a magnetic field provide the damping forces.

A tungsten tip is used in this LT-STM system, because tungsten has a mechanical stiffness and a relatively flat DOS near the ε_F. The tungsten tip was prepared by electrochemical etching of the tungsten wire with a diameter of 0.15 mm in NaOH solution (3 mol/L); such electrochemical etching process is easily achieved using a commercial device (TM-59060, JEOL). Since the tungsten tip is initially fabricated in the atmosphere, in situ tip cleaning in the UHV chamber is necessary to remove oxide layers and impurities covering the tip. High bias voltage applied to the tip induces a field evaporation of the tip–surface atoms, which leads to restructuring of the tip due to a non-uniform electric field. Thus applying the high voltage pulse (10 V) is repeated to obtain the clean and sharp tip apex.

Fig. 1 shows our STM setup for measuring STS, STM-IETS and STM-AS. A main controller for the STM/STS measurements is the "SCALA" system provided by the manufacturer, Omicron. Signals of the tunneling currents are basically sent to the SCALA system and recorded with an oscilloscope

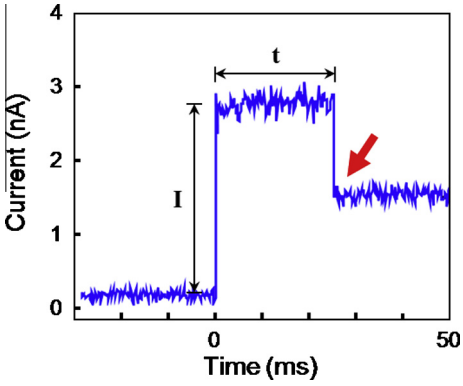

Fig. 2. A typical current trace for an onset of a lateral hopping of a single MT on Cu(1 1 1). *I* and *t* represent the applied tunneling current and time required for a reaction to occur.

(Wave Runner, NF) connected to the data acquisition computer through an IEEE-488 (GPIB) interface. An applied bias voltage and other parameters can be programmed and controlled by a software program named "SCALA Pro" linked to the SCALA controlling system. A function generator (Wave Factory WF1945, NF) was applied for adding dc offsets to the sample bias voltage. In order to measure STS and STM-IETS, two lock-in amplifiers (LI5640, NF) were used to measure both 1st harmonic and 2nd harmonic signals of tunneling current simultaneously for obtaining a change in the ac conductance (dI/dV) and the differential change in the ac conductance (d^2I/dV^2) as a function of the sample bias voltage, respectively.

The STM-AS is obtained simply by measuring reaction yield as a function of applied sample bias. After obtaining an STM image of a molecule, the STM tip is positioned over a target molecule at a fixed tunneling gap resistance followed by feedback loop off. Then the bias voltage is set to zero for a moment (~few tens ms) to stabilize STM junction at zero current. The tunneling electrons are then injected to the molecule at a preset sample bias voltage during a given time duration. The tunneling current is monitored by an oscilloscope in which a sudden current change (increase or decrease) takes place at the moment of reaction as shown in Fig. 2 that recorded during lateral hopping of MT on Cu(1 1 1) [27].

The time required for the single reaction event of the molecule t_{ev} is directly read out from the current trace, I–t plot. Since reaction probability per unit time should be constant, the distribution of t_{ev} for a number of reaction events must follow the exponential distribution $Cf(t)$ where C is a constant and $f(t)$ is normalized exponential function

$$f(t) = \tau \exp(-t/\tau) \tag{1}$$

The time constant τ is obtained by fitting of $Cf(t)$ to the experimentally measured distribution of t_{ev} and R is given by $R = 1/\tau$. The number of injected tunneling electrons n_e for inducing a reaction is calculated by $n_e = It/e$, where e is the elementary charge (1.602×10^{-19} C). The reaction yield Y is then determined as $1/n_e$. [8]. As already mentioned by Ho [3], this τ is the same as simple average of t_{ev} if t_{ev} follows exponential distribution. Sufficient number of the reaction event must give the averaged t_{ev} near the expected value of the exponential distribution given by

$$E_t = \int_0^\infty tf(t)dt = \tau. \tag{2}$$

The resulted E_t is thus identical to the time constant τ obtained by exponential fitting. Therefore, τ and Y can be also obtained from average of t_{ev} if one confirmed that the reaction probability is constant and/or the t_{ev} follow the exponential distribution.

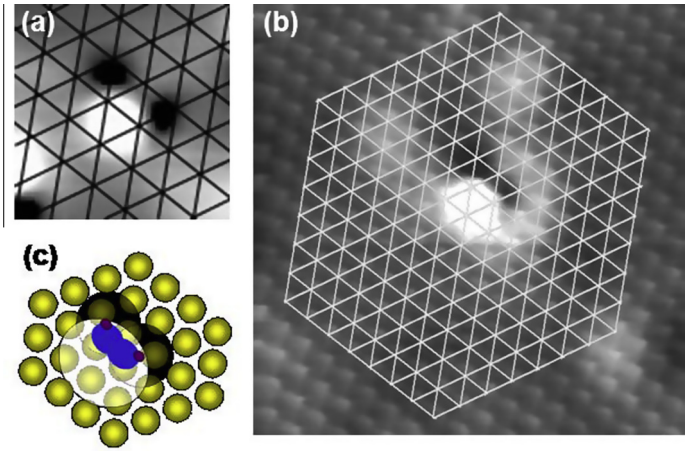

Fig. 3. (a) Topographic STM image of a C_2H_2 molecule on Pd(1 1 1) (V_s = 20 mV, I_t = 0.81 nA, scan area: 3 × 3 nm^2). (b) The hexagonal lattice represents the positions of surface Pd atoms. (c) Schematic drawing of C_2H_2 adsorption structure.

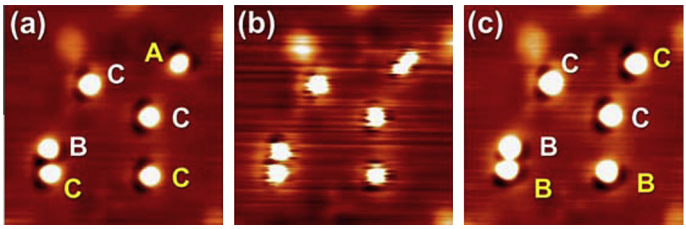

Fig. 4. (a) Topographic STM image of 6 C_2H_2 molecules on Pd(1 1 1) (V_s = 50 mV, I_t = 1.0 nA, scan area: 10 × 10 nm^2). Characters A, B and C represent the adsorption orientations of individual molecules. (b) STM image measured with higher sample bias (V_s = 300 mV, I_t = 1.0 nA, scan area: 10 × 10 nm^2). (c) STM image showing orientation change of 3 molecules labeled with yellow characters (V_s = 50 mV, I_t = 1.0 nA, scan area: 10 × 10 nm^2).

2.2. Detection of the onset bias voltage for a reaction

When the sample bias voltage lies in the range of vibrational excitation, typically between −0.5 and +0.5 V, the STM provides two kinds of reaction mechanisms for inducing reaction. On one hand, the smaller gap resistance (∼MΩ) results in the mechanical, chemical or electrostatic forces between the STM and the molecule due to the proximity effect. STM imaging cannot be normally allowed under the scanning condition with such strong tip-molecule interaction. On the other hand, the greater gap resistance (∼GΩ) provides possible way of exciting molecular vibration by the IET process. The STM-AS is a kind of vibrational spectroscopy, thus the gap resistance should be kept high enough to get rid of direct tip-molecule interaction. In this section, we describe how to distinguish the vibrationally-induced reaction of a single molecule from the proximity-induced reaction by taking a specific system, C_2H_2 on Pd(1 1 1).

Before measuring STM-AS, STM images of individual molecules are obtained with sufficiently high-spatial resolution to determine adsorption site and orientation. Fig. 3(a) shows an STM image of a C_2H_2 molecule obtained at 4.7 K. The Pd(1 1 1) was exposed to a small amount of C_2H_2 molecules at 50 K to form isolated molecules on the surface. The C_2H_2 molecule is observed as a combination of a pair of depressions and a protrusion in the STM image.

In order to determine adsorption structure, an atomically-resolved STM image (Fig. 3(b)) was obtained with a sharp tip modified with a molecule [11]. The intersection of the grid drawn on the STM image indicates the position of each surface Pd atom, where the center of the protrusion is on a 3-fold hollow site and two depressions are located close to the Pd atoms. Molecular structure shown in Fig. 3(c) can be considered as a plausible model for explaining the STM image. The structural studies including theoretical calculations [87], STM [88] and NEXAFS [89] experiments reported that the

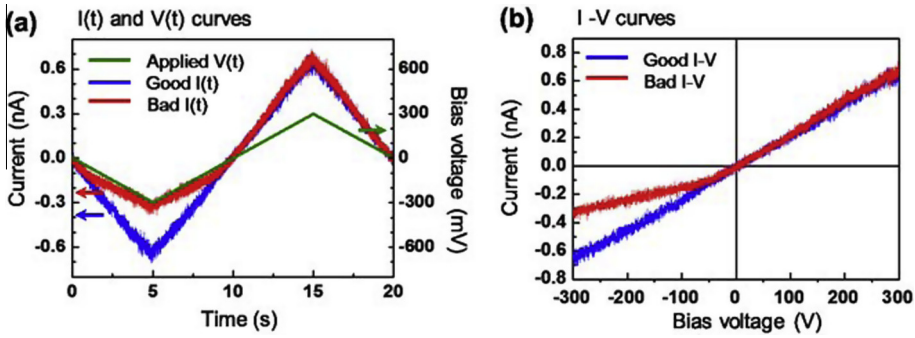

Fig. 5. (a) Traces of tunneling current and sample bias voltage and (b) processed $I - V$ curves obtained with a good (blue line) and a bad (red line) tips on the clean Ag(1 1 1) surface (Set condition: V_s = 50 mV and I_t = 0.5 nA). (For interpretation of the references to color in this figure legend, the reader is referred to the web version of this article.)

adsorption site has 3-fold symmetry, and the C–C bond locates parallel to the $[1\bar{1}0]$ direction with each carbon atom sitting on the Pd atom and hydrogen atoms point towards the vacuum, which is in good agreement with our STM images.

Fig. 4(a) shows 6 individual C_2H_2 molecules with 3 different orientations according to the 3-fold adsorption symmetry. The imaging condition was sample bias voltage $V_s = 50$ mV and tunneling current $I_t = 1$ nA. The molecules are thermally stable and never move during the STM imaging. Scanning with higher V_s of 300 mV at the same tunneling current, the STM image became noisy and streaky as shown in Fig. 4(b). Further imaging of the same area with initial condition produced a clear image (Fig. 4(c)), but some molecules have rotated to change their orientations. This clearly shows that the rotational motion was NOT induced by tip proximity, because the higher gap resistance produced the molecular rotation. Thus, the bias voltage dependent STM imaging can reveal whether the reaction is induced by proximity effect of tip or by vibrational excitation via IET process.

In order to measure STM-AS, one should first determine onset bias voltage of the desired reaction. The easiest way of finding the ranges of bias voltage for injecting tunneling electrons into the target molecule is to measure STM images at various bias voltages. Considering vibrational energies of a given molecule, one can simply examine the occurrence of reaction by STM scanning at slightly higher bias voltage than the energy of the highest vibrational normal mode of the molecule, e.g., ~470 mV for O–H stretching mode, ~410 mV for N–H stretching mode, ~380 mV for C–H stretching mode and ~260 mV for C–O stretching mode. Then, STM scanning is repeatedly performed with decreasing bias voltage until the reaction does not occur any more even with the highest tunneling current as far as the imaging is available. In most cases, the lowest value of bias voltage obtained in this process would be close to the onset bias voltage of the reaction.

2.3. Data acquisition

After making a clean tip for obtaining atomically-resolved STM images, the tip is further optimized for the STM-AS measurement. The first step is to confirm linearity and symmetry of $I - V$ curve on the bare surface. Fig. 5(a) shows the typical $I(t)$ and $V(t)$ signals versus time measured with a good tip and a bad tip on the clean Ag(1 1 1)surface. The tunneling gap resistance was set with the conditions of

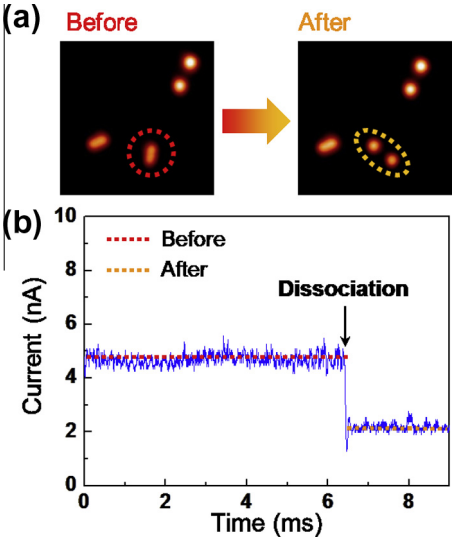

Fig. 6. Topographic STM image of DMDS molecules on Cu(1 1 1) (a) before and after dissociation reaction by injecting tunneling electrons ($V_s = -20$ mV, $I_t = 0.2$ nA, scan area: 1.7×2.2 nm^2). (b) A current trace recorded during the dissociation reaction.

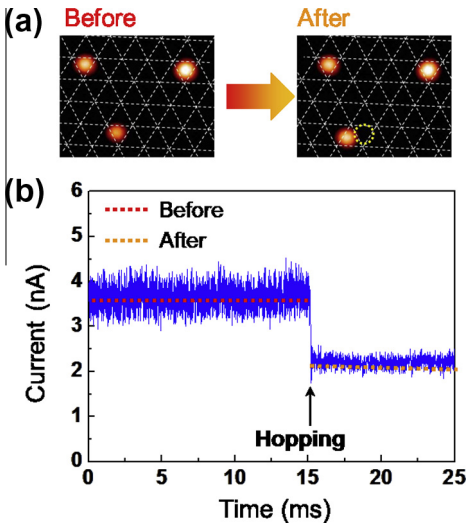

Fig. 7. Topographic STM image of MT molecules on Cu(1 1 1) (a) before and after lateral hopping by injecting tunneling electrons ($V_s = -20$ mV, $I_t = 0.2$ nA, scan area: $(1.2 \times 1.5\ nm^2)$. (b) A current trace recorded during the lateral hopping.

$V_s = 50$ mV and $I_t = 0.5$ nA. The feedback loop was then turned off, followed by sample bias voltage sweeping in the range between −300 and 300 mV with a speed of 60 mV/s. It is clearly shown that the influence of tip condition on the current change according to the bias voltage sweep. A good tip provides perfectly linear and symmetric $I(t)$ and $I - V$ curves, in comparison with the case of a bad tip. Moreover, the maximum tunneling current at a sample bias voltage of ±300 mV was observed to be 3.0 nA, which was numerically expected based on extrapolation of preset tunneling gap resistance.

The next step is to examine the stability of the tip by applying maximum bias voltage to the bare metal surface with high tunneling current for considerably long time in the range of STM-AS measurement, e.g., several nA and a few tens sec. Finally, electrons are then injected to the target molecule to confirm if the desired reaction occurs for the measurement parameter.

Chemical reaction, hopping and rotation of a molecule at the STM junction are fundamental reactions induced by the IET process, which usually lead to the change in the distance between the tip and the surface at the moment of the reaction. Even a small change in the tip–surface distance results in a large change in tunneling current, due to the exponential dependence of the tunneling current on the tip–surface distance. This highly-sensitive response of the change provides technical feasibility to quantitatively analyze reaction rate and reaction yield simply by monitoring current trace, as described in the previous section.

According to the type of reactions, the patterns of current change are classified into two categories. One is a single-shot change of tunneling current for the cases of lateral hopping and chemical reaction involving bond cleavage (breaking of internal chemical bond) and desorption (breaking a chemical bond between a molecule and substrate). The other is two- or more-level switching of tunneling current for the case of reversible change of the molecular configuration at the STM junction, such as the rotation [8], orientation switching [22] or conformational change [90]. In some cases, both types of tunneling current change occurs in a tunneling current trace, which reveals that two or more dynamic processes are induced by a same tunneling condition with a different time domain, e.g., rotation–desorption [91], hopping–rotation [63], rotation–dissociation [73] or two different kinds of orientation change [22,23].

STM images in Fig. 6(a) and (b) show S–S bond scission of a DMDS molecule adsorbed on Cu(1 1 1) surface. Individual DMDS molecules appear as elliptic protrusions in the STM image as in Fig. 6(a). The STM tip was then positioned at the center of a single DMDS molecule and tunneling current of 4.8 nA with a sample bias voltage of 400 mV was applied to the target molecule. Further STM imaging reveals

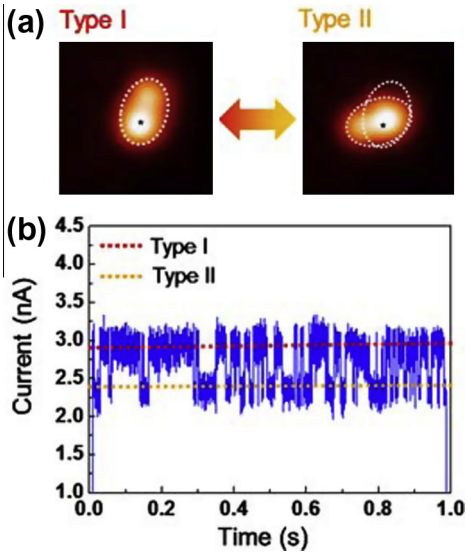

Fig. 8. Topographic STM images showing switching between type I and II adsorption orientations of a *cis*-2-butene molecule on Pd(1 1 0) when tunneling electrons are injected into the center of the brightest part (marked with a star) of the molecule (a). (b) A current trace recorded during the orientation change.

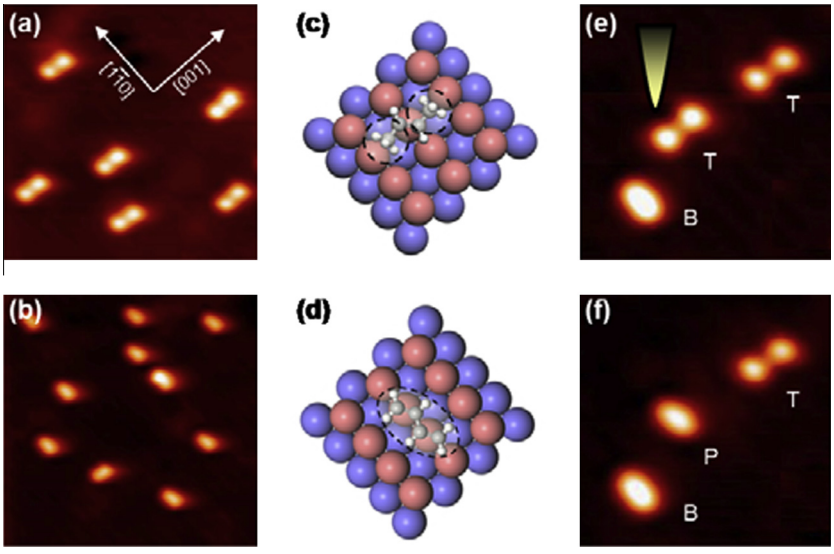

Fig. 9. STM images of (a) *trans*-2-butene and (b) 1,3-butadiene molecules (V_s = 300 mV, I_t = 1 nA, area = 45 × 45 Å^2). Schematic representation of the adsorption site of (c) *trans*-2-butene and (d) 1,3-butadiene molecule on Pd(1 1 0), respectively. STM images of coadsorbed surface (V_s = 200 mV, I_t = 0.86 nA, area = 20 × 20 Å^2) (e) before and (f) after dosing tunneling electrons on a target molecule of *trans*-2-butene marked with an arrow in (e). The *trans*-2-butene, reaction product, and 1,3-butadiene molecules are labeled T, P, and B, respectively, in (f).

that a DMDS dissociates into two identical protrusions corresponding to MT molecules as shown in Fig. 6(b). A sudden drop at 6.5 ms is observed in the trace of tunneling current as in Fig. 6(b), indicating the moment of the S–S bond cleavage. This is a typical single-shot current change, in which a single

reaction event for the target molecule occurs below the STM tip. It is inevitable in this kind of experiment to find a next molecule to react one after another, as also is the case for dehydrogenation of *trans*-2-butene on Pd(1 1 0).

Lateral hopping also gives a single-shot change of tunneling current. Fig. 7(a) shows an STM image of 3 isolated MT molecules on Cu(1 1 1) which were produced by dissociation of DMDS molecules. The crossing points of dotted lines with 3-fold symmetry in the STM image indicate the positions of substrate Cu atoms, and each MT molecule occupies a 3-fold hollow site with its sulfur atom bonding with 3 surrounding Cu atoms. After applying tunneling current of 3.5 nA with a sample bias voltage of 300 mV, a MT molecule laterally hops to the adjacent hollow site as shown in Fig. 7(a). Fig. 7(b) shows a single-shot type tunneling current change at 15 ms in the current trace. Contrary to the case of chemical reaction, a target molecule repeatedly used for the hopping experiments as far as it maintains same adsorption state as before. This was also the case for CO hopping on Pd(1 1 0).

A reversible tunneling current change between two states usually shows a "noisy" current trace. Fig. 8(a) display a reversible change between two identical adsorption structure with different adsorption orientations of a *cis*-2-butene on Pd(1 1 0). Fig. 8(b) displays a current trace for orientation switching (rotation) of a *cis*-2-butene on Pd(1 1 0).

3. Examples of STM-AS

In this section, we provide practical descriptions of constructing and utilizing STM-AS. The chemical transformation of a *trans*-2-butene to a 1,3-butadiene on Pd(1 1 0) was induced by injecting tunneling electrons [43]. The STM-AS was used to reveal the C–H bond scission was caused by excitation of a C–H stretching mode via IET process. The orientation change of *cis*-2-butene on Pd(1 1 1) [22,23] demonstrates that the STM-AS has an ability to detect vibrational modes more efficiently than STM-IETS. We also describe how to detect the vibrational signals from the measured STM-AS spectrum for lateral hopping of a water dimer adsorbed on Pt(1 1 1) [45,92].

3.1. Bond scission induced by the excitation of corresponding vibrational modes: Chemical transformation of a trans-2-butene on Pd(1 1 0)

A mode-selective transformation from a *trans*-2-butene molecule to a 1,3-butadiene molecule on Pd(1 1 0) surface has been studied by combination of the STM imaging, STM-IETS and STM-AS [43].

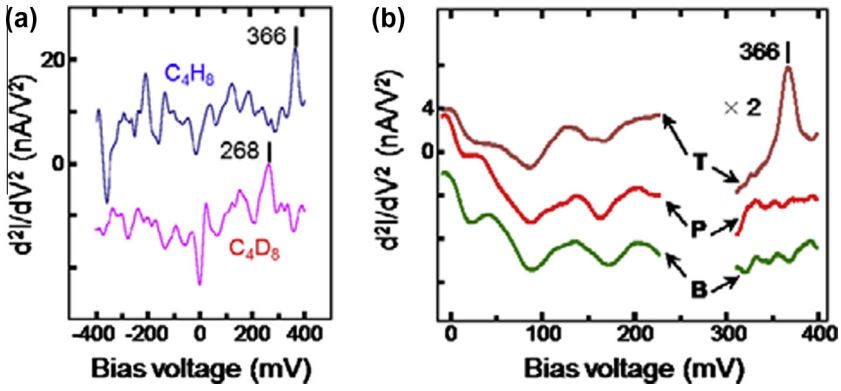

Fig. 10. (a) IETS spectra for *trans*-2-butene and *trans*-2-butene-d_8. The change in conductance for the peaks at ±366 mV (268 mV) is 6% (5%) at positive sample bias, and 7% (3%) at negative sample bias, for the C–H (C–D) stretching mode of *trans*-2-butene (*trans*-2-butene-d_8). (b) IETS spectra for *trans*-2-butene (curve T), reaction product (curve P), and 1,3-butadiene (curve B) shown in Fig. 9(f), respectively. The spectra were taken at a gap resistance of 200 MΩ within the range of 0 and 230 mV, in the region where the dehydrogenation does not occur, and 1.5 GΩ within the range of 300 and 400 mV. Reprinted from Ref. [43].

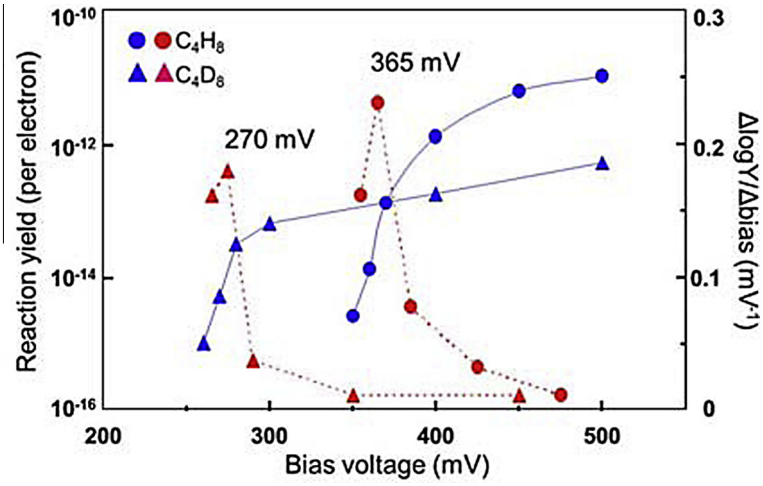

Fig. 11. Transformation yield of *trans*-2-butene on Pd(1 1 0) as a function of bias voltage.

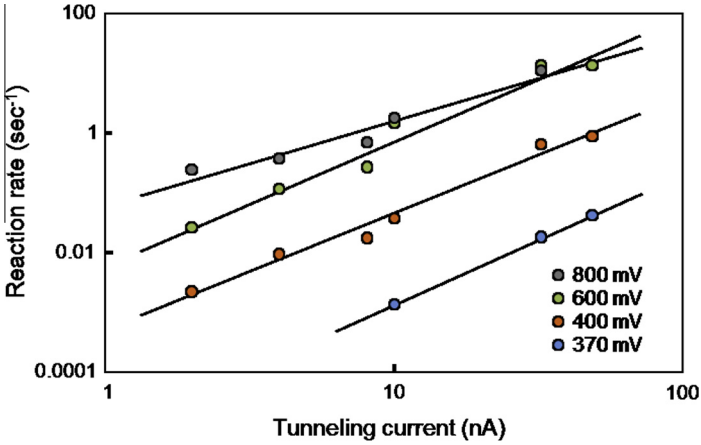

Fig. 12. Reaction rate as a function of tunneling current for various applied bias voltages for *trans*-2-butene. The solid lines are the results of least squares fits to the data, whose slopes for bias voltages correspond to powers (n) in nonlinear power-law dependence, $R \propto I^n$, n = 2.23, 1.96, 2.09, and 1.45 for 370, 400, 600, and 800 mV, respectively.

Topographic STM images of a *trans*-2-butene (Fig. 9(a)) and 1,3-butadiene (Fig. 9(b)) on the Pd(1 1 0) surface are quite different from each other; the former appears as a dumbbell shape where two protrusions are aligned perpendicular to the Pd row. The latter appears as an elliptical protrusion whose long axis is parallel to the Pd row. Fig. 9(e) shows the surface on which molecules of *trans*-2-butene (labeled T) and 1,3-butadiene (labeled B) are coadsorbed. After taking this image, the STM tip is positioned over the *trans*-2-butene molecule, as marked in the figure. The dosing condition is the tunneling current of 7 nA, the sample bias voltage of 450 mV and the dosing period of 1 s with the feedback loop turned off. This causes a topological change of *trans*-2-butene molecules; T of Fig. 9(e) changes to P of Fig. 9(f). Because of the similarity of the STM images between a 1,3-butadiene molecule and the reaction product, the *trans*-2-butene molecule is believed to be converted to a 1,3-butadiene molecule via dehydrogenation.

In order to identify the reaction product, we performed the STM-IETS measurement to obtain the vibrational informations. The STM-IETS measurement was carried out as follows: The STM tip was

precisely positioned over a target molecule and the feedback loop was turned off. Sinusoidal modulation of 397 Hz and 5.7–14.1 mV_{rms} in amplitude was superimposed on the bias voltage. The second harmonic of the modulation frequency was measured with a lock-in amplifier, which is proportional to d^2I/dV^2 showing a peak signal at the threshold energy for excitation of the vibrational mode. Fig. 10(a) represents the characteristic vibrational spectra obtained for *trans*-2-butene on Pd(1 1 0). In a background-subtracted spectrum of *trans*-2-butene molecule the characteristic features at ±366 meV can be assigned to the C–H stretching mode. The feature corresponding to the C–H stretching mode is the most characteristic vibrational fingerprint of hydrocarbon molecules in STM-IETS spectra. It is noted here that in the detection of the C–H stretching mode of *trans*-2-butene molecule, we used considerably high gap resistance of 1 GΩ so as to avoid the dehydrogenation of the molecule during measurement. It was also confirmed that deuteration of the molecule causes a spectral shift of this peak to 268 mV for *trans*-2-butene-d_8 as is also shown. In order to identify the reaction product, STM-IETS measurement was performed on *trans*-2-butene (T), reaction product (P), and 1,3-butadiene (B). In Fig. 10(b) the spectrum of *trans*-2-butene (curve T) is dominated by a strong C–H stretching peak at 366 meV, while no peak is observed in the C–H stretch region both for reaction product (curve P) and for 1,3-butadiene (curve B). The absence of the C–H stretching mode of 1,3-butadiene and reaction product provide spectroscopic evidence for the conversion of a *trans*-2-butene molecule into a 1,3-butadiene molecule.

The transformation yield as a function of the sample bias voltage at a constant tunneling current is shown in Fig. 11, both for *trans*-2-butene and for *trans*-2-butene-d_8. Their slopes are also shown in the same graph. The variation of the reaction yield reveals a rapid increase at the threshold voltages of 365 and 270 mV for a *trans*-2-butene molecule and a *trans*-2-butene-d_8 molecule, respectively. The bias voltages correspond clearly to the C–H and C–D vibrational stretching modes observed in STM-IETS spectra (see Fig. 10(a)). This obviously indicates that the C–H (C–D) stretching mode is a "doorway" to the C–H (C–D) bond dissociation.

Fig. 12 shows the reaction rate $R(I)$ as a function of I at several bias voltages. A feature commonly observed for the vibrational heating mechanism is a nonlinear power-law dependence $R(I) \propto I^n$, where n depends on a bias voltage for"*coherent*" ladder climbing. The solid lines in Fig. 12 are the results of the least squares fits to the data and n = 2.23, 1.96, 2.09, and 1.45 are obtained for 370, 400, 600, and 800 mV, respectively. The experimental result of a transformation yield as a function of the bias voltage at a constant tunneling current of 32 nA is shown as the red circles in Fig. 11.

Although no theory is available to describe a multi-electron coherent ladder climbing in the RC potential, the threshold observed in Fig. 11 indicates that coherent excitation of the C–H stretch mode at $\hbar\Omega = 366$ meV (taken from the corresponding STM-IETS peak shown in Fig. 10) is responsible for the vibrationally mediated transformation of the molecule from *trans*-2-butene to 1,3-butadiene.

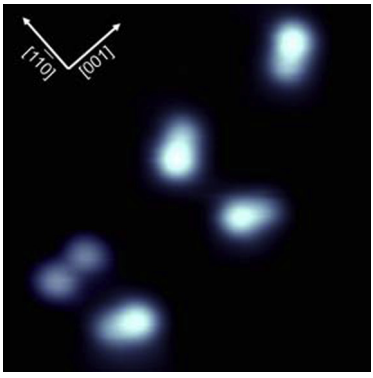

Fig. 13. An STM image of *cis*-2-butene molecules (pear shape) on Pd(1 1 0) surface. A *trans*-2-butene molecule (dumbbell shape) is coadsorbed as a marker. (V_s = −20 mV, I_t = 1.0 nA, scan area: 8 × 8 nm^2).

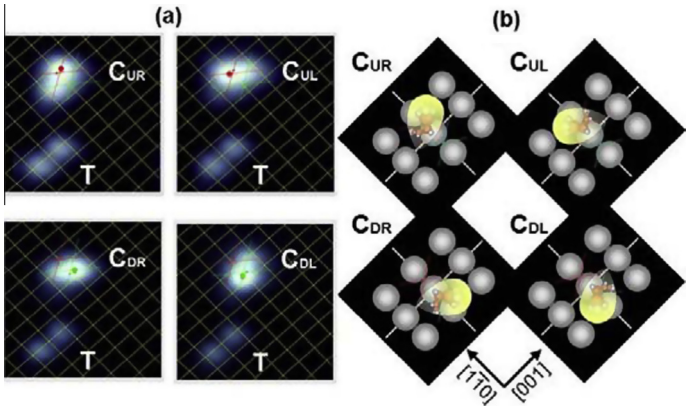

Fig. 14. (a) STM images of a *cis*-2-butene molecule (labeled C) with four equivalent orientations, marked as C_{UR}, C_{UL}, C_{DR} and C_{DL}, which are obtained by rotating a single molecule by injecting tunneling electrons. A *trans*-2-butene molecule (labeled T) was co-adsorbed as a maker. The superimposed grid indicates the position of surface Pd atoms. A filled circle in each molecule represents the center of the large bright region of the molecule in each orientation, where the tunneling electrons were injected. Four lines forming a rhombus correspond to the symmetry lines of the molecule at each orientation. (b) Schematic models of the four orientations corresponding to the STM images.

Besides the motion of the molecule [9], this was the first experimental example to simultaneously reveal, for the chemical reaction, the vibration mode to induce chemical reaction and the detection of the responsible vibrational mode by IETS.

3.2. Usefulness of action spectroscopy as a vibrational spectroscopy of single molecules: Reversible orientation change of cis-2-butene on Pd(1 1 0)

Fig. 13 represents an STM image of individual *cis*-2-butene molecules coadsorbed with a *trans*-2-butene molecule on the Pd(1 1 0) surface. They have characteristic features different from each other in the STM image; a *cis*-2-butene appears as a gourd shape and a *trans*-2-butene appears as a dumbbell shape, respectively. A gourd shape of the *cis*-2-butene consists of a brighter round protrusion region (head) and a pale protrusion region (tail), indicated as a pear shape in the figure. In contrast to the shape of *trans*-2-butene molecule, a geometric isomer, having only one orientation where the long axis of the molecule lies parallel with [0 0 1] direction of the Pd(1 1 0) surface, the *cis*-2-butene molecule was observed to have a total of four kinds of adsorption orientations. Since the Pd(1 1 0) surface has a C_{2v} symmetry, the existence of four kinds of orientations implies that the *cis*-2-butene has a single-bonding configuration with off-symmetric manner.

The *cis*-2-butene molecule easily changes its orientation when the tunneling electrons are injected from the STM tip. Fig. 14(a) shows STM images of a single *cis*-2-butene molecule having four equivalent adsorption orientations, which are obtained by injecting tunneling electrons. Each orientation is labeled as C_{UR}, C_{UL}, C_{DR} and C_{DL}, according to the direction of head part with respect to the crystal surface directions, [0 0 1] and [1 $\bar{1}$ 0]. Fig. 14(b) show schematic models for corresponding adsorption structures of a *cis*-2-butene molecule to each adsorption orientation. It has been reported that the *cis*-2-butene binds through π bonding to a surface Pd atom at the off-centered position [60]. Thus, the molecule is considered to be slightly inclined from the symmetrical position, leading to asymmetric geometry for its two methyl groups, which suggests that the brighter head part of the STM image may reflect the distribution of the electron density of state at the pulled-up methyl group in the highest occupied molecular orbital (HOMO) of the molecule, in addition to the strong hybridization between a molecular π orbital and *d* band of a Pd atom. In the case of *trans*-2-butene molecule adsorbed on the Pd(1 1 0) surface, two equivalent brighter protrusions in the dumbbell-shape STM image have also been assigned to be methyl groups pointing towards vacuum. This is considerably

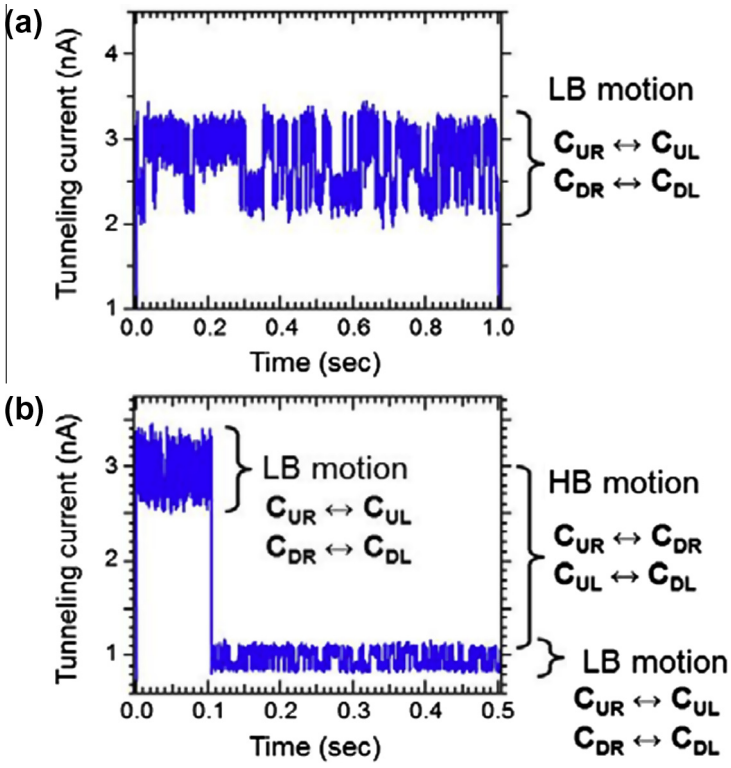

Fig. 15. Current traces for (a) the LB motion at a sample bias voltage of 60 mV (b) the HB motion at a sample bias voltage of 170 mV.

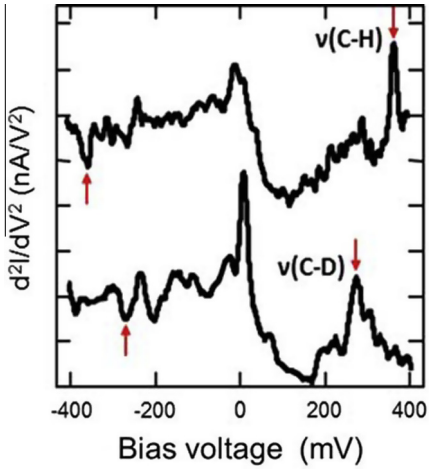

Fig. 16. (a) STM-IETS spectra of C_4H_8 and C_4D_8 on Pd(1 1 0). All spectra were processed by subtracting spectra measured on the bare surface. Tunneling gap resistance was set to be 0.25 nA and 20 mV. $V_{rms} = 15$ mV ac modulation was applied with 797 Hz. Each spectrum has been averaged 16 times.

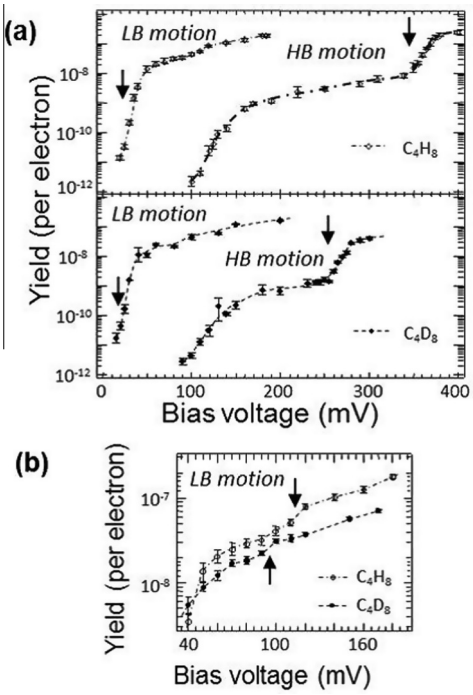

Fig. 17. (a) STM-AS spectra for both LB and HB motions of C_4H_8 (top) and of C_4D_8 (bottom). Data were obtained under fixed tunneling current of 3 nA for C_4H_8 and of 2 nA for C_4D_8. (b) STM-AS spectra for LB motion which is expanded bias voltage range from 20 to 170 mV.

derived from the bent configuration of the C=C–C backbone of the molecule, resulting from the π bonding of C=C bond of the molecule with a surface Pd atom [43].

A *cis*-2-butene molecule hops from one orientation to another when tunneling electrons are injected into the center of the bright region of the STM image, filled circles in Fig. 14(a). The orientation change can be quantitatively measured by monitoring tunneling current change as a function of time as shown in Fig. 15(a) and (b). Based on both STM images and the trace of tunneling current, there are two types of orientation change; one motion is low-barrier (LB) in energy and the other is with high-barrier (HB). A typical tunneling current trace for the LB motion is displayed in Fig. 15(a), where the tunneling current shuttles between two states under the application of sample bias voltage of 60 mV. The STM imaging shows the LB motion occurs only between C_{UR} and C_{UL} or between C_{DR} and C_{DL} orientations. The pairs of (C_{UR} and C_{UL}) and of (C_{DR} and C_{DL}) are mirror images with respect to a plane parallel to $[1\bar{1}0]$, as shown in Fig. 14(b), which implies that the LB motion is achieved by see-saw like switching of asymmetric adsorption sites across the mirror plain along $[1\bar{1}0]$ on a Pd atom. When the higher bias voltage (170 mV in Fig. 15(b)) is applied, a different type of motion, HB motion, occurs. This is the change between C_{UR} and C_{DR} or between C_{UL} and C_{DL}. The pairs of (C_{UR} and C_{DR}) and of (C_{UL} and C_{DL}) are of mirror symmetry about [001], as also shown in Fig. 14(b). According to the schematic models, the HB motion requires a flip-flop like switching of the molecule in addition to the adsorption site change across the mirror plain along [001] on a Pd atom.

Fig. 14(a) clearly shows that the location of STM tip is kept at very near the initial position after orientation change by LB motion, which results in a relatively small change in tunneling current as shown in Fig. 15(a). Whereas, HB motion causes much bigger change in tunneling current after the orientation change as shown in Fig. 15(b). Interestingly, even after HB motion occurs, the current trace displays shuttling with a small change in tunneling current due to the LB motion.

Fig. 16 shows STM-IETS spectra of a *cis*-2-butene (C_4H_8) and fully-duterated *cis*-2-butene (C_4D_8) molecules. The significant signals appear at ~358 mV for C_4H_8 and at ~268 mV for C_4D_8, which are assigned to be the vibrational peaks of $\nu(CH_3)$ and $\nu(CD_3)$ as also obtained in the same experiment on *trans*-2-butene on Pd(1 1 0).

Fig. 17 shows the STM-AS spectra for both LB and HB motions obtained from C_4H_8 and C_4D_8. The clear thresholds are observed at 37 mV and at 115 mV for LB motion, and at 115 mV and at 360 mV for HB motion of C_4H_8 in the upper panel of Fig. 17(a). The STM-AS spectra of C_4D_8 also show thresholds at 31 mV and at 95 mV for LB motion, and at 115 mV and at 270 mV for HB motion. Magnification of the spectra for LB motion of C_4H_8 and C_4D_8 in the range between 30 and 170 mV reveals additional signals at 115 mV for C_4H_8 and 95 mV for C_4D_8. We assigned those thresholds by comparing with the result of high resolution electron energy loss spectroscopy (HREELS) of *cis*-2-butene on Pd(1 1 0), as follows; (1) The first threshold at 37 (31) mV for LB motion of C_4H_8 (C_4D_8) corresponds to the vibrational energy of ν(M–C). (2) Thresholds at 115 mV for LB motion and for HB motion of both C_4H_8 and C_4D_8 correspond to ν(C–C). (3) Thresholds at 115 (95) mV for LB motion of C_4H_8 (C_4D_8) are attributed to $\delta(CH_3)$ ($\delta(CD_3)$). (4) Threshold at 360 (270) mV for HB motion of C_4H_8 (C_4D_8) is assigned to be $\nu(CH_3)$ ($\nu(CD_3)$), which are also obtained in STM-IETS as shown in Fig. 16.

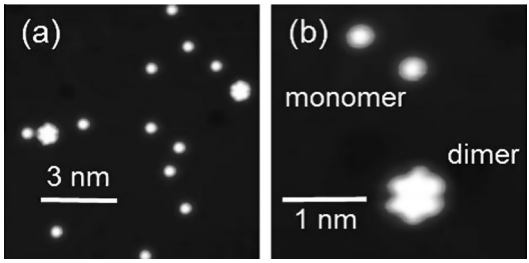

Fig. 18. Topographic STM images of isolated water monomers and dimers on Pt(1 1 1), (a) H_2O, V_s = 20 mV, I_t = 0.5 nA (b) D_2O, V_s = 40 mV, I_t = 0.5 nA.

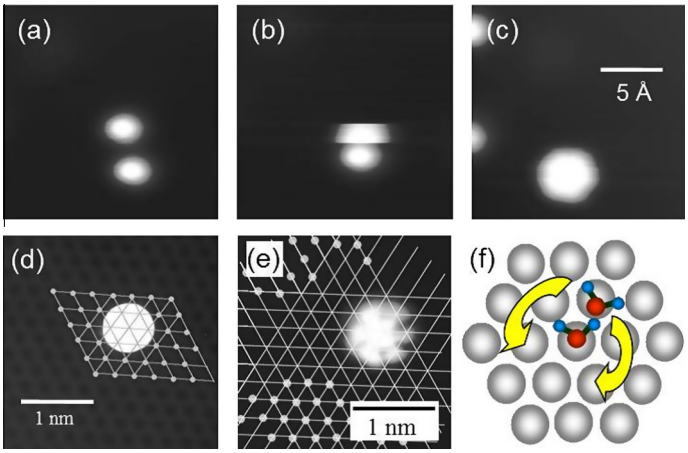

Fig. 19. (a)–(c) Sequential topographic STM images of water dimer formation. (a) Two H_2O monomers, V_s = 30 mV, I_t = 0.5 nA. (b) Hopping motions observed, V_s = 110 mV, I_t = 1.0 nA. (c) A dimer formation completed, V_s = 40 mV, I_t = 0.5 nA. (d) A topographic STM image of H_2O monomer obtained with a tip of which the water molecule is attached to the apex (molecular tip) to resolve the Pt lattice. The grid shows the positions of Pt atoms. V_s = 20 mV, I_t = 0.5 nA. (e) A topographic STM image of H_2O dimer obtained with a molecular tip. V_s = 50 mV, I_t = 0.5 nA. (f) A schematic image of a water dimer. Both molecules are adsorbed on atop site and one is rotating around the other [92].

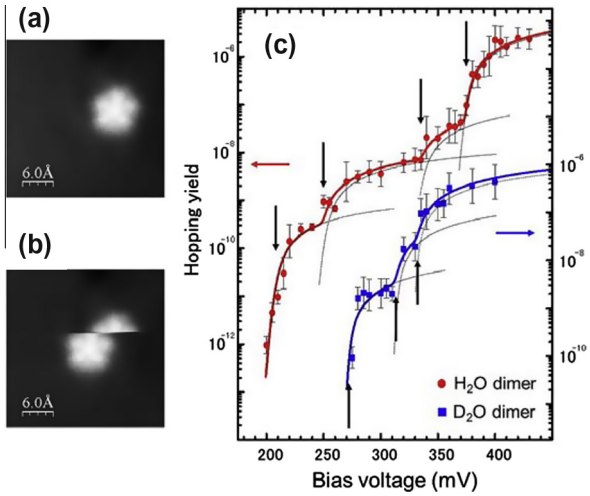

Fig. 20. STM images showing (a) before and (b) after lateral hopping by injecting tunneling electrons into the center of the H_2O dimer (V_s = 50 mV, I_t = 2.0 nA). (c) STM-AS and spectral fit of the lateral hopping of H_2O and D_2O on Pt(1 1 1) [46]. The red circles and blue squares represent the experimental results of the STM-AS for H_2O and D_2O dimer, respectively. The data points at V lower than 370 mV for H_2O and 355 mV for D_2O were taken at constant current of 4 nA and the rest of the data points were taken at 0.5 nA because of the detection limit of oscilloscope. No significant change in hopping yield was detected with respect to the change of tunneling current or tip-sample distance. The thick solid curves represent the best-fit spectra of $Y(V)_{tot}$. The thin dotted curves represent the fraction of simulated $Y(V)_{tot}$, representing the $Y(V)$ of hopping induced by the excitation of each vibrational mode. Arrows indicate the vibrational signals. (For interpretation of the references to color in this figure legend, the reader is referred to the web version of this article.)

From the STM-AS measurement, it turns out that the motion of *cis*-2-butene on Pd(1 1 0) is induced by excitation of ν(M–C), ν(C–C), $\delta(CH_3)$ and $\nu(CH_3)$ vibrational modes, while only $\nu(CH_3)$ is observed in STM-IETS. This would be a good demonstration of how the STM-AS is useful for detecting vibrational signals that cannot be measured by STM-IETS.

3.3. An example for structural characterization of unknown species: Lateral hopping of a water dimer on Pt(1 1 1)

Water monomers and dimers, the simplest building block of water clusters, on well-defined single crystal surface of metals are useful model system for exploring the nature of both water–water hydrogen-bond (H-bond) and water–solid interactions, and have been extensively studied by various kinds of surface spectroscopic techniques as well as by microscopic technique with STM. Since various sizes of water clusters exist on the surface, conventional vibrational spectroscopy always suffers from the difficulty in signal assignment mainly due to its poor spatial resolution. However, STM enables us to characterize structures and orientations of individual water clusters at the molecular level.

On the close-packed surface of noble metals, relatively large clusters such as hexamers, heptamers and nonamers have been observed by STM, which means that the water monomers or dimers are less stable on noble metal surfaces [93–97]. In contrast, on Cu(1 1 0) [38], Ru(0 0 0 1) [98,108,109], and Pd(1 1 1) [35,99], water monomers and dimers were observed as major species at low coverage and low substrate temperature. The orientation of water molecule in a dimer, however, has not been well elucidated yet despite its importance in understanding the growth of clusters and H-bond network. Studies using DFT calculations of a water dimer on Pt(1 1 1) have given different optimized structures [100–103]. Single molecule vibrational spectroscopy is a powerful tool for resolving water dimer structure and more over, STM-AS is suitable for mobile molecules than STM-IETS which requires the stability of the molecule at the STM junction. Cluster-size-specific vibrational spectra of water

measured by STM-AS allows us detailed structural analysis of each water cluster. Therefore, STM-AS was employed to study the structure of water dimer [45,46,92].

Fig. 18(a) and (b) show topographic STM images of isolated water monomers and dimers adsorbed on the Pt(1 1 1) surface at a surface coverage less than 0.005 ML, which was realized by dosing water molecules at a substrate temperature of 20 K. The images of monomers and dimers appear as two different shapes, a small round-shape protrusion and a bigger "flower-like" protrusion with 6-fold symmetry, respectively. Both H_2O and D_2O gave identical protrusions.

The monomers and dimers were assigned by manipulation with STM. Individual water monomers show lateral hopping motion by injecting tunneling electrons under a typical tunneling condition ($V_s = 200$ mV and $I_t = 1.0$ nA for 1 s). The monomer hopping can eventually lead to a collision with a neighboring monomer to form a dimer. A series of STM images during the dimer formation is shown in Fig. 19(a)–(c). The adsorption sites of water monomer is atop site, which was determined by atomically resolved STM image taken with a molecular tip (a water molecule is attached on the apex of the tip) shown in Fig. 19(d). This STM image is supported by the DFT which indicate the atop adsorption of monomers with its molecular plane parallel to the metal substrate [100,102]. DFT also indicated that the lateral rotation barrier of water monomer is sufficiently small for free rotation [101], which results in circular STM images. In the same manner, atomically resolved STM image of water dimer shows that the center of dimer and the center of each lobe are all located on atop sites [Fig. 19(e)]. The anomalous shape of the water dimer can be explained as a "time-averaged" 6-fold shape resulting from one molecule rotating around the other one fixed on the surface as schematically depicted in Fig. 19(f). Six equivalent potential minima for the rotating molecule at the six atop sites result in the flower-shaped protrusion. The adsorption structure model of a water dimer is also supported by the DFT [100–103]. Here we refer to the molecule which rotates and weakly bounds to the surface as an acceptor molecule, and the molecule fixed on the surface as a donor molecule, from accepting and donating a hydrogen atom in H-bond, respectively.

The water dimer exhibits lateral hopping when tunneling electrons are injected into the center of a water dimer, as shown in Figs. 20(a) and (b). After the hopping event, adsorption site is still maintained to be atop site. In order to obtain STM-AS, hopping yield (number of hopping event per an injected electron) was measured as a function of sample bias. The measurement was carried out 16 times for each sample bias voltage ranging from 200 to 430 mV for H_2O and from 270 to 400 mV for D_2O.

The STM-AS for the lateral hopping of both H_2O and D_2O dimers are shown in Fig. 20(c). At a glance, the spectra show roughly total of 5 threshold voltages at ~200 and ~360 mV for H_2O dimer, and at ~270, ~320 and ~340 mV for D_2O dimer. Application of a theoretical fit [29] that will be discussed in Section 4 to the STM-AS spectra enables us reasonable and precise assignment of vibrational signals [46]. The experimental results are well represented by the simulated curves (thick solid curves in Fig. 20(c) with vibrational signals at 208, 250, 335 and 375 meV for H_2O and at 272, 313, and 332 meV for D_2O.

DFT calculations of the vibrational frequencies [46] allow assignment of the vibrational signals observed in the STM-AS. The signal observed at 208 meV corresponds to the HOH scissoring modes δ(HOH) of two water molecules which overlap each other. The small signals at 250 and 335 meV are, respectively, the combination modes of the δ(HOH) and O–Pt stretching modes of the molecule that serves as a hydrogen-bond donor (H-donor molecule) ν(OPt), and of the δ(HOH) and libration modes of the H–O–Pt of the H-donor molecule δ(HOPt). The signal at 375 mV represents the OH stretching mode of the H-donor molecule, which participates in an intermolecular hydrogen bond $\nu(OH)_{HB}$. The signals for D_2O at 272, 313 and 332 meV, respectively correspond to $\nu(OD)_{HB}$, the OD stretching mode of the hydrogen bond acceptor (H-acceptor) molecule that points toward the surface $\nu(OD)_{Pt}$, and the free OD stretching mode of the H-donor ($\nu(OD)_{do}$). A vibrational signal corresponding to $\nu(OH)_{HB}$ at 375 mV in the STM-AS was absent in previously reported infrared reflection absorption spectroscopy (IRAS) [105,106] and HREELS [104,107] spectra for low water coverage, indicating that water dimers were not observed in these macroscopic vibrational studies. STM-AS appears to be the only method so far that can detect the vibrational signals of water dimers on metal surfaces.

The vibrational energy of ν(OH(D)) can be used to deduce the structure of water dimers because it depends on the environment surrounding each OH(D) group. Two structure models were reported, in

which the H-acceptor molecule has two OH(D) groups that are equivalently oriented toward the surface (H-parallel model) [102] or one OH(D) of the H-acceptor molecule points toward the surface and the other points toward the vacuum (H-down model) [101]. To determine which structure occurred in our experiment, we compared the measured vibrational energies with the calculated vibrational energies of the two models. The vibrational energies of ν(OD) obtained by STM-AS (272, 313, and 332 meV) show better agreement with the vibrational energies calculated for the H-down model (264, 309, and 336 meV) [46]. The vibrational energies of the H-parallel model (257, 320, and 335 meV) [102] show significant disagreement, especially in $\nu(\mathrm{OH(D)})_{\mathrm{HB}}$. Thus, we concluded that the water dimer structure on Pt(1 1 1) observed in our STM measurements is well represented by the H-down model. Consequently, this provides valuable information regarding a long-discussed issue of the interaction regime of the water–metal interaction. The H-donor molecule interacts with the substrate Pt atoms via back donation of the oxygen lone pair as commonly thought [101,102]. The H-acceptor molecule interacts with the Pt substrate not through the oxygen lone pair as suggested in the H-parallel model [101] but through an OH–Pt hydrogen bond [107–109].

We demonstrated that the single molecule vibrational spectroscopy with STM-AS enables us the structural analysis of individual molecules and molecular clusters on surfaces through the study of water dimers on Pt(1 1 1). In particular it allows us to determine the positions of the H(D) atoms in individual molecules, which is a difficult task even with using STM.

3.4. Experimental perspectives

In this section, we have shown experimental details about how to measure the STM-AS to detect relevant vibrational modes responsible for dynamic behavior of a single molecule induced by tunneling electrons via IET process. The dynamic behavior of the adsorbate can be described with a potential energy surface in terms of the vibrational energy of the corresponding RC mode and the reaction barrier. In combination with the STM-IETS, one can obtain invaluable information about vibrational modes of an adsorbate in the wide range of vibrational energy from low-frequency surface bound modes to high-frequency internal stretching modes and even combination modes. The measurement of reaction rate as a function of tunneling current at a given bias voltage reveals how many electrons are required to overcome reaction barrier, which enables us to make a rough estimation of reaction barrier. Thus, construction of a 3-dimensional plot that consists of reaction yield, applied bias voltage and tunneling current would be helpful in describing precise potential energy surface for obtaining comprehensive feature of underlying mechanism. The STM-AS detects vibrational modes that are resonantly excited through a local DOS constructed by the hybridization between metal surface and adsorbate MOs near the ε_{F} [27], which implies that the amount of local DOS would significantly affect the reaction yield according to tip position around the target molecule. If a 2-dimensional map of STM-AS is available, one would be able to obtain experimental evidence of correlation between spatial distribution of MOs near the ε_{F} and the IET process at STM junction. Careful measurement of STM-AS will unveil the microscopic underlying mechanism of how the molecular vibration couples to the tunneling electrons leading to dynamic behavior of an adsorbate.

4. Theory of action spectroscopy

In what follows we describe a general theory of STM-AS based on the adsorbate-induced resonance model, which provides a versatile tool to analyze vibrationally mediated reactions of single adsorbates on metal surfaces [42]. This allows us to determine the energy of the excited vibrational mode, the effective broadening of the vibrational DOS (as described by Gaussian or Lorentzian functions), and a prefactor characterizing the elementary process behind the reaction. The underlying different levels of approximations are critically discussed. In addition to the numerical demonstrations of the characteristic AS features, we also point out that observation of reaction yields at both bias voltage polarities can provide additional insight into the DOS of adsorbates near the ε_{F}. In this way STM-AS is a complementary experimental tool to explore the vibrational and electronic properties associated not only

with dynamics of vibrationally mediated single molecule reactions, but in principle also aspects of the electronic structure of the adsorbates.

4.1. Reaction yield

We define a reaction yield $Y(V)$ as a reaction rate $R(V)$ per electron, i.e.,

$$Y(V) = \frac{R(V)}{I(V)/e} \tag{3}$$

where $I(V)$ is electrical current through the adsorbate level at an applied voltage V. The elastic current is generally given by

$$I(V) = \frac{2e}{\hbar}\frac{\Gamma_s\Gamma_t}{\Gamma}\int_{-\infty}^{\infty} d\varepsilon\, \rho_a(\varepsilon + eV)[n_F(\varepsilon) - n_F(\varepsilon + eV)] \tag{4}$$

where a factor 2 is included for spin. Here $\Gamma = \Gamma_s + \Gamma_t$ and $n_F(\varepsilon) = 1/(e^{\beta(\varepsilon-\varepsilon_F)} + 1)$ is the Fermi–Dirac distribution function (Fermi energy ε_F, inverse temperature $\beta = k_BT$) and Γ_j $[= \pi \mid V_{ja}|^2\rho_j$ in the wide-band limit (WBL)] is the coupling with the substrate ($j = s$) or the tip ($j = t$), and the DOS of adsorbate $\rho_a(\varepsilon)$ in the WBL is given by

$$\rho_a(\varepsilon) = \frac{1}{2\pi}\frac{\Gamma}{(\varepsilon - \varepsilon_a)^2 + (\Gamma/2)^2}. \tag{5}$$

We assume that the adsorbate level ε_a is pinned to the substrate chemical potential such that the effect of an applied bias voltage V simply shifts the resonance position by eV with respect to the Fermi level ε_F. We note that this assumption is reasonable under usual STM conditions where $\Gamma_s \gg \Gamma_t$ and that the potential drop thus occurs essentially between the adsorbate and STM tip. The zero-temperature limit is simply

$$I_0(V) = \frac{2e}{\pi\hbar}\frac{\Gamma_s\Gamma_t}{\Gamma}\left[\arctan\frac{2(eV - \varepsilon_a)}{\Gamma} + \arctan\frac{2\varepsilon_a}{\Gamma}\right]. \tag{6}$$

As an alternative to evaluate Eq. (3) in combination with the zero-temperature results Eqs. (4), we shall explore the extended wide band limit (EWBL) by making use of the linearized elastic current

$$I_0(V) \simeq \sigma_0 V \tag{7}$$

where the elastic conductance (around $eV = \pm\hbar\Omega$) is simply given by

$$\sigma_0 = \frac{2e^2}{\hbar}\frac{\Gamma_s\Gamma_t}{\Gamma}\rho_a(\varepsilon_F \pm \hbar\Omega). \tag{8}$$

A reaction rate $R(V)$ in a single electron process is defined by

$$R(V) = K\Gamma_{\mathrm{iet}}(V, \Omega), \tag{9}$$

and

$$Y(V) = \frac{R(V)}{I(V)/e} = K\frac{e\Gamma_{\mathrm{iet}}(V, \Omega)}{I} = K\eta_{\mathrm{iet}}(V, \Omega), \tag{10}$$

where $\eta_{\mathrm{iet}}(V, \Omega) = I_{\mathrm{in}}(V)/I(V)$ is an inelastic tunneling fraction and a prefactor K is specified for an elementary process describing how an inelastic tunneling current $I_{\mathrm{in}} = e\Gamma_{\mathrm{iet}}(V, \Omega)$ exciting a vibrational mode with the energy $\hbar\Omega$ induces reactions of single adsorbates. A key quantity of the vibrational generation rate $\Gamma_{\mathrm{iet}}(V, \Omega)$ is derived below for a single adsorbate-induced resonance model.

4.2. Vibrational generation rate

STM-AS observes a reaction induced by inelastic tunneling current and is free from a complicated competition between the elastic and inelastic tunneling current to determine the observed total current. Following Refs. [110,111], we first describe a formulation of the vibrational generation rate

$\Gamma_{\rm iet}(V)$. We consider the standard Hamiltonian used for a theory of IETS based on an adsorbate-induced resonance model [112,113].

$$H_0 = \varepsilon_a|a\rangle\langle a| + \sum_s \varepsilon_s|s\rangle\langle s| + \sum_t \varepsilon_t|t\rangle\langle t| + \sum_s (V_{sa}|s\rangle\langle a| + h.c.) + \sum_t (V_{ta}|t\rangle\langle a| + h.c.), \tag{11}$$

written in terms of the one particle electron states $|a\rangle, |s\rangle, |t\rangle$ of the adsorbate level, the substrate, and the tip, respectively, and their corresponding one-electron energies $\varepsilon_a, \varepsilon_s$, and ε_t. V_{sa} (V_{ta}) describes the hopping integrals between the substrate (tip) and the adsorbate level. We further consider that a vibrational mode,

$$H_{\rm ph} = \hbar\Omega(b^\dagger b + 1/2), \tag{12}$$

couples to the adsorbate level via a linear coupling term

$$H' = \chi(b^\dagger + b)|a\rangle\langle a|, \tag{13}$$

with χ being the electron–phonon coupling matrix element and b ($b^\dagger$) the phonon annihilation (creation) operator.

As is evident from Eq. (8), a key quantity in the theory of AS is the vibrational generation rate $\Gamma^v_{\rm iet}(V)$ associated with a characteristic vibrational mode v of the adsorbate excited by the inelastic tunnel current. It can generally be expressed as [110]

$$\Gamma^v_{\rm iet}(V) = \int_0^\infty d\omega \rho^v_{\rm ph}(\omega)\Gamma^v_{\rm in}(\omega, V), \tag{14}$$

where $\rho^v_{\rm ph}(\omega)$ is the vibrational DOS and $\Gamma^v_{\rm in}(\omega, V)$ is the spectral generation rate for a mode v corresponding to an excitation of a vibrational mode with the energy $\hbar\omega$. Within Fermi's golden rule the latter is given by

$$\Gamma^v_{\rm in}(\omega, V) = 2\frac{2\pi}{\hbar}\sum_{i,f}\left|\langle f; n+1|H'_v|i; n\rangle\right|^2 \times n_a(\varepsilon_i, V)[1 - n_a(\varepsilon_{\rm F}, V)]\delta_{\varepsilon_i, \varepsilon_{\rm F}+\hbar\omega} \tag{15}$$

where $|i; n\rangle$ ($|f; n \pm 1\rangle$) characterizes the initial (final) electronic state with the harmonic oscillator in a level n ($n \pm 1$). The Pauli exclusion principle is taken into account via the adsorbate level occupation probability $n_a(\varepsilon, V)$, which (under nonequilibrium conditions imposed by a bias voltage V) can be expressed as

$$n_a(\varepsilon, V) = \frac{n_F(\varepsilon + eV)\Gamma_s + n_F(\varepsilon)\Gamma_t}{\Gamma}, \tag{16}$$

With Eq. (13) as the perturbation we obtain

$$\Gamma^v_{\rm in}(\omega, V) = \frac{4\pi}{\hbar}\chi_v^2[n_B(\hbar\omega) + 1]\int_{-\infty}^{\infty} d\varepsilon_i\, \rho_a(\varepsilon_i, V)\rho_a(\varepsilon_i - \hbar\omega, V)n_a(\varepsilon_i, V) \times [1 - n_a(\varepsilon_i - \hbar\omega, V)], \tag{17}$$

where $n_B(\hbar\omega) = 1/(e^{\beta\hbar\omega} - 1)$ is the Bose–Einstein distribution. Note that the summations over initial and final states are replaced with integrals over $\rho_a(\varepsilon, V)$.

Next we describe some different physical approximations that have been applied $\Gamma^v_{\rm in}(\omega, V)$, we apply successively a number of physical approximations. First, with the Lorentzian $\rho_a(\varepsilon)$ in Eq. (17), the spectral generation rate takes the following analytic expression in the zero-temperature limit:

$$\Gamma^v_{\rm in,0}(\omega, V) = \frac{2\chi_v^2\Gamma_s\Gamma_t}{\pi\hbar\Gamma(\Gamma^2 + (\hbar\omega)^2)} \times \begin{cases} \mathcal{I}(eV) - \mathcal{I}(\hbar\omega), & eV > \hbar\omega \\ \mathcal{I}(0) - \mathcal{I}(eV + \hbar\omega), & eV < -\hbar\omega \\ 0, & |eV| \leqslant \hbar\omega \end{cases} \tag{18}$$

where

$$\mathcal{I}(X) \equiv \mathcal{A}(X+\varepsilon_F-\varepsilon_a)+\mathcal{L}(X+\varepsilon_F-\varepsilon_a), \tag{19}$$

$$\mathcal{A}(X) \equiv \arctan\frac{2X}{\Gamma}+\arctan\frac{2(X-\hbar\omega)}{\Gamma}, \tag{20}$$

$$\mathcal{L}(X) \equiv \frac{\Gamma}{2\hbar\omega}\log\frac{X^2+(\Gamma/2)^2}{(X-\hbar\omega)^2+(\Gamma/2)^2}. \tag{21}$$

The zero-temperature limit (denoted by subscript 0) is always justified in STM manipulation experiments as the thermal energy is the smallest energy scale, e.g., at $T = 4.2$ K the thermal energy is $k_BT \approx 0.1$ mV, which is significantly smaller than typical vibrational excitations $\hbar\omega$, applied voltages eV, and life-time broadenings Γ of the adsorbate resonance.

Secondly, as we are mostly interested in the behavior around the onset of vibrational excitation, it is a good approximation to perform a linear expansion of Eq. (18) around $eV = \pm\hbar\omega$. This can be written as

$$\Gamma^{v,\mathrm{lin}}_{\mathrm{in},0}(\omega,V) = \alpha(V)\gamma^v_{\mathrm{eh}}(\omega)\times\frac{\Gamma_s\Gamma_t}{\Gamma^2}\frac{|eV|-\hbar\omega}{\hbar\omega}\theta(|eV|-\hbar\omega), \tag{22}$$

where we define $\gamma^v_{\mathrm{eh}}(\omega) = 4\pi\omega\chi_v^2\rho_a^2(\varepsilon_F)$ as the electron–hole pair damping rate at ε_F and $\alpha(V) = \rho_a(\varepsilon_F+\mathrm{sgn}(V)\hbar\omega)/\rho_a(\varepsilon_F)$ as an asymmetric factor taking into account variations in the adsorbate DOS on the energy scale of the vibrational energy. For an unoccupied resonance $\varepsilon_a-\varepsilon_F \gg \hbar\omega$ one has $\alpha(+V) > 1 > \alpha(-V)$, which according to Eq. (22) implies that the spectral generation rate is larger for positive sample voltage than for negative one. This leads to an asymmetric feature in the spectral generation rate (also in the vibration generation rate) with respect to the polarity of the bias voltage.

Although almost all the experiments of single adsorbate reactions observed for positive V except hopping of a single Co atom on a Cu(1 1 1) by incoherent multiple ladder climbing followed by a vibrationally assisted tunneling (VAT) [39,111], a molecular switch utilizing current driven rotation of Sc_3N cluster within an icosahedral C_{80} fullerene cage [14], hopping of MT and dissociation of DMDS on a Cu(1 1 1) [27], the theory presented in Ref. [42] proposes that an observation of AS with both polarities provides additional insight into the molecular orbitals near the ε_F involved in the excitation of vibrational modes responsible for reactions. A factor $\alpha(V)$ in Eq. (22) eventually manifests itself in the reaction yield at a positive and negative bias voltage. As explicitly shown in Section 5 dissociation of DMDS and hopping of MT molecule exhibit noticeable difference of the reaction yield at positive and negative voltage as a result of their differences of $\rho_a(\varepsilon)$ below and above ε_F. Since it is premature to estimate $\alpha(V)$ from the calculated $\rho_a(\varepsilon)$, the fitting of the experimental reaction yield for dissociation of DMDS and hopping of MT molecule using the present theory is made using a simplified relation $Y(V) = \alpha' Y(-V)$ for a negative V, where $\alpha' = \alpha(V)/\alpha(-V) = \rho_a(\varepsilon_F+\hbar\omega)/\rho_a(\varepsilon_F-\hbar\omega)$ phenomenologically takes care of a difference of the overall feature of $\rho_a(\varepsilon)$.

Thirdly, in the EWBL the adsorbate DOS is considered to be constant over the vibrational energy scale $\hbar\omega$, i.e., $\rho_a(\varepsilon\pm\hbar\omega)\approx\rho_a(\varepsilon)$ so that $\alpha(V) = 1$. With this additional approximation, Eq. (22) reduces to the well-known form [110,113]

$$\Gamma^{v,\mathrm{EWBL}}_{\mathrm{in},0}(\omega,V) = \gamma^v_{\mathrm{eh}}(\omega)\frac{\Gamma_s\Gamma_t}{\Gamma^2}\frac{|eV|-\hbar\omega}{\hbar\omega}\theta(|eV|-\hbar\omega), \tag{23}$$

leading to a symmetry of a reaction rate or yield w.r.t. a bias polarity. This is indeed a case observed for a single-molecule switch based on tunneling electron-driven rotation of a triangular Sc_3N cluster within an icosahedral C_{80} fullerene cage [14]. Here the experimental quantum yields for enantiomorphic switching as a function of bias voltage, which reveal excitation of the antisymmetric Sc–N stretch vibration of a Sc_3N molecule, are symmetric w.r.t. $V = 0$ and the experimental dI/dV spectra of $Sc_3N@C_{80}$ molecule as well as the calculated PDOS are flat within $\sim\pm500$ mV below and above the ε_F.

4.3. Effect of the vibrational density of state

As mentioned above, we take the vibrational DOS $\rho_{\rm ph}(\omega)$ explicitly into account for the vibrational generation rate $\Gamma^{v}_{\rm iet}(V)$. We consider three different spectral forms as characterized by either a δ-function or Gaussian/Lorentzian functions centered around a characteristic vibrational energy $\hbar\Omega$, i.e.,

$$\rho^{\delta}_{\rm ph}(\omega) = \delta(\hbar\omega - \hbar\Omega) - \delta(\hbar\omega + \hbar\Omega), \tag{24}$$

$$\rho^{G}_{\rm ph}(\omega) = \frac{1}{\sigma_G\sqrt{2\pi}}\frac{1}{\mathrm{Erf}(\Omega/\sqrt{2}\sigma)} \times \left\{ \exp\left(-\frac{(\hbar\omega - \hbar\Omega)^2}{2\sigma_G^2}\right) - \exp\left(-\frac{(\hbar\omega + \hbar\Omega)^2}{2\sigma_G^2}\right)\right\}, \tag{25}$$

$$\rho^{L}_{\rm ph}(\omega) = \frac{1}{4\arctan(2\hbar\Omega/\sigma)} \times \left\{ \frac{\sigma_L}{(\hbar\omega - \hbar\Omega)^2 + (\sigma_L/2)^2} - \frac{\sigma_L}{(\hbar\omega + \hbar\Omega)^2 + (\sigma_L/2)^2}\right\}. \tag{26}$$

These DOS all satisfy the physical conditions $\rho_{\rm ph}(0) = 0$ and $\int_0^\infty \rho_{\rm ph}(\omega)d\omega = 1$. When $\sigma_{G(L)}$ is sufficiently small compared with $\hbar\Omega$, a use of a single Gaussian or Lorentzian, i.e.,

$$\rho^{G}_{\rm ph}(\omega) = \frac{1}{\sigma_G\sqrt{2\pi}}\left\{ \exp\left(-\frac{(\hbar\omega - \hbar\Omega)^2}{2\sigma_G^2}\right)\right\}, \tag{27}$$

$$\rho^{L}_{\rm ph}(\omega) = \frac{1}{2\pi}\left\{ \frac{\sigma_L}{(\hbar\omega - \hbar\Omega)^2 + (\sigma_L/2)^2}\right\}, \tag{28}$$

are good enough for the most practical applications for positive V.

In the EWBL one thus reaches the following simple analytic expression for the reaction yield

$$Y^{\rm EWBL}(V) = K_{\rm eff}\mathcal{F}(V, \rho_{\rm ph}). \tag{29}$$

where

$$K_{\rm eff} = \pi\frac{\gamma_{\rm eh}(\Omega)}{\Omega}\frac{\varepsilon_a^2 + (\Gamma/2)^2}{\Gamma^2}K, \tag{30}$$

$$= \frac{\gamma_{\rm eh}(\Omega)}{2\Omega}\frac{1}{\rho_a(\varepsilon_{\rm F})\Gamma}K, \tag{31}$$

is an effective (dimensionless) prefactor determined by the elementary process [K is the proportionality constant in $R(V) = K\Gamma_{\rm iet}(V)$ as specified below for different elementary processes] and $\mathcal{F}$ is a voltage-dependent (dimensionless) function

$$\mathcal{F}(V, \rho_{\rm ph}) = \frac{1}{|eV|}\int_0^{|eV|} d\omega\rho_{\rm ph}(\omega)(|eV| - \hbar\omega) \tag{32}$$

which has the different analytic expressions for the considered phonon DOS. It is easy to show, from a normalization condition of $\rho_{\rm ph}(\omega)$, that

$$\lim_{|eV|\to\infty}\mathcal{F}(V, \rho_{\rm ph}) = 1, \tag{33}$$

so that the property $\mathcal{F} \leqslant 1$ in the high-bias limit implies that $K_{\rm eff} \sim Y(eV \to \infty)$, i.e., that the effective prefactor is essentially the saturation value of the reaction yield at high voltages.

It is worth describing a relation between Eq. (32) and a formula previously proposed by Motobayashi et al. [29]. They define a reaction yield as

$$Y(V) = K^{\rm OB}\frac{I_{in}(V)}{I(V)} \simeq K^{\rm OB}\frac{I_{in}(V)}{I_0(V)} = K^{\rm OB}\frac{I_{in}(V)}{\sigma_0 V}, \tag{34}$$

where $K^{\rm OB}$ is a prefactor for a over barrier process, and I_0 and I_{in} are the *pure* elastic and inelastic tunneling currents, respectively. Ueba and Persson [28] have shown

$$\frac{d^2 I_{in}(V)}{dV^2} \simeq \frac{\gamma_{eh}(\Omega)}{\hbar\Omega}\frac{\Gamma_t^2}{\Gamma_s^2}\rho_{ph}(eV), \tag{35}$$

i.e., the second derivative I_{in} w.r.t V is proportional to $\rho_{ph}(eV)$ in the EWBL. This relation leads Motobayashi et al. [29] to define I_{in} in terms of an inelastic conductance σ_{in} as

$$I_{in} = \sigma_{in}\int_0^V \rho_{ph}(V')dV' \int_0^{V'} \rho(V'')dV'' \equiv \sigma_{in} f(V). \tag{36}$$

Then we rewrite Eq. (34) to

$$Y(V) = K_{\text{eff}}\frac{ef(V)}{eV}. \tag{37}$$

where $K_{\text{eff}} = K^{\text{OB}}\sigma_{in}/\sigma_0$.

For a normalized single Gaussian $\rho_{\text{ph}}(V)$ peaked at $V = \hbar\Omega/e$ with the broadening σ_G, the integration in Eq. (36) gives

$$Y(V) = K_{\text{eff}}\left[\left(1-\frac{\hbar\Omega}{eV}\right)\left[\text{Erf}\left(\frac{eV-\hbar\Omega}{\sqrt{2}\sigma_G}\right)+\text{Erf}\left(\frac{\hbar\Omega}{\sqrt{2}\sigma_G}\right)\right]+\sqrt{\frac{2}{\pi}}\frac{\sigma_G}{eV}\left(\exp\left(-\frac{(eV-\hbar\Omega)^2}{2\sigma_G^2}\right)-\exp\left(-\frac{(\hbar\Omega)^2}{2\sigma_G^2}\right)\right)\right], \tag{38}$$

where

$$\text{Erf}(x) = \frac{2}{\sqrt{\pi}}\int_0^x e^{-t^2}dt.$$

Also for a single Lorentzian DOS,

$$Y(V) = K_{\text{eff}}\left[\frac{2}{\pi}\left(1-\frac{\hbar\Omega}{eV}\right)\left[\arctan\frac{2(eV-\hbar\Omega)}{\sigma_L}+\arctan\frac{2\hbar\Omega}{\sigma_L}\right]+\frac{\sigma_L}{2\pi eV}\log\frac{(\hbar\Omega)^2+(\sigma_L/2)^2}{(eV-\hbar\Omega)^2+(\sigma_L/2)^2}\right]. \tag{39}$$

Eqs. (38) and (39) exactly coincide with that calculated from Eq. (32). This agreement is also proved by a relation

$$\int_0^{eV} d\omega\rho_{\text{ph}}(\omega)(eV-\hbar\omega) \equiv \int_0^{eV} d\omega\rho_{\text{ph}}(\omega)\int_0^{\omega} d\omega'\rho_{\text{ph}}(\omega'). \tag{40}$$

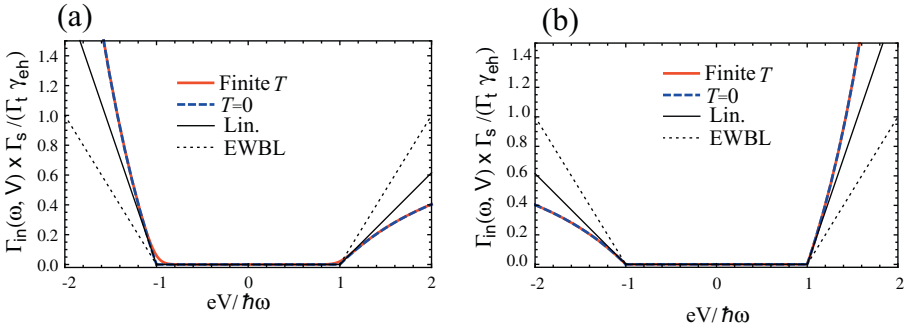

Fig. 21. Generic illustration of the spectral generation rate $\Gamma_{\text{in}}(\omega, V)$ at the various levels of approximations: The finite-temperature expression Eq. (17) (thick red line) and the zero-temperature expressions Eq. (18) (thick dashed blue line), Eq. (22) (linear expansion, thin black line), and Eq. (23) (EWBL, dash-dotted black line). The model parameters are (a): $\Gamma_s = 1000\Gamma_t = \varepsilon_F - \varepsilon_a = 90k_BT = 3\hbar\omega$, corresponding to a relatively sharp occupied electronic resonance at high temperatures (chosen to illustrate the differences between the various approximations), and (b) $\Gamma_s = 1000\Gamma_t = \varepsilon_a - \varepsilon_F = 900k_BT = 3\hbar\omega$, corresponding to a relatively sharp unoccupied resonance state at almost $T = 0$. By symmetry $V \to -V$ and $(\varepsilon_a - \varepsilon_F) \to -(\varepsilon_a - \varepsilon_F)$ gives the same result. Namely (a) and (b) are mirror image with respect to $V = 0$. (For interpretation of the references to color in this figure legend, the reader is referred to the web version of this article.)

For a double-Gaussian DOS defined in Eq. (25) the voltage-dependent function $\mathcal{F}$ given by Eq. (32) takes the following analytic form for a double Gaussian DOS [Eq. (25)]

$$\mathcal{F}_G(V,\Omega,\sigma_G) = 1 + \frac{|eV|-\hbar\Omega}{|eV|}\mathcal{E}_G(|eV|-\hbar\Omega) - \frac{|eV|+\hbar\Omega}{|eV|}\mathcal{E}_G(|eV|+\hbar\Omega) + \frac{\rho_{\rm ph}(|eV|)\sigma_G^2}{|eV|},$$
$$\mathcal{E}_G(X) = \frac{1}{2}\frac{\mathrm{Erf}(X/\sqrt{2}\sigma_G)}{\mathrm{Erf}(\Omega/\sqrt{2}\sigma_G)}, \tag{41}$$

and for a double Lorentzian DOS defined in Eq. (25)

$$\mathcal{F}_L(V,\Omega,\sigma_L) = \frac{2}{\pi}\arctan\left(\frac{2\hbar\Omega}{\sigma_L}\right) + \frac{|eV|-\hbar\Omega}{\pi|eV|}\arctan\left(\frac{|eV|-\hbar\Omega}{\sqrt{2}\sigma_L}\right) - \frac{|eV|+\hbar\Omega}{\pi|eV|}\arctan\left(\frac{|eV|+\hbar\Omega}{\sqrt{2}\sigma_L}\right),$$
$$- \frac{\sigma_L}{4\pi|eV|}\log\left(1 - \frac{4|eV|\hbar\Omega}{(\sigma_L/2)^2 + (|eV|+\hbar\Omega)^2}\right). \tag{42}$$

4.4. Numerical comparison

Above we gave analytic expressions for the spectral generation rate $\Gamma_{\rm in}(\omega,V)$ at various levels of approximations. Here we compare them numerically and discuss the qualitative differences. Fig. 21(a) shows the spectral generation rate for a specific set of parameters for the resonance adsorbate level, $\Gamma_s = 1000\Gamma_t = \varepsilon_F - \varepsilon_a = 90k_BT = 3\hbar\omega, \sigma_{G,L} = \hbar\Omega/15$ corresponding to a relatively sharp

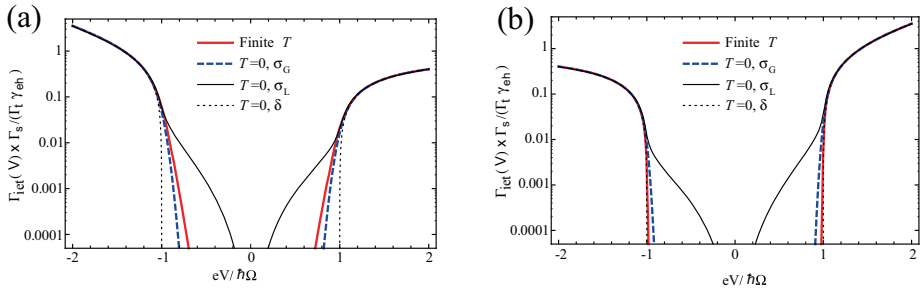

Fig. 22. Generic illustration of the vibrational generation rate $\Gamma_{\rm iet}(V)$ on a logaritmic scale for the whole bias range. The different curves correspond to the cases where the broadening is dominated by temperature (thick red line) in (a) or by a width in the vibrational DOS characterized by either a Gaussian ($\sigma_G = \hbar\Omega/15$, thick dashed blue line) or a Lorentzian ($\sigma_L = \hbar\Omega/15$, thin black line) distribution in (b). For comparison the result with a δ-DOS at zero temperature is also shown (dotted curve). The rest of model parameters used herein are the same as Fig. 21. (For interpretation of the references to color in this figure legend, the reader is referred to the web version of this article.)

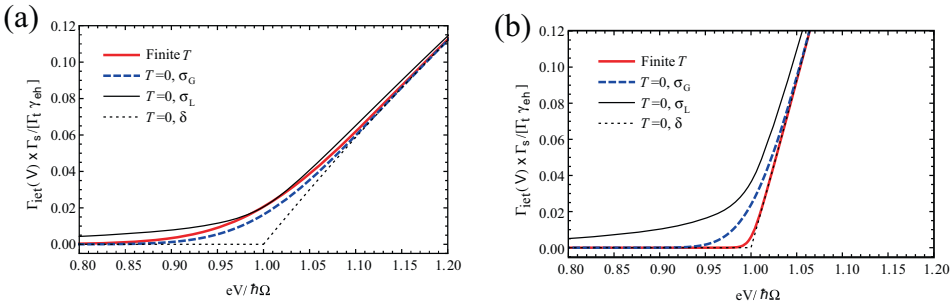

Fig. 23. Same as Fig. 22 in a linear scale around the threshold at a positive bias voltage.

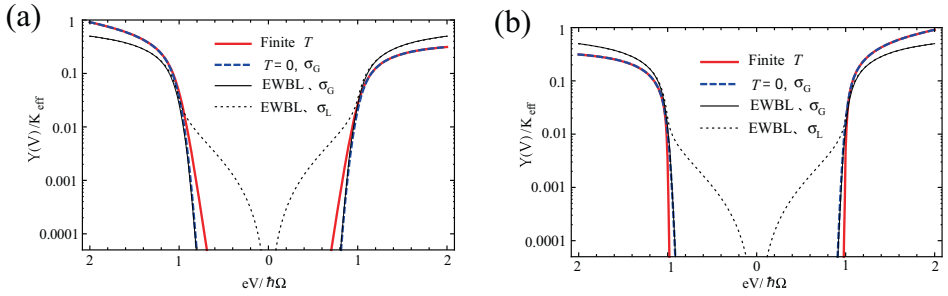

Fig. 24. Generic illustration of the reaction yield $Y(V)$ in different limits. Two exact cases correspond to broadening dominated by temperature (thick red line) or by a Gaussian vibrational DOS (thick dashed blue curve). Two approximations are also shown: EWBL with a Gaussian (thin black line) and a Lorentzian (dotted black curve) vibrational DOS. The model parameters used herein are the same as before. (For interpretation of the references to color in this figure legend, the reader is referred to the web version of this article.)

occupied electronic resonance at high temperatures, chosen to illustrate the differences between the various approximations. The finite temperature result Eq. (17) (thick red line) and the zero-temperature limit Eq. (18) (thick dashed blue) coincides for voltages above the emission threshold $eV = \hbar\Omega$. Around the onset finite temperatures manifests itself in a smearing and finite emission probability below the threshold. Both expressions show a nonlinear dependence on V which originates from the energy dependence of the adsorbate resonance DOS $\rho_a(\varepsilon)$. For obvious reasons the linear expansion (Eq. (22)) (thin black line) and the EWBL Eq. (23) (dash-dotted black line) do not capture this nonlinearity, but the former maintains the asymmetry with respect to bias inversion through the inclusion of the energy variation $\rho_a(\varepsilon_F - \hbar\omega) \neq \rho_a(\varepsilon_F + \hbar\omega)$. For almost all practical purposes the zero-temperature limit is valid to describe low-temperature STM-based experiments. The tiny effect of temperature observed in Fig. 21(a) is only visible because we chose an artificially high temperature compared with typical vibration frequencies of adsorbates at metal surfaces (we used $k_BT = \hbar\omega/30$ which implies that $T \sim 120$ K if take $\hbar\Omega = 300$ meV).

Fig. 21(b) shows the opposite situation where $\Gamma_{in}(\omega, V > 0)$is larger than that for $V < 0$ for a set of parameters $\Gamma_s = 1000\Gamma_t = \varepsilon_a - \varepsilon_F = 900k_BT = 3\hbar\omega$, corresponding to a relatively sharp unoccupied resonance state. The smearing at $eV \simeq \hbar\omega$ disappears for $k_BT = \hbar\omega/300$ and almost coincides with the case of $T = 0$ (blue dashed curve). It is clear that $\Gamma_{in}(\omega, V)$ and $\Gamma_{iet}(\omega, V)$ shown below follow the similar behaviors and the symmetric reaction yield $Y(V)$ is confirmed for $\varepsilon_a = \varepsilon_F$. By symmetry $V \to -V$ and $(\varepsilon_a - \varepsilon_F) \to -(\varepsilon_a - \varepsilon_F)$ gives the same result. Namely, $\Gamma_{in}(\omega, V)$ and $\Gamma_{iet}(\omega, V)$ are a mirror image with respect to $V = 0$. For $\varepsilon_a = \varepsilon_F$, both $\Gamma_{in}(\omega, V)$ and $\Gamma_{iet}(\omega, V)$ exhibit the symmetric features with respect to $V = 0$.

Fig. 22 explores the role of the different vibrational DOS (Eqs. (24)–(26)) in the vibrational generation rate $\Gamma_{iet}(V)$. In general we see that $\Gamma_{iet}(V)$ is qualitatively different depending on the dominant source of broadening, namely temperature or widths in the vibrational DOS. Here we compare $\Gamma_{iet}(V)$ for a pure thermal broadening (red curve) and a Gaussian or Lorentzian broadening ($\sigma = \sigma_G = \sigma_L = \hbar\Omega/15$ in (a) and $\hbar\Omega/30$ in (b) for $T = 0$. A choice of Gaussian or Lorentzian DOS does not affect $\Gamma_{iet}(V)$ when V becomes larger than $\hbar\Omega$. Away from the emission threshold $eV = \hbar\Omega$, the temperature and the Gaussian broadening display a similar voltage dependence, essentially exponential in the low-bias regime as seen in the linear scale shown in Fig. 23. As can be seen in the red and blue dashed curve, the broadening due to a finite temperature effect is well represented by a Gaussian broadening [111], rather than the Lorentzian broadening associated with the intrinsic vibrational relaxation due to electron–hole pair excitation. It is also found that the Lorentzian lineshape leaves a distinct shoulder on the logarithmic scale. From Fig. 23 it is clear that, even when parameter are chosen appropriately, each of the four cases also behave differently close to the emission threshold. It is remarked here that a long lived tail found in $\Gamma_{iet}(V)$ when the Lorentzian DOS is used may mislead to add another lower vibrational mode than the mode with $\hbar\Omega$ in the analysis of $R(V)$ or $Y(V)$. It is remarked here that, since

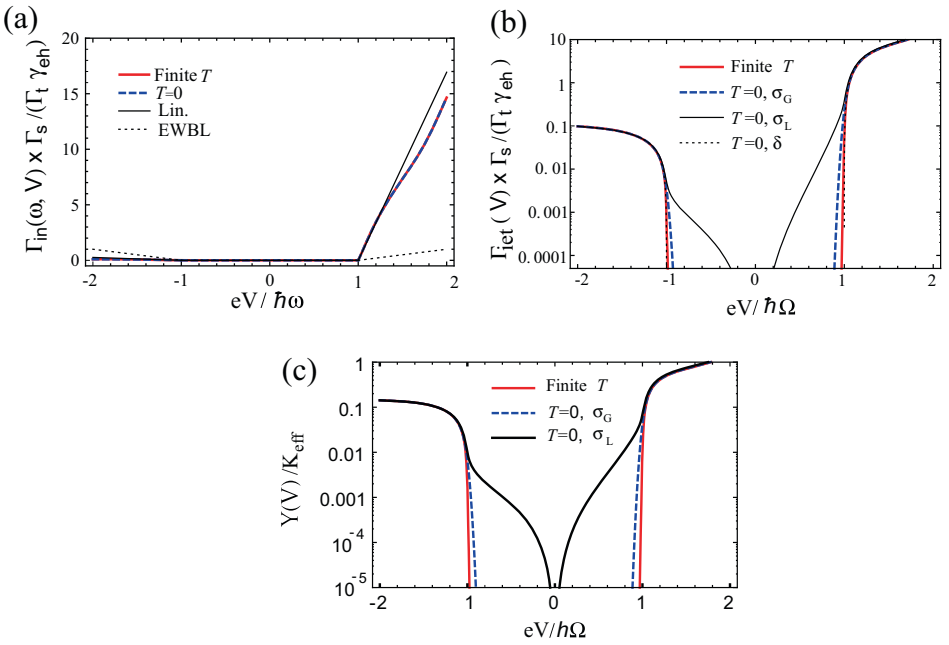

Fig. 25. (a) Asymmetric spectral generation rate $\Gamma_{in}(V)$ (compare this with Fig. 1(a) and (b)), the red curve is for a finite temperature, the blue dashed is for $T = 0$, the solid and dashed black curve are for a linear expansion of Eq. (18) around $eV = \pm\hbar\omega$ and extended wide band limit (EWBL), respectively. (b) vibrational generation rate $\Gamma_{iet}(V)$, the solid red curve is for a finite temperature, the dashed blue curve is for $T = 0$ with a Gaussian DOS, the solid black curve is for $T = 0$ with a Lorentzian DOS, and dashed black curve is $T = 0$ with δ-function DOS, and (c) reaction yield $Y(V)$. For a set of the parameters $\Gamma_s = 1000\Gamma_t$, $k_BT = \hbar\Omega/300$, $\varepsilon_a = \hbar\Omega$ and $\sigma_{G,L} = \hbar\Omega/30$. the red curve for a finite temperature, the dashed blue curve for $T = 0$ with a Gaussian DOS, and the solid black curve for $T = 0$ with Lorentzian DOS, respectively. (For interpretation of the references to color in this figure legend, the reader is referred to the web version of this article.)

$I_{in}(V) = e\Gamma_{iet}(V)$, Fig. 23 also exhibits generic features of $I_{in}(V)$ around the threshold for a vibrational excitation leading to a single molecule reaction. As for a real system $I_{in}(V)$ for exciting the C–O stretch mode responsible for hopping of a CO molecule on Pd(1 1 0) are calculated later in Section 5.2.

Fig. 24 shows numerical example of evaluating Eq. (29) with Gaussian (thin black line) and Lorentzian (dashed black line) vibrational DOS and to demonstrate how a choice of different vibrational DOS manifests itself in the reaction yield $Y(V)$, here the parameters used are the same in Fig. 22. It highlights a drawback of the EWBL approximation, namely the loss of the fundamental asymmetry between the two bias polarities. In most cases the Gaussian distribution for the vibrational DOS provides the best agreement with experiments. This can be rationalized by considering that this distribution is most adequate to take into account *all broadening effects* encountered in practice (thermal, noise/instrumental, intrinsic lifetime broadening, and inhomogeneous broadening associated with random modulation of a vibrational energy) in a single parameter (the total width). Tikhodeev and Ueba [110] have shown that the broadening in the vibrational DOS due to finite temperature effects is well represented by a Gaussian broadening, rather than the Lorentzian broadening associated with intrinsic vibrational relaxation due to electron–hole pair excitation. When broadening of the reaction yield is dominated by temperature (i.e., not by vibrational broadening) one can evaluate Eq. (9) (and hence Eq. (3) in combination with Eq. (4). A numerical example of this procedure is shown in Fig. 24 with red lines.

Contrarily, when broadening of the reaction yield is dominated by effects well-described by broadened vibrational spectra one can resort to the zero-temperature limits for the spectral generation rate

[Eq. (18)] as well as for the current given by Eq. (6). A numerical example of evaluating Eq. (10) with Eqs. (14), (18), (25), and (6) is shown in Fig. 24 with blue dashed lines.

The most pronounced difference between the Gaussian and Lorentzian is found below the threshold, i.e., the Lorentzian DOS gives an extended tail below the threshold. The motivation for a Gaussian distribution is to take into account all broadening effects in a single parameter. It is well-known that a Gaussian function is appropriate for a system with an inhomogeneous broadening. This is certainly a case of a hydrogen atom (proton) relay reaction in a water–hydroxyl chain on a Cu(1 1 0) surface [15] where the energy of the shared O–H stretch mode is very sensitive to the distance between the neighboring two oxygen atoms belonging to H_2O and OH. A difference between Gaussian and Lorentzian DOS manifests itself in those tails, in other words, below the threshold at $eV = \hbar\Omega$ where $Y(V)$ approaches the detection limit (with a large error bar) of the experiment. Since any reaction may involve a direct or indirect excitation of the low energy vibrational modes associated with the vibrational degree of freedoms of the nuclear motions, care should be paid to the choice of $\rho_{\mathrm{ph}}(\omega)$.

As a final example of the numerical demonstrations Fig. 25 shows a case where a large asymmetry of the reaction yield is observed. Within the present adsorbate-induced resonance model, the vibrational modes are resonantly excited through a MO tunneling electrons and excitation probabilities of vibrational modes depend on the population of the MOs at the corresponding energy. In this sense STM-AS probes not only vibrational states but also electronic states near ε_F within a span of the vibrational energy of interest. An asymmetric reaction yield with respect to a bias polarity is expected, for example, for a case $\varepsilon_a \simeq \hbar\Omega \gg \Gamma$, i.e., a narrow resonance and $Y(V)$ for a set of the parameters; $\Gamma_s = 1000\Gamma_t, k_BT = \hbar\Omega/300, \varepsilon_a = \hbar\Omega$ and $\sigma_{G,L} = \hbar\Omega/30$. The spectral generation rate $\Gamma_{\mathrm{in}}(V)$ is very large for positive V and the EWBL (black dashed curve) does not work in this situation. This gives an order of magnitude larger $\Gamma_{\mathrm{in}}(V)$ and $Y(V)$ for a positive V than that for a negative V. This suggests an experimental effort to observe $Y(V)$ for both polarities as almost all the STM-IETS's have done so in order to identify the vibrational signal superimposed on very noisy backgrounds. The asymmetric $Y(V)$ observed at positive and negative bias voltages suggests a breakdown of the EWBL and reflects a difference in $\rho_a(\varepsilon)$ at $eV = \hbar\Omega$ below and above ε_F. This is qualitatively a case for dissociation of a single DMDS molecule on a Cu(1 1 1) [27] as demonstrated below in the analysis of experimental results.

When excitation of several vibrational modes v by tunneling electrons are involved the total reaction, the yield should be expressed as the sum over contributions from each mode,

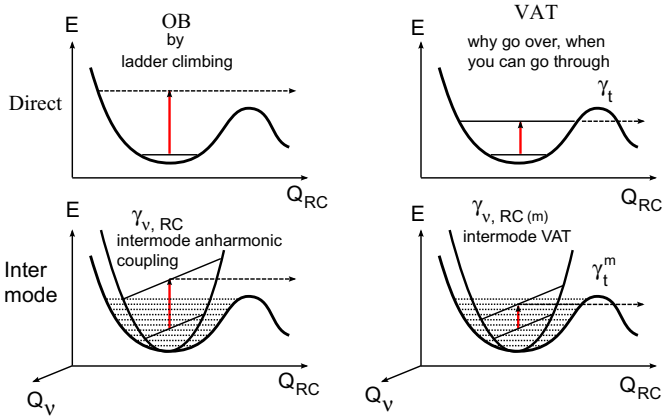

Fig. 26. Schematics illustration of four different elementary processes induced by single-electron inelastic tunneling events. The process may involve over-barrier (OB, $\hbar\Omega_v \geqslant E_B$, left column) or tunneling (T, $\hbar\Omega_v \leqslant E_B$, right column), and the accepting mode v may be the RC itself (direct, D, top row) or involve intermode (IM) anharmonic coupling to the RC as characterized by the interconversion rate $\gamma_{v,\mathrm{RC}}$.

$$Y(V) = \sum_v K_{\mathrm{eff}}^v \mathcal{F}(V, \rho_{\mathrm{ph}}^v) \tag{43}$$

Eqs. (25) and (43), in combination with a suitable model for the vibrational DOS, constitute the general formulas which can be used for the fitting of the experimentally observed reaction yields. This can be rationalized by considering that this distribution is most adequate to take into account all broadening effects encountered in practice (thermal, noise/instrumental, intrinsic lifetime broadening, and inhomogeneous broadening associated with random modulation of a vibrational energy) in a single parameter (the total width). It is also noted that for most practical applications a single Gaussian or Lorentzian is good enough when a broadening σ is sufficiently small compared a vibrational energy $\hbar\Omega$. It is emphasized here that what is important in the analysis of AS is not only a determination of the vibrational mode responsible for a reaction, but also a prefactor K_{eff} which contains the elementary processes involved therein. In this sense STM-AS differs from STM-IETS. The former detects the vibrational mode in the RC potentials (for direct excitation of the RC mode) or the one coupled to the RC mode, while the latter observes the vibrational modes that fulfills the so-called propensity (selection) rules [24].

We have presented a versatile formula of AS to analyze the reaction yield of single molecules induced by vibrational excitation with STM. In the present form it applies to any single-electron processes (over-barrier, vibrationally assisted tunneling, or coherent multiple vibrational excitation [114], but can readily be generalized multi-electron cases such as incoherent step-by-step vibrational ladder climbing [113,110]. Although the assignment of vibrational mode energies can be made from conventional $\Delta \log Y(V)/\Delta V$ plots, the present formula can be used even with a limited number of the experimental data points. The present theory also underlines the relevance of observing yields $Y(V)$ at both polarities as this would in principle provide information about variations in the adsorbate DOS near the ε_{F} on the energy scale of the vibrational mode excited by tunneling electrons. In this way STM-AS is a complementary experimental tool to explore not only dynamics of vibrationally mediated single molecule reactions, but in principle also aspects of the electronic structure of the adsorbates near the ε_{F} within a span of a vibrational energy of concern.

5. Elementary processes of vibrationally mediated reactions

At low temperatures, where molecular vibrations are almost completely frozen, the probability for a given adsorbate reaction or motion to occur will be related to the efficiency for the tunneling electrons to excite the vibrational modes and thus to leave the adsorbate with sufficient energy to either overcome or tunnel through the energy barrier E_B associated with the reaction along the RC. In this scenario we can distinguish different elementary processes (sketched in Fig. 26) depending on whether it involves over-barrier (OB, $\hbar\Omega_v \geqslant E_B$) process by a direct excitation of the RC mode or by vibrationally assisted tunneling (VAT, $\hbar\Omega_v \leqslant E_B$), and whether the accepting mode v is the RC itself (direct, D) or involves intermode (IM) anharmonic coupling to the RC as characterized by the intermode coupling rate $\gamma_{v,\mathrm{RC}}$. Fig. 26 is a schematic illustration of these different elementary processes induced by IET events.

5.1. Vibrational ladder climbing

When a reaction occurs by a direct excitation of a vibrational mode in the RC potential well, there are two different ways to climb up the vibrational ladders over the reaction barrier. The so called "*incoherent* process" via a single step-by-step ladder climbing was formulated by Gao et al. [113] for atom transfer (bond-breaking) using the tip of STM. In this theory the bond is broken by overcoming the associated potential barrier by gaining energy from the tunneling electrons. The rate of atom transfer was shown to be Arrhenius-like with an "*effective*" vibrational temperature T_{eff} (vibrational heating) set by the inelastic tunneling rate. The essence of this theory is that the ladder climbing undergoes a step-by-step *real* population (transition) in the excited states below the barrier in competition between the vibrational depopulation (energy relaxation) rate and the vibrational generation rate.

The reaction rate of this incoherent ladder climbing can be expressed as

$$R_{\mathrm{inc}}(V) = \sum_m \Gamma_m P_m(V), \tag{44}$$

where Γ_m stands for the excitation rate from the vibrational level m with population probability P_m to the unbound state above the barrier by a tunneling electron. For a truncated harmonic oscillator with a linear inelastic electron-vibration coupling, an elegant treatment has been made by Gao et al. [113]. They showed that the transitions among the different vibrational levels is described by a Pauli master equation for P_m. They showed that the reaction rate R is determined by the quasi stationary population of the level $n-1$ (the highest level in the RC potential) times the rate for transitions from this level to the level n above the barrier, i.e., the reaction rate $R_{\mathrm{inc}}(V)$ by this incoherent ladder climbing is then expressed in a form of an Arrhenius-type law characterized by T_{eff} as

$$R_{\mathrm{inc}}(V) = n\Gamma_\uparrow \exp\left(-\frac{(n-1)\hbar\Omega}{k_{\mathrm{B}}T_{\mathrm{eff}}}\right) \tag{45}$$

$$= n\Gamma_\uparrow \left(\frac{\Gamma_\uparrow}{\Gamma_\downarrow}\right)^{n-1} \tag{46}$$

$$\simeq \frac{n\Gamma_{\mathrm{iet}}^n(V)}{\gamma_v^{n-1}}, \tag{47}$$

where the final step holds for a condition $\gamma_v \gg \Gamma_{\mathrm{iet}}$. Here the quasi stationary distribution is given by the stationary solution of the master equation in the situation of infinite barrier height and is given by a Boltzmann distribution among the different vibrational levels uniquely characterized by an effective temperature T_{eff},

$$T_{\mathrm{eff}} = \frac{\hbar\Omega}{k_{\mathrm{B}} \ln\left(\frac{\Gamma_\downarrow}{\Gamma_\uparrow}\right)}, \tag{48}$$

where

$$\Gamma_\uparrow = n(\hbar\Omega)\gamma_v + \Gamma_{\mathrm{iet}}(V) \tag{49}$$

$$\Gamma_\downarrow = [1 + n(\hbar\Omega)]\gamma_v + \Gamma_{\mathrm{iet}}(V), \tag{50}$$

here $n(\hbar\Omega) = 1/(\mathrm{e}^{\hbar\Omega/k_{\mathrm{B}}T} - 1)$, and $\Gamma_\uparrow$ ($\Gamma_\downarrow$) stands for an excitation (de-excitation) rate between the nearest vibrational levels and γ_v is the vibrational relaxation rate. The effective distribution function is then written as

$$n(T_{\mathrm{eff}}, \hbar\Omega) = n(T, \hbar\Omega) + \frac{\Gamma_{\mathrm{iet}}(V)}{\gamma_v}, \tag{51}$$

and $\Gamma_{\mathrm{iet}}(V)/\gamma_v$ play a key factor of the vibrational heating by inelastic tunneling currents. It has been proved that the inelastic tunneling current $I_{\mathrm{in}} \simeq \mathrm{e}\Gamma_{\mathrm{iet}}(V)$ is a good approximation [110] and $\Gamma_{\mathrm{iet}}(V)$ is linear in V except in the vicinity at $eV = \hbar\Omega$. This gives a power law dependence from Eq. (47)

$$R_{\mathrm{inc}}(V) \propto V^n \propto I^n, \tag{52}$$

where n is the number of electrons (i.e., reaction order) required to overcome the barrier by a step-by-step vibrational ladder climbing. The rate of a Xe atom transfer between a Ni substrate and W tip [1] and a single Co atom hopping on Cu(1 1 1) [39] have been basically explained by this incoherent excitation of the frustrated translation mode by inelastic tunneling. [113,115,116].

As we have seen above a key quantity in $R_{\mathrm{inc}}(V)$is a ratio $\Gamma_{\mathrm{iet}}/\gamma_v$ as a consequence of the step-by-step real transitions between the vibrational levels in the RC potential. There is, however, another channel to be excited above the barrier via *virtual* excitation to the intermediate excited states in the temporal ionic (negative (positive) for electron (hole) tunneling) states. This *coherent* multiple ladder climbing is nothing to do with the vibrational relaxation rate γ_v because this does not occur via real populations of the intermediate vibrational excited state. Salam et al. [114] established a simple criterion under what condition the coherent mechanism dominates over the incoherent one. Accord-

ing to them, atom transfer by coherent multiple excitation is favored in situation where the vibrational relaxation rate is high or when the tunneling current (rate) is small. For instance, estimated γ_v is $\simeq 3 \times 10^{10}$/s due to phonon damping for Xe atom transfer on Ni(1 1 0). This gives a threshold current for the cross over to incoherent multiple excitation is about 10 nA at $V_s \simeq 10$ mV. This suggests that for this system the rare of transfer by incoherent single step-by-step multiple ladder climbing dominate over the coherent one in the range V_s = 20–200 mV used in the experiment. On the other hand, for most adsorbed molecules on metal surface γ_v's are orders of magnitude of 10^{10}/s due to electron–hole pair excitations. This value for the relaxation rate corresponds to a crossover current as high as μA, which is several orders larger than usually used for vibrationally mediated manipulation of single molecules on metal surfaces. It underlines that a criterion for coherent and incoherent vibrational excitation is determined by a relative rate of vibrational damping and current rate. This qualitative arguments are consistent why coherent ladder climbing is responsible for dissociation of a single O_2 molecule on Pt(1 1 1) [10] and chemical transformation of *trans*-2-butene on Pd(1 1 0) [43]. This will also explain why most of the vibrationally mediated motions and reactions so far reported are induced by anharmonic mode coupling of the high frequency mode excited by tunneling electron with a low frequency of RC modes.

5.2. Vibrationally-assisted tunneling

A theory of vibrationally-assisted tunneling (VAT) is proposed by Tikhodeev and Ueba [111]. This mechanism couples together with the incoherent vibrational ladder climbing. The main idea of VAT is explained schematically in Fig. 26. The left potential well is the initial position of the reactant (adatom or molecule), and is separated by a potential barrier from another potential well. In a simple truncated harmonic potential well, the reaction occurs when the reactant reaches a vibrational level n_c just above the barrier [113]. If, however, the barrier is semi-transparent for quantum tunneling, there will be a tunneling component in the overall reaction rate. In the equilibrium situation at low temperatures, although the tunneling rates γ_t^m are expected to grow exponentially with a higher vibrational level m because of a lower and a narrower barrier, the role of tunneling from the higher levels is quenched by their exponentially decreased population. Under the STM tip, with the overheating by IET process, their population grows, and the tunneling from higher excited states can make a significant impact on the overall reaction rate, thus enabling VAT to play a important role.

We now add tunneling processes γ_t^m from the m-th level and write the Pauli master equation in a form

$$\frac{dP_0}{dt} = -\gamma_t^0 P_0 + \Gamma_\downarrow P_1 - \Gamma_\uparrow P_0, \tag{53}$$

$$\frac{dP_m}{dt} = -\gamma_t^m P_m + (m+1)\Gamma_\downarrow P_{m+1} + m\Gamma_\uparrow P_{m-1} - [m\Gamma_\downarrow + (m+1)\Gamma_\uparrow]P_m, \tag{54}$$

here we assume no backward tunneling. For $\gamma_t^m = 0$ these equations reduce to the conventional ones for a single step-by-step ladder climbing.

In a case where the tunneling γ_m^t is negligibly small, terms with γ_t^0 in Eq. (53) and γ_t^m in Eq. (54) can be omitted, and the quasi stationary solution of the Pauli master equation gives the Arrhenius type formula for reaction rate, governed by the effective temperature due to the vibrational overheating [113]. In the low-temperature limit $k_B T \ll \hbar\Omega$ this gives a power-law dependence for the reaction rate

$$R_{\mathrm{inc}}(V) \propto (|eV| - \hbar\Omega)^n \theta(|eV| - \hbar\Omega). \tag{55}$$

However, if the barrier is thin, and the vibration levels can be emptied via atomic quantum tunneling as described in Eqs. (53) and (54), the power law of Eq. (55) no longer holds. The resulting transfer rate is then given by

$$R_{\mathrm{VAT}} = A^{-1} \sum_{m=0}^{n_c-1} \gamma_t^m P_m + n_c \Gamma_\uparrow P_{n_c-1}, \tag{56}$$

with a normalization factor $A = \sum_{m=0}^{n_c-1} P_m$. Here the first term represents VAT and the second term arises from the incoherent ladder climbing as described above. There is no simple Arrhenius-type solution in this case. The master equation can be easily solved numerically if the tunneling rates γ_t^m are known (or can be estimated). This multi-level VAT during incoherent vibrational ladder climbing has been taken into account for a Xe atom transfer [115]. Eq. (56) has been successfully applied to reproduce the experimental result of a single Co atom hopping on a Cu(1 1 1) surface [39,111]. Note that this is one of a few experiment which observed the hopping rate at both polarities and the symmetric reaction rate was observed, thereby implying that the EWBL works pretty well in this system.

For a tunneling from the ground state and from the first excited state, we are allowed to neglect the population of higher vibrational levels, and to assume $P_0 \gg P_1$. In this case Eq. (56) reduces to

$$R(V) \simeq \gamma_t^0 + \frac{\gamma_t^1}{\gamma_v}\Gamma_{\text{iet}}(V), \tag{57}$$

where $\gamma_t^{0(1)}$ is a tunneling rate from the ground (first excited) state in the potential well. Here the prefactor γ_1/γ_v represents a competition of a rate between tunneling and relaxation from the first excited state of the mode excited by a tunneling electron. Eq. (57) was successfully employed to reproduce the reaction rate of hydrogen-bond exchange within a single water dimer on Cu(1 1 0) [38,111].

5.3. Mode coupling followed by vibrationally-assisted tunneling

Even when an inter-mode coupling $\gamma_{v,\text{RC}}$ is not strong enough to excite the RC mode above the barrier, a reaction can still occur via the VAT from the intermediate excited states of the RC mode populated by the inter-mode coupling (see the illustration on the light in the lower panel). In this case there will be a bundle of levels n which satisfy the energy conservation $\hbar\Omega_v - \hbar\omega_n - \varepsilon_v = 0$, here ε_v stands for an energy of a heat bath (electron–hole pair excitation and/or phonons) in the substrate [117] Let γ_t^m be the tunneling probabilities from the m th-level such that the reaction rate is described by

$$R^{\text{IM-VAT}}(V) = \sum_m \gamma_{\text{RC(n)}}^t P_{\text{RC(n)}}, \tag{58}$$

where $\gamma_{\text{RC(n)}}^t$ stands for a tunneling rate from the m-th level and $P_{\text{RC(n)}}$ is the (quasi-) stationary population of the n-th excited state of the RC mode. Again, assuming $P_{\text{RC(n)}} \ll 1$, the excited state population is determined from

$$\frac{dP_{\text{(n)}}^{\text{RC}}}{dt} = -(\gamma_t^{\text{RC(n)}} + \gamma_{\text{RC(n)}})P_{\text{(n)}}^{\text{RC}} + \gamma_{v,\text{RC(n)}}P_1^v = 0, \tag{59}$$

where $\gamma_{\text{RC(n)}}$ describes the damping rate of the level n and $\gamma_{v,\text{RC(n)}}$ the interconversion rate from v to n. We then obtain

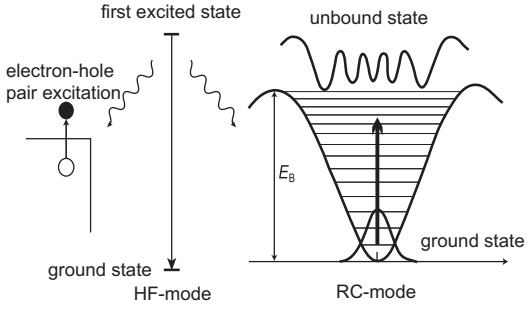

Fig. 27. Schematics of elementary process illustrating how the energy stored in the high-frequency mode (for example the C–O stretch mode of CO molecule) activates the RC mode (for example the frustrated translational mode for lateral hopping) from the ground state to the continuum scattering state above the barrier, in competing with the vibrational relaxation due to EHP excitation in a metal substrate.

$$R^{\mathrm{IM-VAT}}(V) = K^{\mathrm{IM-VAT}}\Gamma^{v}_{\mathrm{iet}}(V). \tag{60}$$

where

$$K^{\mathrm{IM-VAT}} = \sum_{n} \frac{\gamma^{t}_{\mathrm{RC(n)}}}{\gamma^{\mathrm{RC}}_{\mathrm{n}}} \frac{\gamma_{v,\mathrm{RC(n)}}}{\gamma^{v}_{\mathrm{eh}}}, \tag{61}$$

here the first factor is interpreted as a competition between the rate of tunneling out and deexcitation of the RC mode from the excited state, while the second factor as ratio of excitation rate of the RC mode to the n-th level by inter-mode coupling with v-mode and the damping rate of the v mode. This type of the IM-VAT process is expected when a reaction occurs by primary excitation of a v-mode with the energy lower than the barrier. No experimental result, however, suggesting this IM-VAT process has been reported so far.

5.4. Anharmonic mode coupling – Indirect excitation of RC mode

As a final example in the elementary processes depicted in Fig. 27 we briefly describe an over-barrier process via an inter-mode anharmonic coupling between the high energy mode v (E_{B}) excited by tunneling electrons and the RC mode. Experimental results have shown that the excitation of the C–O stretch vibration for CO on Pd(1 1 0) and the N–H vibration for NH_3 on Cu(1 0 0) are trigger for transnational motion of these single molecules. Similarly, excitation of the C–H stretch mode for C_2H_2 on Cu(1 0 0) induces the rotation of the molecule. A common feature of these reactions is the appearance of a threshold bias voltage (corresponding to the excitation of the high frequency (HF) C–O, N–H, and C–H stretch mode) in $R(V)$ above which transnational or rotational motion of the molecules is induced in a single electron process, i.e., $R(I) \propto I^{n}$. Fig. 27 depicts a single-electron process where anharmonic mode coupling between the HF mode and the low energy RC mode leads to activation of the RC mode above E_{B} in competing with the vibrational damping due to electron–hole pair excitations in the substrate.

Here we consider the intermode-coupling in a single electron processes, where the energy deposited in an accepting mode v is transferred into the RC-mode characterized by the interconversion rate $\gamma_{v,\mathrm{RC}}$. For an over-barrier (OB) process the reaction rate is simply given by the mode coupling rate $\gamma_{v,\mathrm{RC}}$ times the (quasi-) stationary population P^{v}_{1} of the first excited state of the mode v, i.e.,

$$R^{\mathrm{OB}}(V) = \gamma_{v,\mathrm{RC}} P^{v}_{1}(V). \tag{62}$$

The population P^{v}_{1} is determined from the steady-state solution of the master equation (assuming $P^{v}_{1} \ll P^{v}_{0} \approx 1$)

$$\frac{dP^{v}_{1}}{dt} = -\left(\gamma^{v}_{\mathrm{eh}} + \gamma_{v,\mathrm{RC}}\right) P^{v}_{1} + \Gamma^{v}_{\mathrm{iet}}(V) = 0. \tag{63}$$

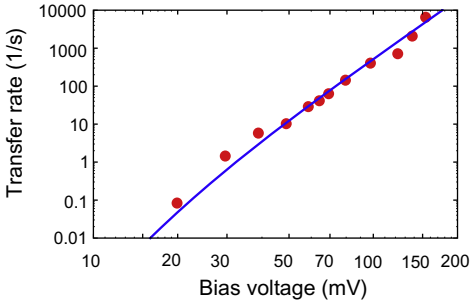

Fig. 28. Xe atom transfer rate as a function of bias voltage. Red circles are experimental and blue line is calculated result. See the text for the rest of parameters used herein. (For interpretation of the references to color in this figure legend, the reader is referred to the web version of this article.)

This immediately leads to

$$R^{\mathrm{OB}}(V) = K^{\mathrm{OB}}\Gamma^{v}_{\mathrm{iet}}(V), \tag{64}$$

where the prefactor K^{OB} for the OB process by an anharmonic mode coupling becomes

$$K^{\mathrm{OB}} = \frac{\gamma_{v,\mathrm{RC}}}{\gamma^{v}_{\mathrm{eh}} + \gamma_{v,\mathrm{RC}}} \simeq \frac{\gamma_{v,\mathrm{RC}}}{\gamma^{v}_{\mathrm{eh}}}. \tag{65}$$

In the above we include only the electron–hole pair damping (EHP) γ^{v}_{eh} of the mode v, but other damping mechanisms can be easily included. For the HF mode like C–O, N–H and C–H stretch mode, the EHP damping is the most efficient energy dissipation bath compared to the phonon bath in the substrate because of a continuum nature of the EHP excitation and large energy mismatch between these HF mode and the substrate phonons.

6. Analysis of experimental results

In this section we apply the theory of AS described above to analyze several representative experiments reported by M. Kawai group over the decade since 2002 [6]. Before that we attempt to reproduce a pioneering experimental work of single Xe atom transfer [1] using an incoherent step-by-step vibrational ladder climbing (vibrational heating) in the RC potential well.

6.1. Xe atom shuttling-Eigler switch

Immediately after having spelled the first atomic letters "IBM" with 35 Xe atoms on a Ni(1 1 1) surface using controlled manipulation of single Xe atoms [118], Eigler et al. demonstrated the first fabrication of an atomic switching device using high and low conductance states corresponding to a single

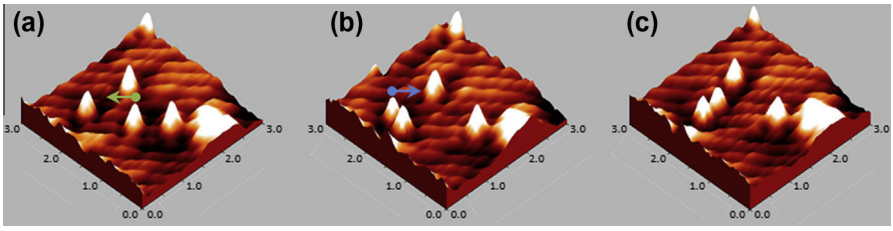

Fig. 29. STM images of four CO molecules on Pd(1 1 0) observed at V_s = 50 mV and I_t = 1 nA; before and after dosing tunneling electrons onto the target molecule marked by arrows at I_t = 7 nA and V_s = 350 mV.

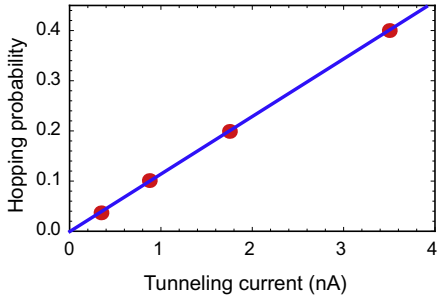

Fig. 30. Hopping probability as a function of the tunneling current with sample bias voltage of 350 mV. The current is tuned by changing the gap distance. The blue straight line is an eye-guide for the experimental result (red circles). (For interpretation of the references to color in this figure legend, the reader is referred to the web version of this article.)

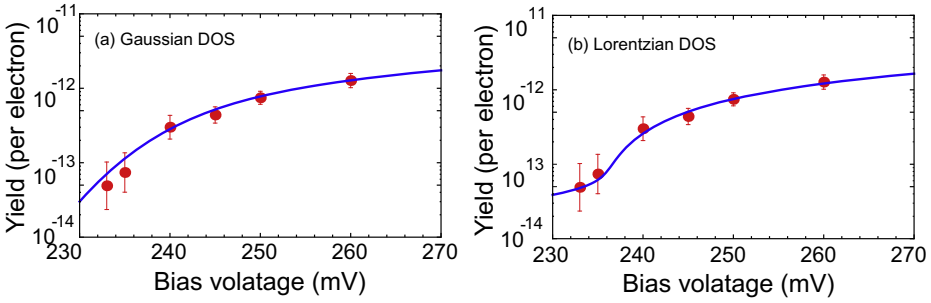

Fig. 31. Hopping yield per electron as a function of bias voltage for CO on Pd(1 1 0), here the red circles are the experimental result [6] and the blue curves are calculated using (a) Gaussian and (b) Lorentzian DOS. See the text for a set of parameters used herein. (For interpretation of the references to color in this figure legend, the reader is referred to the web version of this article.)

Xe atom shuttling between a Ni(1 1 0) surface and a tungsten tip of STM by application of a bias voltage with the positive and negative polarity [1]. This reversible Xe atom transfer by a voltage pulse at ±0.8 V excludes any electronic excitation as a plausible physical mechanism underneath the motion of the atom. The power-law dependence of the atom transfer rate $R(I) \propto I^{4.9\pm0.2}$ on the tunneling current I suggests that the atom overcomes the potential barrier through stepwise climbing of a vibrational ladder of the adatom-substrate bond excitations through a competition between energy gain from tunneling electrons and dissipation to the heat bath in the substrate.

We apply Eq. (47) using a set of the parameters ($\hbar\Omega = 4$ meV, $\gamma_{\rm eh} = 3.3 \times 10^8$/s, $\gamma_{\rm ph} = 3 \times 10^{10}$/s, $\Gamma_t/\Gamma_s = 0.07$, $n = 5$) determined in a detailed formulation by Gao et al. [113], and the calculated result of $R(V)$ are shown together with the experimental result (red circles) as shown in Fig. 28. A more advanced theoretical study of a Xe atom transfer has been done by Gao et al. [113]. A similar analysis has also been made by Walkup et al. [115] using a double well potential associated with the bound state of Xe atom on the Ni surface and on the STM tip. They claimed that, in addition to a stepwise vibrational ladder climbing, vibrational-assisted tunneling plays a role for levels near the top of the barrier.

6.2. Lateral hopping of a single CO molecule on Pd(1 1 0)

One of the pioneering works in motions and reactions in single molecules is a lateral hopping of a CO molecule on Pd(1 1 0) [6]. The STM instrument used in this experiment was commercially available (Omicron) low temperature STM. The STM observation was carried out at the sample temperature of 4.8 K in ultrahigh vacuum condition. The molecules of CO were dosed on the surface at low temperature (<50 K). It is well known that CO adsorbs at the bridge site at low coverage on Pd(1 1 0). When a certain amount of tunneling current is dosed to an isolated CO molecule, lateral motion of the molecule along the [1 1 0] direction is induced. Fig. 29 shows STM images before and after dosing tunneling electrons to the isolated CO molecule indicated by the arrow. Thermal hopping is negligible at 4.8 K, and scanning the STM tip causes no change of the adsorption site of CO when it is scanned under normal tunneling conditions (typically sample bias voltage V_s = 100 mV and tunneling current I_t = 1 nA). Fig. 29 shows a sequence of the STM images observed at V_s = 50 mV and I_t = 1 nA (a) before and (b) and (c) after dosing tunneling electrons for 1 s at V_s = 350 mV and I_t = 7 nA. The CO molecule has jumped three Pd lattice spacing to the left along the [1 1 0] direction, while no change in bonding position is observed for other molecules. At V_s = 200 mV, it was observed that a position of the target CO molecule remains unchanged, while at V_s = 300 mV the CO molecule shows a hopping to the nearest-neighbor bridge site along [1 1 0] direction.

The hopping probability as a function of I at V_s = 350 mV is shown in Fig. 30. Here the probability is defined as the number of events in which the change of the adsorption site occurs out of the total number of dosing events. The linear increase of the hopping rate as a function of I is a clear evidence that a CO hoping occurs in a single-electron process.

The hopping yield per electron as a function of V is shown in the red circles in Fig. 31. It shows a sharp increase beyond a threshold voltage at about 240 meV. The isotope shift of the threshold voltage from 240 meV for a normal CO to 235 meV for $^{13}C^{16}O$ was also confirmed. These findings clearly suggest that excitation of the C–O stretch mode is a trigger for inducing lateral hopping of a single CO molecule on Pd(1 1 0).

A similar experiment was performed for a single CO molecule on a Cu(1 1 0) surface under the same condition as for CO/Pd(1 1 0). The result showed that no lateral hopping was observed under the same conditions for V_s up to 550 meV. It should be noted that the hopping barrier for CO on Cu(1 1 0) has been estimated to be 97 meV, which is considerably lower than 180 meV for CO on Pd(1 1 0). It was puzzling why a weakly chemisorbed CO on Cu(1 1 0) with the lower hopping barrier than a strongly chemisorbed CO on Pd(1 1 0) does not move on the surface when the C–O stretch mode is excited by tunneling electrons. Since the C–O stretch mode is nothing to do with the nuclear motion associated with the lateral hopping, one immediately notices that the energy stored in the C–O stretch mode with the higher energy than the hopping barrier is transferred to the frustrated translation mode (RC mode for lateral hopping) in competing to its rapid damping due to electron–hole pair excitations in the substrate.

Thanks for extensive experimental and theoretical studies of the vibrational properties of CO molecules on metal surfaces in mid 1980's [119]. It has been observed that the peak position and the width of the C–O stretch mode observed by infrared absorption spectroscopy exhibit the noticeable change as a function of temperature on Ni [120] and on Ru [121], while no temperature dependence was observed on Cu(1 0 0) [122]. Such a temperature dependence of the C–O stretch mode is due to a vibrational dephasing caused by the anharmonic coupling between the C–O stretch mode and the low energy mode including the frustrated translation or rotation mode.

We attempt to reproduce the experimental result of $Y(V)$ for CO hopping using the Gaussian or Lorentzian DOS with a set of parameters $(\hbar\Omega, \sigma_{ph}, K_{\rm eff})$. Fig. 31 compares the experimental (the red circles) and the calculated one; the blue curve in (a) using the Gaussian DOS with the parameters (236 meV, 6 meV, 6.9×10^{-12}), and (b) the Lorentzian DOS with the parameters (236 meV, 0.8 meV, 6.5×10^{-12}). Here we use a single vibrational DOS given by Eqs. (25) and (26). The Gaussian broadening of 6 meV is quite large compared to the intrinsic lifetime τ of 0.5 ps (=1.3 meV) for the C–O stretch mode on Pd(1 0 0) [123,124]. The origin of such large $\sigma_{\rm ph}$ might be attributed to unknown inhomogeneous broadenings caused by instrumental factors, statistical errors, and effects of an unstable tip–surface junction [29]. On the other hand the Lorentzian DOS gives a better agreement with the experimental result, in particular, in the low bias region below $V \simeq 240$ mV with $\sigma_{\rm ph} = 0.8$ meV which corresponds to τ = 0.83 ps, being in very close compared to the theoretical [123] and the experimental value measured in the linewidth of the infrared absorption spectrum of CO molecules on Pd [124]. As shown in a generic feature of $Y(V)$ (Fig. 24), a noticeable difference between Lorentzian and Gaussian function manifests itself in the tail below the threshold. In STM-AS the tail approaches the detection limit with large experimental error bars so that a special care of the measurement in this region is required to choose a Gaussian or Lorentzian DOS for a vibrational mode of interest.

Except the difference observed in the calculated $Y(V)$, the experimental result of $Y(V)$ is satisfactory reproduced using a similar prefactor $K_{\rm eff} = 6.5 \times 10^{-12}$. This allows us to extract a key quantity $\gamma_{v,\rm RC}$ if we can estimate coupling ratio Γ in Eq. (31). In doing so we use a formula of the elastic conductance $\sigma_0 = G_0\Gamma_s\Gamma_t/((\varepsilon_{\rm F} - \varepsilon_a)^2 + (\Gamma_s + \Gamma_t)^2)$ for a single adsorbate level ε_a, where $G_0 = 2e^2/h$ is a quantum conductance. The tunneling gap set point condition I_t = 1 nA at V_s = 100 mV (before increasing V_s over 220 mV to observe CO hopping) gives $\sigma_0 = 10$ nA/V [6]. The inverse photoemission experiment for CO on Pd(1 1 1) exhibits the $2\pi^*$ state ε_a with the width Γ_s of 1 eV at about 0.9 eV above the $\varepsilon_{\rm F}$ [125]. Since $\Gamma_s \gg \Gamma_t$, we roughly estimate $\Gamma_t/\Gamma_s = 2.6 \times 10^{-4}$. Thus determined Γ_t/Γ_s, however, should only be viewed as a rough estimate because the PDOS of the $2\pi^*$ level of CO molecules on metal surfaces is not always a Lorentzian shape. Also it should be noted that, in $Y(V)$ experiment as a function of V, the tip-sample distance d is under control in order to keep a constant tunneling current I. Strictly speaking this means $\Gamma_t \sim e^{-\alpha d}$ (α: constant). In the experiments of the present concern, V varies between 230 and 270 mV so that the elastic current changes just a factor, not an order. This permits us to assume the same Γ_t even in the constant current mode to measure $Y(V)$. Using thus determined coupling ratio of $\Gamma_t/\Gamma_s = 2.6 \times 10^{-4}$ we obtain a key quantity of the transition rate

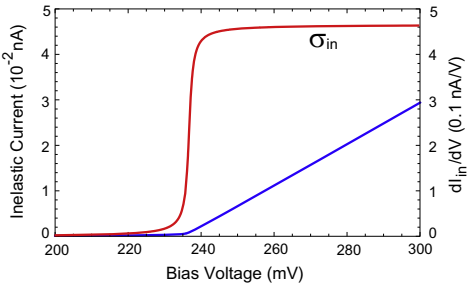

Fig. 32. Inelastic tunneling current (blue curve) exciting the C–O stretch mode at 236 meV. Also shown is dI_{in}/dV (red curve), where the constant part gives the inelastic conductance σ_{in}. (For interpretation of the references to color in this figure legend, the reader is referred to the web version of this article.)

$\gamma_{v,\mathrm{RC}} = 3.6 \times 10^2/\mathrm{s}$ for the mode coupling between the C–O stretch mode ($\hbar\Omega = 236$ meV) and the frustrated translation mode ($\hbar\omega_0 = 25$ meV). Using $\sigma_{\mathrm{ph}} = 0.8$ meV, we obtain the branching ratio $P = \gamma_{v,\mathrm{RC}}/\gamma_{\mathrm{eh}} = 2.9 \times 10^{-10}$, describing a fraction of the vibrational excited molecule which decays by transferring (a part of) the energy into the RC to overcome the barrier in competing the damping due to electron–hole pair excitation.

Persson and Ueba [6,126] derived a formula of P as

$$P \simeq \frac{\eta^2}{\sqrt{2\pi}} \frac{1 - E_{\mathrm{B}}/(\hbar\Omega)}{2 - E_{\mathrm{B}}/(\hbar\Omega)} \left(\frac{\lambda}{\varepsilon_B}\right)^2 n^{3/2} \mathrm{e}^{-2n}, \tag{66}$$

where η takes care of the reduced weight of the plane wave function for a continuum state above a potential barrier and $n = E_{\mathrm{B}}/\hbar\omega_0$. Note that it is to be resolved why $P(n)$ exhibits a maximum as a function of n. Assuming $\eta = 0.01$ and using $\hbar\Omega = 236$ meV (the C–O stretch), $\hbar\omega_0 = 25$ meV (FT mode of CO on Pd(1 1 0)) and the barrier height $E_{\mathrm{B}} = 150$ meV (this gives a number of vibrational level $n = 6$) and $P = 2.8 \times 10^{-10}$ we obtain λ = 3.6 meV. On the basis of a similarity of the bridge bonding configuration and electronic structure between CO/Ni(1 1 1) and CO/Pd(1 1 0), and considering a simplicity of our model and many approximations to obtain the formula of $Y(V)$ and P, thus estimated anharmonic coupling λ through the full analysis of $Y(V)$ for a lateral hopping of CO on Pd(1 1 0) is very close to $\hbar\delta\omega = 4.3$ meV determined by the temperature dependence of the infrared absorption spectra of the bridge-bonded CO molecule [127] and theoretically calculated one as an origin of a vibrational dephasing brought about by energy exchange between anharmonically coupled high and low frequency mode of CO on Ni(1 1 1) [120]. This is the first theoretical determination of λ from the full analysis of the reaction yield [59]. A final remark is to answer why CO on Cu (1 1 0) does not move even when the C–O stretch mode is excited by tunneling electrons. In addition to an order of magnitude smaller λ on Cu(1 1 0) than on Pd(1 1 0) [128], a key factor is n in Eq. (66), i.e., $\hbar\omega_0 = 4$ meV [129] and $E_{\mathrm{B}} \simeq 97$ meV [130]. This gives $n \simeq 25$ leading to $P \sim 10^{-26}$ so that excitation of the C–O stretch mode is almost unable to induce a hopping on C(1 1 0).

Having achieved an excellent agreement between the experimental and calculated AS for a CO hopping, we are now able to calculate the inelastic tunneling current $I_{in}(V) = e\Gamma_{iet}(V)$ inducing hopping of a single CO molecule on Pd(1 1 0) (Note reaction rate $R(V) = K\Gamma_{iet}$). The blue curve in Fig. 32 shows $I_{in}(V)$ calculated using the same parameters as used to calculate $Y(V)$. Since $I_{in}(V)$ is linear in V except near $V \simeq \hbar\Omega/\mathrm{e}$, it is a good approximation to define $I_{in}(V) \simeq \sigma_{in}V$ in terms of the inelastic conductance σ_{in}. From the linear part of $dI_{in}(V)/dV$ as shown in the green curve, we obtain $\sigma_{in} = 0.46$ [nA/V], which gives the change of conductance $\Delta\sigma = \sigma_{in}/\sigma_0 = 4.6 \times 10^{-2}$ due to excitation of the C–O stretch mode. This value of $\Delta\sigma$ is very reasonable from a view of its theoretical prediction [112].

An important and novel finding here is not a determination of the C–O stretch mode energy from the analysis of AS for a CO hopping. That is an evaluation of the anharmonic mode coupling from the transition rate $\gamma_{v,\mathrm{RC}}$ and a branching ratio P estimated in the excellent reproduction of the

experimental result for the first time since they were calculated in Ref. [6]. It has taken more than ten years to complete a full analysis of hopping of a single CO molecule on a Pd(110) surface. Our generic and versatile formula of AS allows us to reproduce the experimental result over a full range of the applied bias voltage. This has provided us the vibrational mode and its energy responsible for hopping. In this sense STM-AS can be viewed as a unique single molecule vibrational spectroscopy (when it couples to the RC mode for motions and reactions) in complementary to STM-IETS. More importantly a success of reproduction of the reaction yield has permitted us to determine the key quantity of the mode coupling with a knowledge of an elastic conductance, vibrational damping and hopping barrier. All of these are combined to obtain the inelastic tunneling current to induce the reaction, a change of the conductance upon vibrational excitation and the vibrational DOS [59].

6.3. Dissociation of $(CH_3S)_2$ and hopping of CH_3S molecule on Cu(111)

Many single molecule motions and reactions reported so far [5] are single electron process where the vibrational mode, whose energy is larger than the reaction barrier, excited by tunneling electrons is coupled with the low energy RC mode to excite it above the barrier. Exceptional cases are two-electron process of NH_3 desorption from Cu(100) following a double excitation of the umbrella mode [131] and selective dissociation of chlorine atoms from single chlorobenzene molecule adsorbed on a Si(111)-7 × 7 surface [132]. As we show below, DMDS on Cu(111) exhibits a unique behavior. The evidences from the STM imaging, the current dependence of the reaction rate $R(I)$ and the bias dependence of the reaction yield $Y(V)$ indicate: (1) Injection of tunneling electrons dissociates DMDS into two methyl thiolate molecules. (2) The reaction order estimated from a current dependence of the dissociation rate $R(I)$ changes from $n = 2$ to 1 with an increase in the applied bias voltage. (3) Either ν(C–H) or the combination mode of ν(C–H) and the S–S stretch mode ν(S–S) is needed to be excited. (4) The role of molecular orbitals (MOs) in the vibrationally-induced reaction is understood in terms of the resonance tunneling mechanism in which a tunneling electron is temporarily captured in the MO to undergo electron-vibration coupling. (5) A quite large asymmetric $Y(V)$ feature for DMDS dissociation and small difference in $Y(V)$ for MT hopping observed at positive and negative bias voltages are qualitatively consistent to the characteristic difference in the PDOS of DMDS and MT on Cu(111).

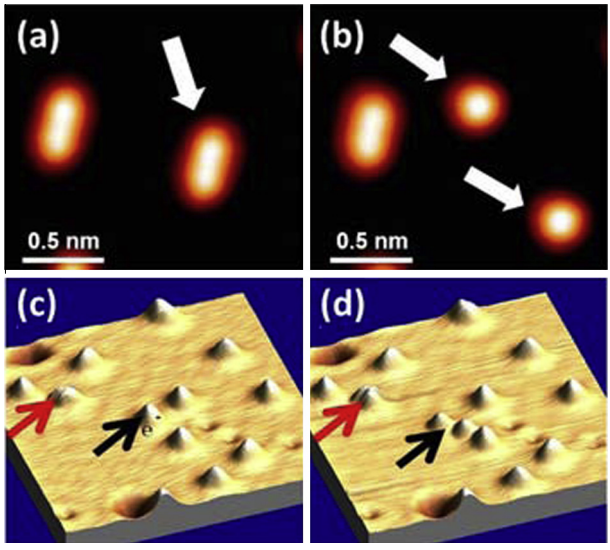

Fig. 33. STM images of dissociation of a single DMDS molecule to two isolated MT molecules on Cu(111) observed at V_s = 20 mV and I_t = 0.2 nA (a) before and (b) after electron injection (V_s = 400 mV and I_t = 1 nA for 2 s) into the target molecule marked by the white arrow in (a). (c) and (d) are bird's view of the extended scan. Other DMDS molecules remain unchanged.

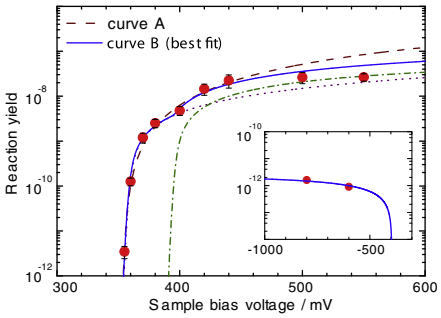

Fig. 34. Dissociation yield as a function of sample bias voltage for DMDS on Cu(1 1 1). Red circles are experimental data measured at 5 K and 4 nA [27]. Curve A is calculated for double excitation of ν(C–H) shown for comparison. Curve B is the best fit to the data, which is sum of the reaction yield induced by simultaneous excitation of ν(C–H) and ν(S–S) (purple dotted curve), and the combination mode excitation (green chain curve). The inset is an action spectrum of DMDS dissociation for a negative sample bias, which is reproduced by $Y(V) = \alpha' Y(-V)$ for $V < 0$, where with the asymmetric factor of $\alpha' = 2.4 \times 10^{-5}$ for the combination band excitation. (For interpretation of the references to color in this figure legend, the reader is referred to the web version of this article.)

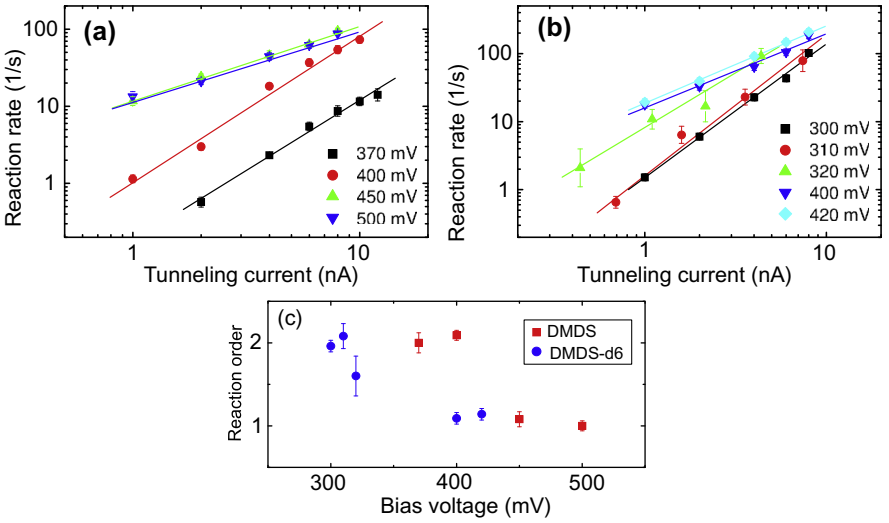

Fig. 35. (a) Dissociation rate $R(I)$ as a function of I at several V for DMDS (a) and DMDS-d_6 (b) on Cu(1 1 1) at 5 K. The solid lines are the least square fitting of a power law $R(I) = cI^n$ to the measured data and the reaction orders are plotted in the red squares for DMDS and blue circles for DMDS-d_6 (c). Reproduction from [58]. (For interpretation of the references to color in this figure legend, the reader is referred to the web version of this article.)

Although action spectra offer rich informations of a vibrationally mediated reaction of single molecules, the precise mechanism by which a particular vibrational mode induces molecular reactions by inelastic tunneling electrons has not yet been fully examined. Many theoretical attempts to explain the tunneling electron-vibration coupling [4,5] in a molecule have been based on a resonance model. A detailed knowledge of the MOs of the adsorbate is necessary for understanding the underlying mechanism of electron-vibration coupling and for predicting which vibrational mode is actually excited by tunneling electrons. A role of MOs near the ε_F in the excitation of vibrational modes of a single molecule has been clearly addressed by Ohara et all. [27] in their study of a dissociation of DMDS and a lateral hopping of an isolated MT on a Cu(1 1 1). Based on the experimental findings

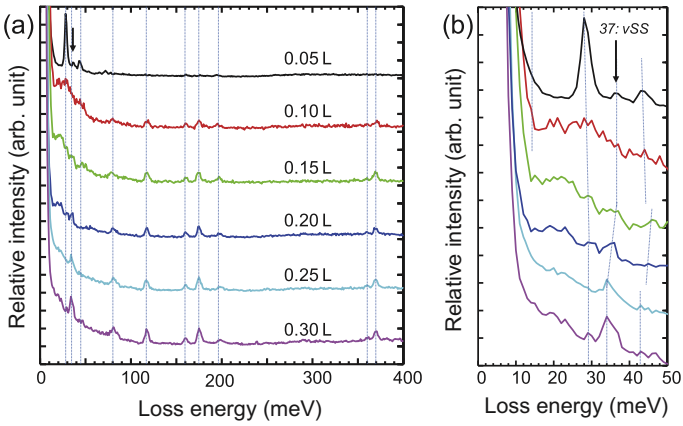

Fig. 36. (a) HRELLS spectra of DMDS on Cu(1 1 1) for various DMDS exposures. The intensities are normalized by the elastic peak height. Reproduction from [58].

and on DFT calculations of the PDOS and spatial distribution of MOs, they clarified how the MOs of an adsorbate near the ε_F affect electron-vibration coupling and thereby affect the molecular motions and reactions by vibrational excitations of a single DMDS and MT molecule on Cu(1 1 1).

6.3.1. Dissociation of a single $(CH_3S)_2$ molecule on Cu(1 1 1)

Details of the experimental procedures have been reported previously [27]. The clean Cu(1 1 1) surface was exposed to DMDS vapor at a temperature below 50 K. The typical condition for obtaining STM images was $V_s = -20$ mV and $I_t = 0.2$ nA. AS for S–S bond scission of DMDS molecules were taken when STM tip was positioned over the center of a target molecule. In order to assign the vibrational modes from the threshold bias voltage in AS, we acquired HREELS spectra [58]. All HREELS spectra were taken with a primary beam energy of 4.5 eV at a specular configuration with an incident angle of 60° respect to the surface normal. The energy resolution was 3.1 ± 0.4 meV, as determined from the full width at half-maximum of the elastic peak. The substrate temperature was 20 K.

Fig. 33 shows the STM images of dissociation of a single DMDS molecule on Cu(1 1 1) before and after electron injection of the target molecule [27]. By injecting tunneling electrons with $V_s = 400$ mV and $I_t = 1$ nA for 2 s into the target molecule, we find that a single DMDS molecule is broken into two identical ball-shaped protrusions, implying S–S bond scission to form two isolated MT molecules. The bird's view of the extended area [Fig. 33(c) and (d)] shows that a single DMDS (marked by a black arrow) dissociates to two single MT molecules, while the other molecules remain unchanged.

The experimental result of the AS for dissociation of DMDS on Cu(1 1 1) is shown in the red circles in Fig. 34. The AS exhibits a clear threshold voltage at 359 mV. This threshold voltage corresponds to the vibrational excitation energy of the ν(C–H) of the CH_3 group in the molecule. It was also observed that the sharp peak in the $\Delta \log Y(V)/\Delta V$ at 357.5 mV is accompanied with another small peak at $V = 410$ mV. This weaker thresholds does not match with any of the vibrational normal modes of DMDS molecule, and may correspond to excitation of a combination band of ν(C–H) and ν(S–S) modes of DMDS in a single electron process.

In order to determine the reaction order we observed the tunneling current dependences of a dissociation rate $R(I)$ of DMDS and deuterated DMDS (DMDS-d_6) [58]. Fig. 35(a) is for several fixed bias voltages from 370 to 500 mV for DMDS and (b) from 300 to 420 mV for DMDS-d_6. All $R(I)$ exhibit a power law dependence, and the reaction order n estimated from the slopes as a function of V is shown in Fig. 35(c). It is observed that n changes from 2 to 1 with an increase in V and the crossover is found around $V = 400$–450 mV for DMDS. A similar behavior is also observed for DMDS-d_6, and n changes from 2 to 1 around $V = 300$–400 mV as a result of the vibrational isotope shift of ν(C–H) mode and ν(C–D) mode which are the component of the combination mode.

Our assignment of the ν(S–S) mode at 37 meV is confirmed by the HREELS spectra shown in Fig. 36 for sub-monolayer DMDS on Cu(1 1 1) at energy loss between 0 and 400 meV [58]. Several peaks are clearly assigned to the asymmetric ν_a(C–H) at 370 meV, the symmetric ν_s(C–H) mode at 361 meV, the bending $\delta_a(CH_3)$ at 175 meV, $\delta_s(CH_3)$ mode at 160 meV, the rocking $\rho_r(CH_3)$ mode at 117 meV, and ν(C–S) mode at 81 meV. In addition, we assign a weak peak at 37 meV (indicated by the black arrow in the expanded spectrum at 0–50 meV) to the ν(S–S) mode. Although ν(S–S) have a surface parallel motions of atoms, it is expected to have also a surface normal component of transition dipole due to the mixing with other vibrational modes such as ν(Cu–S) and ν(C–S) modes, or due to the oscillatory charge transfer between DMDS and Cu atoms depending on the S–S bond distance. The weakened S–S bond due to the formation of the Cu–S bond shifts the ν(S–S) energy much lower than that for condensed phase of DMDS multilayer [133,134] at 63 and 62 meV.

In the conventional scenario, the requirement of two electrons for the reaction implies that double excitation of a vibrational mode is necessary to overcome the activation barrier E_B. For DMDS, the observation that $n = 2$ for ν(C–H) excitation indicates that $E_B \geqslant 360$ meV, while $n = 1$ for the combination band excitation suggests $E_B \leqslant 400$ meV. For DMDS-d_6, however, 310 meV $\leqslant E_B \leqslant$ 330 meV is obtained from $n = 2$ for ν(C–D) and $n = 1$ for the combination band. Since E_B should be independent of isotopic substitution, the above estimate of E_B from the behavior of $Y(V)$ and $R(I)$ based on the conventional scenario cannot be accepted. Thus, from energetic point of view, the participation of a double excitation of the ν(C–H) mode inducing the dissociation is excluded.

Simple analysis of the temperature dependence of DMDS dissociation observed in STM images gave us a rough estimation of takes care of the reduced The coverage of non-dissociated DMDS is described as $\theta = \theta_0 \exp(-kt)$, here θ_0 is the initial coverage and t is a time after adsorption. The dissociation rate constant k is given by $k = \nu \exp(E_B/k_B T)$, here a prefactor $\nu = k_B T/h$ and h is a Planck's constant. We hardly observed the dissociated molecules (the fraction of dissociated molecules was less than 0.1%) when DMDS was adsorbed at 50 K within 100 s. In contrast, thermally dissociated molecules appeared (at least 1%) when the substrate temperature was kept at 77 K for an hour. These observations gives $k < 1.0 \times 10^{-4}$/s at 50 K and $k > 2.8 \times 10^{-6}$/s at 77 K. The Arrhenius equation then permits us to estimate $E_B = 170$—270 meV [58], which is very low compared to the threshold voltage (357.5 meV) of the dissociation yield [27]. The above discussion also support that the reason for $n = 2$ for ν(C–H) excitation does not follow the conventional scenario. It seems that a deexcitation of ν(C–H) mode excited by a tunneling electron provides sufficient energy to the ν(S–S) mode for S–S bond cleavage; however, the experimental result of $R(I)$ clearly excludes this single electron process. It is implied that a coupling between the ν(C–H) excited state and ν(S–S) mode in the ground state is too small to cause S–S bond cleavage for DMDS dissociation.

These facts encourage us to look for the other elementary two-electron process for DMDS dissociation in addition to excitation of the ν(C–H) mode. As demonstrated here, we have proposed a novel process of two-electron process where two electron excite different vibrational modes: one electron excites the ν(C–H) mode and another electron excite the partner mode of ν(S–S) (the RC mode) [58]. As bias voltage exceeds the sum of these two modes, a single-electron process exciting the ν(C–H) + ν(S–S) combination band leads to further dissociation of DMDS.

To clarify this new scenario, we now come to a stage to reproduce the experimental $Y(V)$ for dissociation of a single DMDS molecule on Cu(1 1 1) shown in the red circles in Fig. 34 based on the qualitative discussions presented above. The reaction rate $R(V)$ for the two-electron process exciting two different vibrational modes is given by

$$R^{(2)}(V) = \Sigma_n \gamma_{\nu_1:1\to 0,\nu_2:n\to k} P_1^{\nu_1}(V) P_n^{\nu_2}(V), \tag{67}$$

where the first factor represents the transition rate which describes a decay of the ν_1 mode in the first excited state transfers a part of its energy to the hot vibrational state n of the ν_2 mode excited by a tunneling electron. Here $P_1^{\nu_1}$ is the population of the ν_1 mode in the first excited state, while $P_n^{\nu_2}$ is the population of the ν_2 mode in the n-th excited state. It is assumed that the vibrational energy of the ν_1 mode (ν(C–H) mode in the present system) is higher than that of the ν_2 mode (S–S stretch mode for the S–S bond scission). Here n can be 1 or higher if the coherent ladder climbing is allowed and k is

the scattering state of the v_2 mode above the dissociation barrier. The rate equations for $P_1^{v_1}$ and for $P_n^{v_2}$ in a similar manner as Eq. (63) immediately lead to

$$R^{(2)}(V) = \Sigma_n \gamma_{v_1:1\to 0, v_2:n\to k} \frac{\Gamma_{\text{iet}}^{v_1}(V)}{\gamma_{\text{eh}}^{v_1}} \frac{\Gamma_{\text{iet}}^{v_2}(V)}{\gamma_{\text{eh}}^{v_2}}, \tag{68}$$

and is explicitly expressed as

$$R^{(2)}(V) = K \frac{\Gamma_{\text{iet}}(V, \Omega_{\text{C-H}})}{\gamma_{\text{C-H}}} \frac{\Gamma_{\text{iet}}(V, \Omega_{\text{S-S}})}{\gamma_{\text{S-S}}}, \tag{69}$$

where the prefactor K includes the activation rate of the S–S mode over the barrier via the inter-mode coupling to the C–H mode. We assume hereafter $n = 1$, i.e., v_2 of the S–S stretch mode is excited to the first excited state by a tunneling electron. Then the yield $Y^{(2)}(V)$ is given by using a notation defined in Eq. (32) in the EWBL

$$Y^{(2)}(V) = \frac{K_{\text{eff}}^{(2)}}{\text{e}} \mathcal{F}(V, \rho_{\text{ph},v}) \mathcal{R}(V, \rho_{\text{ph},v}) \tag{70}$$

where $\mathcal{R}(V, \rho_{\text{ph},v}) = \mid eV \mid \mathcal{F}(V, \rho_{\text{ph},v})$ and $K_{\text{eff}}^{(2)}$ is given by

$$K_{\text{eff}}^{(2)} = \frac{\gamma_{v_1\times v_2:\text{RC}}}{2\Omega_{v_1}} \frac{1}{\rho_a(\varepsilon_{\text{F}})} \frac{1}{\hbar\Omega_{v_2}} \frac{\Gamma_t}{\Gamma_s}, \tag{71}$$

where $\gamma_{v_1\times v_2:\text{RC}}$ is a prefactor of Eq. (68) and the dimensionless $K_{\text{eff}}^{(2)}$ is ensured by the numerical dimension of $\mathcal{R}(V, \rho_{\text{ph},v})$ in [eV]. It is important to note that the lifetime of the v_2 (i.e., the S–S mode ($\tau_{\text{S-S}} = 1/\gamma_{\text{S-S}}$) should be long enough compared to the average time interval of two electrons, otherwise the excited S–S mode returns to the ground state before it is excited above the barrier via the inter-mode coupling with the C–H mode. It is also noted that because of a step function $\theta(eV - \hbar\Omega_{\text{C-H}}) \times \theta(eV - \hbar\Omega_{\text{S-S}})$ for the vibrational excitation, the threshold is determined by the high energy v(C–H) mode.

The higher threshold observed at V near 410 meV corresponds to the vibrational energy of a sum of the v(C–H) and v(S–S) mode. A formal theory of combination band excitation in a single electron process has been recently formulated using the Keldysh Green's function in a study of rotation of a single acetylene molecule on Cu(1 0 0) by Shchadilova et al. [135,136]. It is also noted that a role of excitation of a combination band in a single electron process has been addressed for chirality change of a chloronitrobenzene molecule on Au(1 1 1) [40], switching chirality of a propene molecule on Cu(2 1 1) [31], and water dimer hopping on Pt(1 1 1) [46].

The rate of a combination band excitation takes the same form as for a single-phonon excitation rate $\Gamma_{\text{in}}(\Omega, V)$, where a single vibrational frequency is simply replaced by the sum of two vibrational frequencies, i.e.,

$$\Gamma_{\text{in}}(V) = \frac{\gamma_{\text{eh}}^{v_1+v_2}}{\Omega_{v_1+\Omega_{v_2}}} \frac{\Delta_t}{\Delta_s} (|eV| - \hbar\Omega_1 - \hbar\Omega_2) \theta\left(\frac{|eV|}{\hbar\Omega_{v_1+\hbar\Omega_{v_2}}} - 1\right), \tag{72}$$

here $\gamma_{\text{eh}}^{v_1+v_2}$ is a damping rate of the combination band. Note that the linewidth of infrared absorption spectrum of a combination band is given by a sum of each fundamental mode [137].

The AS for the combination band excitation in a single electron process is given by the same form as Eq. (29) i.e.,

$$Y^{(1)}(V) = K_{\text{eff}}^{(1)} \mathcal{F}(V, \rho_{\text{ph}}). \tag{73}$$

where

$$K_{\text{eff}}^{(1)} = \frac{\gamma_{\text{eh}}^{v_1+v_2}}{2(\Omega_{v_1+\Omega_{v_2}})} \frac{1}{\rho_a(\varepsilon_{\text{F}})\Gamma} K = \frac{1}{2(\Omega_{v_1+\Omega_{v_2}})} \frac{\gamma_{v_1+v_2:\text{RC}}}{\rho_a(\varepsilon_{\text{F}})\Gamma}, \tag{74}$$

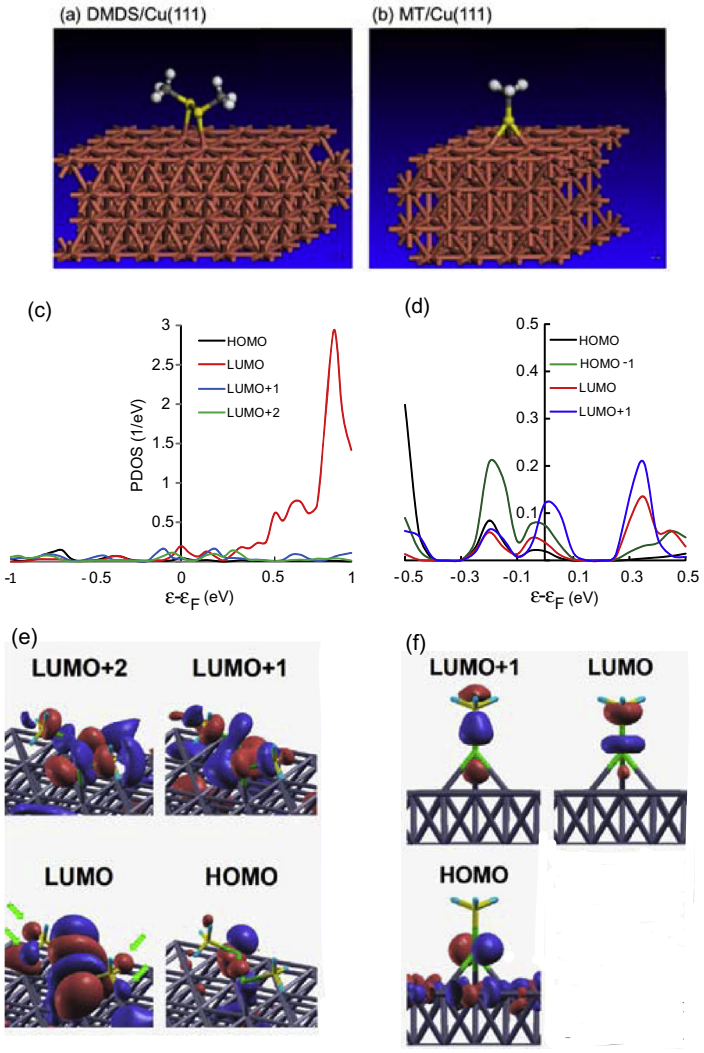

Fig. 37. DFT calculated optimized adsorption geometry of (a) a single DMDS molecule and (b) MT molecule on Cu(111). (c) PDOS of a single DMDS molecule on Cu(111). (d) PDOS of a single MT molecule on Cu(111). Redrawn near ε_F. (e) The spatial distribution of LUMO+2, LUMO+1, LUMO and HOMO for a single DMDS molecule. MOs on the C–H bond in DMDS molecule are indicated by arrows. (f) The spatial distribution of LUMO+1, LUMO and HOMO for a single MT molecule. H, C, S and Cu atoms are drawn in blue, yellow, green, and gray, respectively. Redrawn from Fig. 3 in Ref. [27]. (For interpretation of the references to color in this figure legend, the reader is referred to the web version of this article.)

where $\gamma_{v_1+v_2:\mathrm{RC}}$ differs from $\gamma_{v_1\times v_2:\mathrm{RC}}$ in Eq. (71). Although both stand for the excitation rate of the S–S mode over the barrier, in the latter process each v_1 (C–H) and v_2 (S–S) mode is excited in a two-electron process.

Curve A in Fig. 34 is the calculated $Y(V)$ using Eq. (7) in Ref. [29] for the conventional scenario that involves double excitation of v(CH). This curve does not involve a contribution from the combination mode, and the transition from $n = 2$ to $n = 1$ does not occur. Therefore Curve A cannot reproduce the experimental results [58]. The solid blue curve (curve B) is a sum of following two contributions: The dashed purple curve is calculated using Eq. (69) with $\hbar\Omega_{\mathrm{C-H}} = 359$ meV, $\hbar\Omega_{\mathrm{S-S}} = 37$ meV, $\sigma_{\mathrm{ph}} = 3$ meV

and $K_{\mathrm{eff}}^{(2)} = 1 \times 10^{-10}$ for the double excitation of two modes in a two-electrons process. The dashed green curve in Fig. 34 is calculated with $\hbar\Omega_{\mathrm{C-H}} + \hbar\Omega_{\mathrm{S-S}} = 394$ meV, $\sigma_{\mathrm{ph}} = 2$ meV and $K_{\mathrm{eff}}^{(1)} = 1 \times 10^{-7}$ for the combination band excitation in a single electron process. As shown in the curve B in Fig. 34, the experimental result of AS is nicely reproduced by the numerical simulation using Eqs. (69) and (73) which is based on the scenario of the two-electron process exciting ν_1(C–H) and ν_2(S–S) mode. It means that the simulation supports our new scenario for the two-electron process.

This convinces us that, in addition to the excitation of ν(C–H), the excitation of ν(S–S) is required for DMDS dissociation in both reaction processes with $n = 2$ below $V \simeq 390$ mV and with $n = 1$ above $V \simeq 400$ mV. This is plausible from a view that dissociation needs the S–S bond breaking of DMDS. The dissociation occurs when the RC mode, we believe that it should be ν(S–S), is multiply excited to overcome the reaction barrier. The excitation of ν(C–H) is required as an energy source that transfers sufficient energy to the RC mode via anharmonic mode coupling for overcoming the reaction barrier. The excitations of ν(S–S) is additionally required for inducing the reaction. It is expected that the anharmonic coupling rate of the ν(C–H) with the ν(S–S) is enhanced for the hot excited state of the ν(S–S) mode compared to the ground state. This is because excitation of ν(S–S) mode expands its wave function leading to a larger overlap between the wave function of ν(S–S) and ν(C–H) modes. It leads to efficient multiple excitation of the ν(S–S) mode and a subsequent S–S bond dissociation when the ν(C–H) mode is excited. It is noted here that DMDS dissociation via above mechanism can be induced only if the lifetime of the ν(S–S) mode is sufficiently long compared to the rate of electron tunneling. This is the first clear evidence regarding the contribution of simultaneously existing excited states of two vibrational modes, and the participation of a combination mode in a single molecule reaction.

The contribution of MOs to the vibrationally induced reaction is discussed in terms of the DFT calculation of PDOS and the polarity dependence of $Y(V)$. Fig. 37(c) shows that the LUMO is mainly located about 1 eV above the ε_F and also have certain contribution at above $\varepsilon_F + 0.3$ eV. It indicates that the most electrons injected from an STM tip at 300 mV $< V <$ 500 mV is first captured by LUMO of DMDS. The spatial distribution of individual MOs for DMDS illustrated in Fig. 37(e) shows that the LUMO of DMDS is clearly localized at both the S–S and C–H bonds in the molecule. Resonant model for vibrational excitation through IET process [112] suggests that a resonantly captured electron in

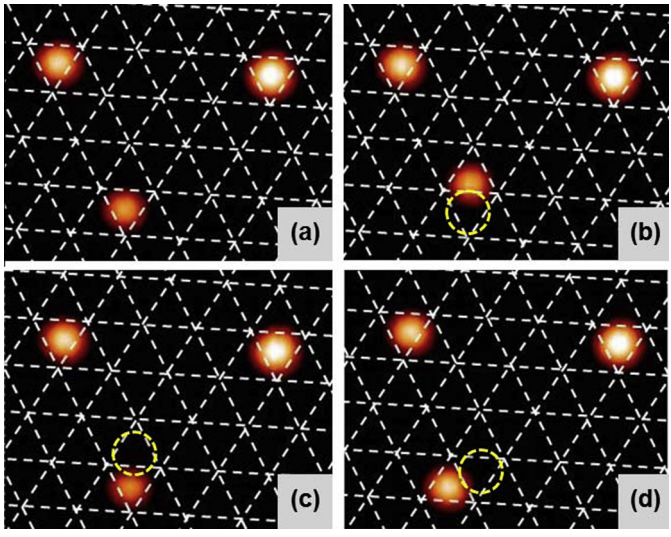

Fig. 38. Sequential STM images of the hopping motion of a MT molecule on Cu(1 1 1), $V_s = -20$ mV and $I_t = 0.2$ nA, 15 nm × 12 nm. The original position of the hopped MT molecule in the previous STM images are indicated by yellow dotted circle. The hopping direction of the MT molecule on Cu(1 1 1) depends on the injection point of the tunneling electrons as explained in Fig. 39. The grid shows the position of Cu atoms determined from the position of co-adsorbed CO molecules [56]. (For interpretation of the references to color in this figure legend, the reader is referred to the web version of this article.)

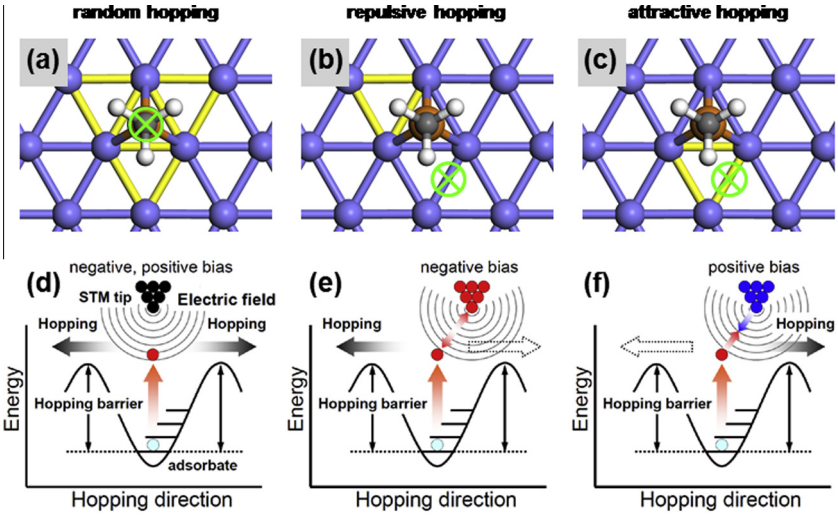

Fig. 39. Top views of the relative position between the hopping direction(s) of MT and the STM tip in (a) random, (b) repulsive, and (c) attractive hopping motions. The molecule hops toward the hollow sites, marked by yellow lines, when the tunneling electrons are injected (or extracted) at the positions indicated by ⊗. Schematics for (d) random, (e) repulsive, and (f) attractive hopping. Each electric field contour is depicted with a point charge at the STM tip apex [44]. (For interpretation of the references to color in this figure legend, the reader is referred to the web version of this article.)

the LUMO influences the S–S and C–H bond. This results in the Fig. 34 where the ν(C–H) and the ν(S–S) are excited to induce the dissociation at $V > 350$ mV. On the other hand, as shown in the inset of Fig. 34, $Y(V)$ for negative V is much smaller than $Y(V)$ for positive V. The $Y(V)$ at negative V is reproduced by $Y(V) = \alpha' Y(-V)$, where α' is defined in the text and the asymmetric factor of $\alpha' = 2.4 \times 10^{-5}$ for the combination band excitation. This asymmetry factor is consistent for the calculated PDOS of the LUMO shown in Fig. 37(c), where almost no weight is observed for $V < 0$. The reaction yield for dissociation showed distinctly different dependence on polarity, where the contribution of the LUMO state apparently dominates. In addition, the small contributions of the LUMO+1 and HOMO states are broadly distributed within a span of the vibrational energies of interest. The LUMO+1 as well as the HOMO is not distributed along C–H bond but along Cu–S bond, indicating the small contributions of these MOs to the dissociation of DMDS. Thus, all the experimental results shown here can be reasonably explained by using resonant model. This characteristic asymmetry feature of the dissociation AS with respect to the bias polarity (Fig. 34) and the distribution of the PDOS are in contrast to a lateral hopping of a single MT molecule on Cu(1 1 1) as described in detail below.

In summary the successful curve fitting of AS data for DMDS dissociation revealed that the reaction includes a significant contribution of the two-electron process where one electron excites ν(C–H) mode and another one excites ν(S–S). We have clarified that the vibrational modes play different role, i.e., where excitation of ν(C–H) acts as an energy source and excitation of ν(S–S) enhances the rate of the anharmonic coupling with ν(C–H). This is the first clear evidence regarding the contribution of simultaneously existing excited states of two vibrational modes, and the participation of a combination mode in a single molecule reaction. The present analysis also underlines an importance of the PDOS of an isolated DMDS. The LUMO state of DMDS lies mainly above 0.35 eV and its contribution is larger than half of the total DOS, while the population and contribution of the LUMO are extremely small in the negative energy region. According to the resonance model, this leads to the small probability that tunneling electrons are captured by the LUMO, and hence the small probability of excitation of vibrational modes responsible for the dissociation. The very small prefactor K at the negative bias relative to that at the positive one is thus understood in terms of the asymmetry of the PDOS population. This result emphasizes that the vibrational modes are resonantly excited through a temporal occupation of the MO by tunneling electrons, and that the excitation probabilities of vibrational modes depend on the population of the MOs at the corresponding energy.

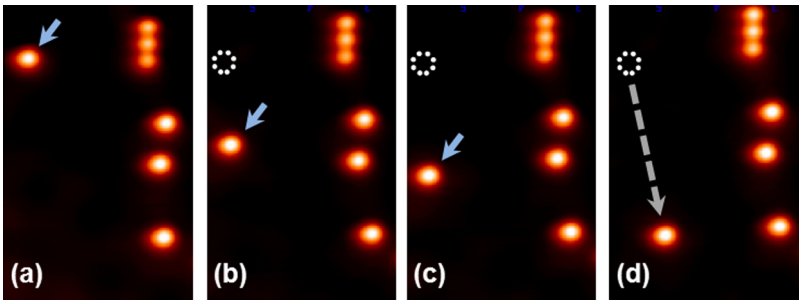

Fig. 40. (a)–(d) Sequential STM images showing the long-distance transport of a MT molecule on Cu(1 1 1) observed at $V_s = -20$ mV and $I_t = 0.2$ nA, 40 nm × 26 nm. Off-center injection of tunneling electrons induce the hopping of the MT molecule indicated by blue arrows [56]. (For interpretation of the references to colour in this figure legend, the reader is referred to the web version of this article.)

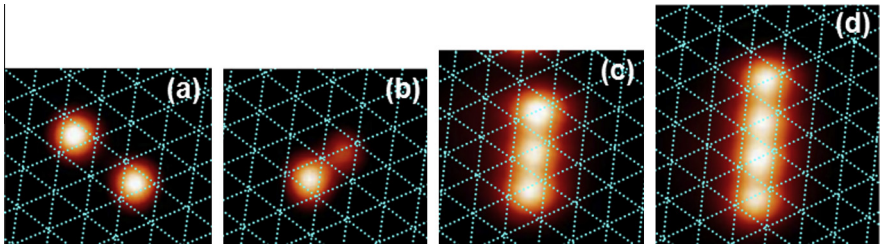

Fig. 41. STM images of two MT molecules (a), a MT dimer (b), MT trimer (c), and MT tetramer (d) on Cu(1 1 1) observed at $V_s = -20$ mV and $I_t = 0.2$ nA [56]. Scan size: (a) and (b) 11.2 nm × 13.3 nm, (c) 12.2 nm × 13.3 nm, (d) 14.4 nm × 15.3 nm.

6.3.2. Lateral manipulation of a single CH_3S molecule on Cu(1 1 1)

One of two isolated MT molecules prepared by the S–S bond cleavage of a single DMDS molecule was further manipulated to undergo a lateral hopping on Cu(1 1 1) [56]. The hopping is understood as the result of vibrational excitation of ν(C–S), where the bias voltage of $\nu(\text{C–S}) \leqslant |V|$ is necessary. Fig. 38(a) shows the STM image of three isolated MT molecules on a Cu(1 1 1) observed at $V_s = -20$ mV and $I_t = 0.2$ nA. After injecting tunneling electrons at $I_t = 1$ nA with $V_s = 400$ mV to the center of a MT molecule for 2 s, the target molecule moves laterally to the nearest neighboring hollow site, as shown in Fig. 38(b). This molecular hopping was observed repeatedly for each electron injection event.

Each MT molecule has three equivalent nearest-neighbor hollow sites around itself. When the tunneling electrons are injected at the center of a target molecule, the hopping direction of the MT molecule is random as illustrated in Fig. 39(a) and (d). We could, however, control the direction of MT hopping by an off-center injection of tunneling electrons at positive or negative bias voltage. The off-center electron injection enabled the target molecule to hop to the nearest neighboring hollow site opposite to the injection point as shown in (b) and (e) for a negative bias, and (c) and (f) for a positive bias, respectively [44]. To explain the mechanism of the controlled molecular hopping, we discuss the relationship between the charge on the STM tip determined by the applied bias voltage and the hopping direction of the molecule. The STM tip was negatively charged during the injection of tunnel electrons into the molecule and positively charged during extraction. It means that local electric field gradient is generated near the STM junction, which is intensified at the sharp apex of the tip. When the apex of the tip was positioned on the molecular center, the local electric field in an STM junction is approximately homogeneous parallel to the surface [Fig. 39(d)]. Therefore, the hopping direction of a MT molecule is not restricted by the electric field and the molecule hops randomly on the surface irrespective to the polarity of the applied bias. On the other hand, when the apex of the tip was positioned at off-center of the molecule, certain electric field gradient parallel to the surface is generated by applied bias [Figs. 39(e), (f)]. Since a MT molecule is always negatively charged on the Cu(1 1 1)

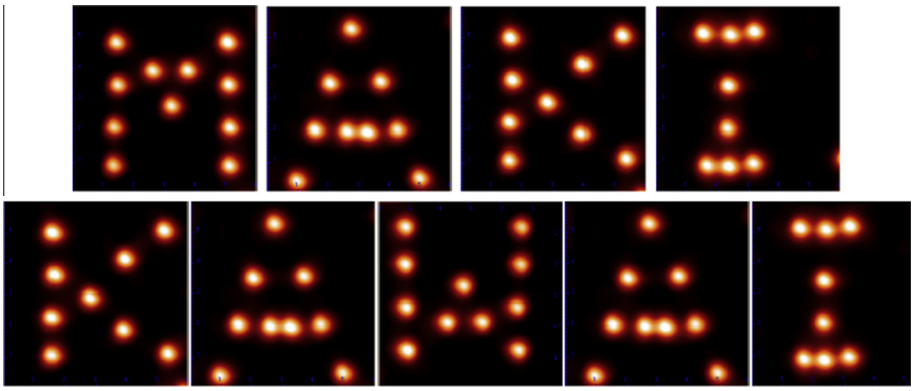

Fig. 42. STM images of "MAKI KAWAI" fabricated by a controlled manipulation of single MT molecules on Cu(1 1 1) surface.

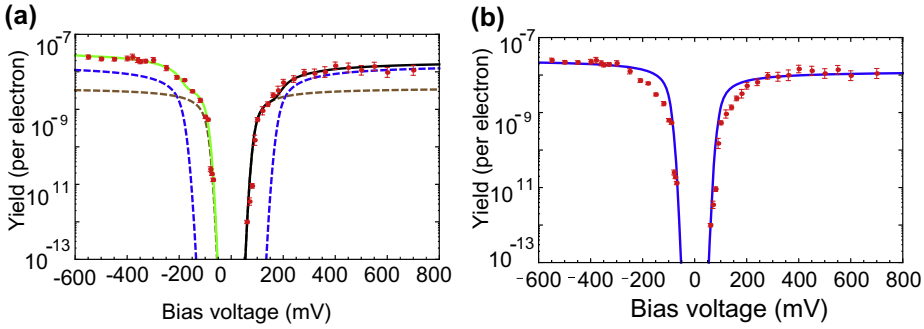

Fig. 43. (a) Action spectrum $Y(V)$ for the hopping of MT molecules on Cu(1 1 1) in both positive and negative bias. Initial current was set to 4 nA. The dashed blue and brown curves are calculated with two vibrational modes at 87 and at 140 meV. The black (green) curve for $V > 0$ ($V < 0$) in (a) is a sum of two contribution from the modes at 87 meV and at 180 meV, Here a factor $\alpha' = 1.9$ is multiplied for both modes at $V < 0$. Introduction of additional mode with 180 meV improves the curve fitting to the experimental result around $V \simeq 100$–200 mV as seen in (b) where $Y(V)$ is calculated using the mode at 87 meV only and $Y(V) = 1.9Y(-V)$. (For interpretation of the references to color in this figure legend, the reader is referred to the web version of this article.)

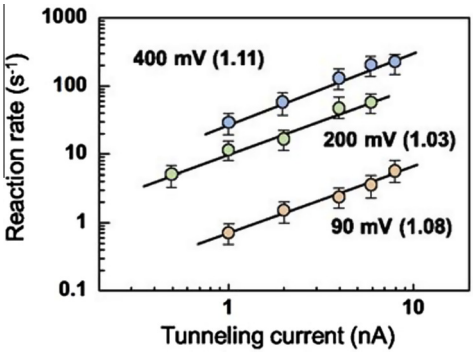

Fig. 44. Hopping rate $R(I)$ of an isolated MT molecule as a function of tunneling current I for various bias voltages V. Solid lines are the results of least-squares fits of $R(I) \propto I^n$ to the data, whose slope 1.08, 1.03 and 1.11 for $V = 90$, 200 and 400 mV, respectively. The power $n \simeq 1$ suggests a single electron process for all V examined here.

surface [138–140], a negative bias causes a repulsive force between the tip and the molecule, which induces the hopping of MT molecules to the nearest-neighbor hollow site to move away from the STM tip. In contrast, if a positive bias is applied, the molecule is attracted toward a positively charged STM tip and prefers to hop to the site near the STM tip. This mechanism was confirmed by the observation that negatively charged CO molecules on Pd(1 1 0) [141] hop toward the tip at $V_s \leqslant 0$ and hop away from the tip at $V_s \geqslant 0$.

By repeated injection of tunneling electrons at the off-center of the molecule, we achieved long-distance transport of a single MT molecule over 2.2 nm in the intended direction as shown in Fig. 40 [56]. This manipulation technique of MT molecules in a controlled manner allows us to fabricate various nanostructures on the surface. We demonstrated it by achieving the formation of molecular clusters with intended sizes [56]. Injection of tunneling electrons into one of the two MT molecules located nearby [Fig. 41(a)] induces lateral hopping of the molecule to form a gourd-shaped entity that consists of a brighter and a darker protrusion, as shown in Fig. 41(b). The gourd-shaped species rotates and moves laterally like a single molecule with the injection of additional tunneling electrons. This implies a formation of a dimer of two MT molecules in which one MT molecule is bonded to the other in an asymmetric configuration. The dimer formation of alkyl thiolates on Au(1 1 1) at 375 K was already reported by Kluth et al. based on HREELS observation of ν(S–S) [142]. They proposed that one sulfur atom in a dimer sits in a hollow site and the other sits near a bridge site, which is very similar to our STM observations. In this work, we successfully fabricated MT dimers using a non-thermal process with an STM at 4.7 K. In a same manner, a trimer and a tetramer of MT molecules were formed by successive lateral manipulation as shown in Figs. 41(c) and (d), respectively. As in the case of the dimer, these molecular clusters can rotate on the surface with the injection of tunneling electrons. This means that each molecule binds with other molecules in these clusters. The molecular chains all have MT molecules at (1×1) bridge sites in the $[1\,\bar{1}\,0]$ direction. This noncontact process for manipulating and positioning individual molecules offers some advantages that are not provided by conventional manipulation such as rapid movement of molecules between two sites and the extremely low probability of the STM tip breaking or of molecular dissociation often caused by strong tip-molecule interaction. It offers a controllable way of precisely positioning individual molecules to fabricate nanostructures, as demonstrated by the patterned arrays of single molecular characters "MAKI KAWAI" shown in Fig. 42. Our approach will provide a possible general basis for tailoring the architecture of molecule-based electronics.

Now let's go back to a main stream of this review, i.e., the AS for hopping of a MT molecule on Cu(1 1 1). Fig. 43 shows the experimental result (red circles) of a hopping yield $Y(V)$ observed as a function of V at a fixed $I = 4$ nA. The AS shows only one threshold at $V \simeq 85$ mV for positive V. Fig. 44 shows the hopping rate of an isolated MT molecule on Cu(1 1 1) as a function of tunneling current I for three bias voltages $V = 90$, 200 and 400 mV [44]. Solid lines are the results of least-squares fits to the data, whose slope at given V corresponds to the power $n \simeq 1$, i.e., single electron process for all V examined here.

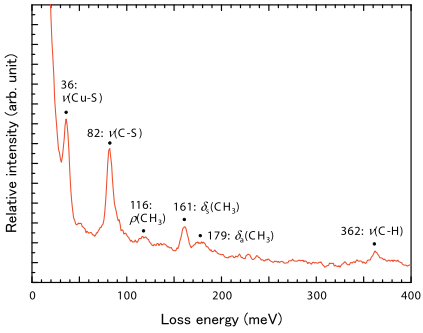

Fig. 45. HREELS spectra of sub-monolayer MT on Cu(1 1 1). The vibrational energy and the assignment of each peak is also shown.

For the assignment of the vibrational mode, we measured HREELS spectra of MT molecules on Cu(1 1 1). Adsorption of submonolayer MT for HREELS measurement was performed by exposing the clean Cu(1 1 1) to DMDS vapor for 0.05 L at room temperature, where dissociative adsorption of DMDS resulted in MT adsorption. Measurement condition including substrate temperature is same as that for DMDS as described in previous section. We observed six vibrational peaks as shown in Fig. 45: ν_s(C–H) at 362 meV, $\delta_a(CH_3)$ at 179 meV, $\delta_s(CH_3)$ at 161 meV, $\rho_r(CH_3)$ at 117 meV, ν(C–S) at 82 meV, and ν(Cu–S) at 36 meV. The assignment was straightforward since similar peaks have been observed for HREELS spectra of MT on Au(1 1 1), Cu(1 0 0), Ni(1 1 1), Pt(1 1 1) [133,134,143,144]. Therefore, we concluded that the vibrational mode at 85 meV for MT molecules on Cu(1 1 1) shown in AS (Fig. 43) corresponds to ν(C–S). Since the frustrated translation and/or rotation modes constitute the RC mode for hopping, the indirect excitation of the RC mode via the anharmonic coupling with the ν(C–S) mode is primarily responsible for hopping of MT molecule on Cu(1 1 1).

The blue curves in Fig. 43(b) is calculated using the ν(C–S) mode; $(87, 10, 1.3\times10^{-8})$ for $V > 0$ and $(87, 10, 2.5.\times10^{-8})$ for $V < 0$, where we again assume $Y(V) = \alpha' Y(-V)$ and factor $\alpha' = 1.9$ is multiplied to $Y(V)$ for negative V. In the original publication [44] it was noted that the hopping yield is identical for the applied voltage of both polarities. The present fitting, however, finds a tiny, but noticeable difference of $Y(V)$ for positive and negative V. A single mode of the ν(C–S) at 87 meV appears to explain the experimental result (see the blue curves in Fig. 43(b). However, a noticeable deviation from the experimental result is found at $100\,\text{mV} < V < 200\,\text{mV}$. This deviation is improved by introducing additional component $\hbar\Omega = 180$ meV, $\sigma_{ph} = 13$ meV and $K_{eff} = 1.6 \times 10^{-8}$), in addition to the ν(C–S) (in this case best fit is achieved with $\hbar\Omega = 87$ meV, σ = 10 meV and $K_{eff} = 3.8 \times 10^{-9}$) as shown in the blue and brown dashed curve, respectively, in Fig. 43(a). Here the green solid curve in negative V is multiplied by an asymmetric factor $\alpha' = 1.9$ for the black solid curve at positive V. Although a tentative candidate of the mode at 180 meV could be the $\delta(CH_3)$ shown in Fig. 45, the possibility of the overtone of ν(C–S) cannot be excluded since the double of $\hbar\Omega$ for ν(C–S) is near 180 meV. There remains a room to be clarified by other vibrational spectroscopic experiments and/or theoretical calculation of the vibrational modes of MT on Cu(1 1 1).

Fig. 37(d) shows the calculated PDOS of MOs of a single MT molecule on Cu(1 1 1). In contrast to DMDS, most MOs distribute more homogeneously around the ε_F, and slightly larger population can be found below ε_F. The spatial distribution of MOs such as HOMO, LUMO, and LUMO+1, shown in Fig. 37(f) are located around C–S bond, while almost no distribution can be found around C–H bond. Along the same logic described in the previous section, this explains why ν(C–S) signal appears in the AS of MT whereas ν(C–H) does not, and why DMDS shows ν(C–H) signal, whereas MT does not. Thus, detailed interpretation of the spatial distribution of individual MOs based on resonant model successfully explains our experimental AS, where the excitation of the ν(C–H) and ν(S–S) mode are cooperatively active for the S–S bond breaking of DMDS, while the ν(C–S) mode is responsible for lateral hopping of MT.

It should be emphasized that the hopping yield of MT is almost identical for both bias polarities in contrast to dissociation of DMDS. This is also explained by the almost homogeneous distribution of the PDOS of most MOs across the ε_F, while that of the HOMO contributes much more in the unoccupied state as shown in Fig. 37(d). It is qualitatively seen that all the MOs shown in Fig. 37(d) except for LUMO+1 have slightly larger population at below ε_F. This small asymmetry of the PDOS below and above ε_F for MT molecule on Cu(1 1 1) results in asymmetric factor $\alpha' = 1.9$ in our model of the EWBL.

In summary, we both experimentally and theoretically studied hopping of MT molecules on Cu(1 1 1) depending on the position of the STM tip and applied bias voltage. It is found that the electron injection at positive (negative) sample bias voltages on the off-center of a MT molecule results in attractive (repulsive) hopping of the molecule, in contrast to the random hopping induced by electron injection at the center of the molecule. The hopping itself is induced by the IET process and subsequent excitation of RC mode through vibrational mode coupling, but the direction of the hopping is determined by the attractive (repulsive) electrostatic force between positively (negatively) charged STM tip and negatively charged MT molecules. This controllable manipulation technique allows us to fabricate various nanostructures composed of molecules on surfaces. STM-AS of MT hopping induced by electron injection on the center of the molecule showed that the hopping yield increase when ν(C–S) and probably $\delta(CH_3)$ are excited, but does not drastically change when ν(C–H) is excited. This is due to the localization of MOs near the ε_F at the C–S bond in the molecule and poor distribution around the

methyl group, in contrast to the DMDS where MOs are distributed around S–S bond and methyl group resulted in the hopping induced by the excitation of ν(S–S) and ν(C–H). In addition, the hopping yield of MT is almost identical for both bias polarities, which possibly reflects the almost homogeneous distribution of the PDOS across the ε_F of the MOs responsible for the IET process. This result again emphasizes that the vibrational modes are resonantly excited through a temporal occupation of the MO by tunneling electrons, and that the excitation probabilities of vibrational modes depend on the population of the MOs at the corresponding energy. These findings leads us to conclude that STM-AS probes not only the vibrational modes responsible for reactions, but also the adsorbate electronic properties near the ε_F within a span of the vibrational energy so that it probes the PDOS of single molecules to some extent.

7. Concluding remarks

STM allows the real-space observation of site-resolved single-molecule motions and reaction [3–5]. The reaction rate as a function of applied bias voltage and tunneling currents provides important information about the elementary processes of electronic or vibrational excitation by tunneling electrons. Since STM-AS reflects a purely inelastic tunneling current (free from a competition with an elastic current), it plays a complementary role to be compared to the STM-IETS. The identification of the vibrational mode responsible for various surface motions and reactions, is essential for achieving mode-selective control of chemical reactions at surfaces. While $R(I)$ tells us how many electron is required (reaction order) to induce reactions, a full reproduction of a reaction yield $Y(V)$ using a formal theory presented here provides all the key quantities in vibrationally mediated reactions of single molecules. A knowledge of the reaction order is indispensable in reproduction of an experimental $Y(V)$ using the formula presented in this review.

Although the assignment of vibrational mode energies can be made from a conventional $\Delta \log Y(V)/\Delta V$ plot [9], the proposed formula can be used even with a limited number of the experimental data points. Moreover, a prefactor K_{eff} obtained from a fitting of experimental $Y(V)$ allows to gain insights into the microscopic mechanisms of vibrationally mediated motions and reactions of single molecules on metal surfaces.

What matters is how deeply we can shed a light into elementary processes of a vibrationally mediated reactions. The formula of $Y(V)$ presented here and $\gamma_{v,\text{RC}}$ obtained in the analysis of $Y(V)$ is the one that remains to be compared to a sophisticated extensive *ab initio* calculations to look for the RC modes. Our versatile formula presented here also underlines an importance to observe $Y(V)$ at both polarities. In STM-IETS it becomes conventional to observe it at both polarities in oder to make sure the vibrations signal superimposed on very noisy back ground as a consequence to detect weak change of tunneling current associated with a vibrational excitation. Even when an asymmetric IETS is observed, it is not direct manifestation of the electronic DOS of adsorbed molecules near the ε_F because of a competing elastic component in the presence of an electron-vibration interaction. On the other hand, AS probes purely inelastic component of a tunneling current and asymmetric AS is a direct consequence of a difference of the DOS below and above the ε_F within a span of the vibrational energy of interest. In this way STM-AS is a complementary experimental tool to explore not only dynamics of vibrationally mediated single molecule reactions, but in principle also aspects of the electronic structure of the adsorbates.

Acknowledgements

We would like to thank all members who have worked with M. Kawai in the STM-AS related projects in RIKEN and in Department of Advanced Materials Science, the Univ. of Tokyo. We also thank N. Lorente for his preliminary work on DMDS and for many stimulating discussions. This work is supported in part by a Grant-in-Aid for Scientific Research on Priority Areas "Electron Transport Through a Linked Molecule in Nano-scale" and a Grant-in-Aid for Scientific Research (S) "Single Molecule Spectroscopy using Probe Microscope" (No. S-21225001) from the Ministry of Education, Culture, Sports, Science, and Technology (MEXT) of Japan. K.M. is supported by the Japan Society for the

Promotion of Science (JSPS) fellows. T.F. acknowledges support from the Basque Departamento de Educacion and the UPV/EHU (Grant No. IT-756-13), the Spanish Ministerio de Economy Competitividad (Grant No. FIS2010-19609-CO2-00), and the European Union Integrated Project PAMS. H.U. was also supported by a Grant (No. C-25390007) from JSPS.

References

[1] D.M. Eigler, C.P. Lutz, W.E. Rudge, An atomic switch realized with the scanning tunneling microscope, Nature 352 (1991) 600–603.
[2] A.J. Mayne, G. Dujardin, G. Comtet, D. Riedel, Electronic control of single-molecule dynamics, Chem. Rev. 106 (2005) 4355–4378.
[3] W. Ho, Single-molecule chemistry, J. Chem. Phys. 117 (2002) 11033–11061.
[4] H. Ueba, Motions and reactions of single adsorbed molecules induced by vibrational excitation with STM, Surf. Rev. Lett. 10 (2003) 771–796.
[5] H. Ueba, S.G. Tikhodeev, B.N.J. Persson, Current-driven phenomena in nanoelectronics: Inelastic tunneling current-driven motions of single adsorbates, Pan Stanford Publishing, 2010. pp. 373 Ch. 2.
[6] T. Komeda, Y. Kim, M. Kawai, B.N.J. Persson, H. Ueba, Lateral hopping of molecules induced by excitation of internal vibration mode, Science 295 (2002) 2055–2058.
[7] J.I. Pascual, N. Lorente, Z. Song, H. Conrad, H.P. Rust, Selectivity in vibrationally mediated single-molecule chemistry, Nature 423 (2003) 525–528.
[8] B.C. Stipe, M.A. Rezaei, W. Ho, Inducing and viewing the rotational motion of a single molecule, Science 279 (1998) 1907–1909.
[9] B.C. Stipe, M.A. Rezaei, W. Ho, Coupling of vibrational excitation to the rotational motion of a single adsorbed molecule, Phys. Rev. Lett. 81 (1998) 1263–1266.
[10] B.C. Stipe, M.A. Rezaei, W. Ho, S. Gao, M. Persson, B.I. Lundqvist, Single-molecule dissociation by tunneling electrons, Phys. Rev. Lett. 78 (1997) 4410–4413.
[11] H.J. Lee, W. Ho, Single-bond formation and characterization with a scanning tunneling microscope, Science 286 (1999) 1719–1722.
[12] T. Kudernac, N. Ruangsupapichat, M. Parschau, B. Macia, N. Katsonis, S.R. Harutyunyan, K.-H. Ernst, B.L. Feringa, Electrically driven directional motion of a four-wheeled molecule on a metal surface, Nat. Nanotechnol. 479 (2012) 208–211.
[13] W. Auwarter, K. Seufert, F. Bischoff, D. Ecija, S. Vijayaraghavan, A surface-anchored molecular four-level conductance switch based on single proton transfer, Nat. Nanotechnol. 7 (2012) 41–46.
[14] T. Huang, J. Zhao, M. Feng, A. Popov, S. Yang, L. Dunsch, H. Petek, A molecular switch based on current-driven rotation of an encapsulated cluster within a fullerene cage, Nano Lett. 11 (2011) 5327–5340.
[15] T. Kumagai, A. Shiotari, H. Okuyama, S.S. Hatta, T. Aruga, I. Hamada, T. Frederiksen, H. Ueba, H-atom relay reactions in real space, Nat. Mater. 11 (2012) 167–172.
[16] B. Hammer, Y. Morikawa, J.K. Nørskov, CO chemisorption at metal surfaces and overlayers, Phys. Rev. Lett. 76 (1996) 2141–2144.
[17] G. Meyer, B. Neu, K.H. Rieder, Controlled lateral manipulation of single molecules with the scanning tunneling microscope, Appl. Phys. A 60 (1995) 343–345.
[18] L. Bartels, G. Meyer, K.H. Rieder, Controlled vertical manipulation of single CO molecules with the scanning tunneling microscope: A route to chemical contrast, Appl. Phys. Lett. 71 (1997) 213–215.
[19] P. Brumer, M. Shapiro, Coherence chemistry – Controlling chemical reactions with lasers, Acc. Chem. Res. 22 (1989) 407–413.
[20] M. Kawai, T. Komeda, Y. Kim, Y. Sainoo, S. Katano, Single-molecule reactions and spectroscopy via vibrational excitation, Phil. Trans. R. Soc. Lond. A 362 (2004) 1163–1171.
[21] Y.S. Choi, T.S. Kim, H. Petek, K. Yoshihara, R.L. Christensen, Evidence for quantization of the transition state for *cis–trans* isomerization, J. Chem. Phys. 100 (1994) 9269.
[22] Y. Sainoo, Y. Kim, T. Okawa, T. Komeda, H. Shigekawa, M. Kawai, Excitation of molecular vibrational modes with inelastic scanning tunneling microscopy: Examination through action spectra of cis-2-butene on Pd(110), Phys. Rev. Lett. 2005 (2005) 246102.
[23] Y. Sainoo, Y. Kim, T. Komeda, M. Kawai, H. Shigekawa, Observation of cis-2-butene molecule on Pd(110) by cryogenic STM: Site determination using tunneling-current-induced rotation, Surf. Sci. 536 (2003) L403–L407.
[24] M. Paulsson, T. Frederiksen, H. Ueba, N. Lorente, M. Brandbyge, Unified description of inelastic propensity rules for electron transport through nanoscale junctions, Phys. Rev. Lett. 100 (2008) 226604.
[25] N. Lorente, M. Persson, Theory of single molecule vibrational spectroscopy and microscopy, Phys. Rev. Lett. 85 (2000) 2997–3000.
[26] H. Ueba, T. Mii, S.G. Tikhodeev, Theory of inelastic tunneling spectroscopy of a single molecule – Competition between elastic and inelastic current, Surf. Sci. 601 (2007) 5220–5225.
[27] M. Ohara, Y. Kim, S. Yanagisawa, Y. Morikawa, M. Kawai, Role of molecular orbitals near the Fermi level in the excitation of vibrational modes of a single molecule at a scanning tunneling microscope junction, Phys. Rev. Lett. 100 (2008) 136104.
[28] H. Ueba, B.N.J. Persson, Action spectroscopy for single-molecule motion induced by vibrational excitation with a scanning tunneling microscope, Phys. Rev. B 75 (2007) 041403.
[29] K. Motobayashi, Y. Kim, H. Ueba, M. Kawai, Insight into action spectroscopy for single molecule motion and reactions through inelastic electron tunneling, Phys. Rev. Lett. 105 (2010) 076101.
[30] S. Katano, Y. Kim, Y. Kagata, M. Kawai, Single-molecule vibrational spectroscopy and inelastic-tunneling-electron-induced diffusion of formate adsorbed on Ni(110), J. Phys. Chem. C 114 (2010) 3003–3007.

[31] M. Parschau, D. Passerone, K.-H. Rieder, H.J. Hug, K.-H. Ernst, Switching the chirality of single adsorbate complexes, Angew. Chem., Int. Ed. 48 (2009) 4065–4068.
[32] K. Motobayashi, S. Katano, Y. Kim, M. Kawai, Spectral fitting of action spectra for motions and reactions of single molecules on metal surfaces, Bull. Chem. Soc. Jpn. 86 (2013) 75–79.
[33] T. Huang, J. Zhao, M. Feng, A.A. Popov, S. Yang, L. Dunsch, H. Petek, A multi-state single-molecule switch actuated by rotation of an encapsulated cluster within a fullerene cage, Chem. Phys. Lett. 552 (2011) 1–12.
[34] L. Lauhon, W. Ho, Electronic and vibrational excitation of single molecules with a scanning tunneling microscope, Surf. Sci. 451 (2000) 219–225.
[35] E. Fomin, M. Tatarkhanov, T. Mitsui, M. Rose, D.F. Ogletree, M. Salmeron, Vibrationally assisted diffusion of H_2O and D_2O on Pd(1 1 1), Surf. Sci. 600 (2006) 542–546.
[36] Y. Kitaguchi, A. Shiotari, H. Okuyama, S. Hatta, T. Aruga, Imaging sequential dehydrogenation of methanol on Cu(1 1 0) with a scanning tunneling microscope, J. Chem. Phys. 134 (2011) 174703.
[37] V. Simic-Milosevic, M. Mehlhorn, K.-H. Rieder, J. Meyer, K. Morgenstern, Electron induced ortho-meta isomerization of single molecules, Phys. Rev. Lett. 98 (2007) 116102.
[38] T. Kumagai, M. Kaizu, S. Hatta, H. Okuyama, T. Aruga, I. Hamada, Y. Morikawa, Direct observation of hydrogen-bond exchange within a single water dimer, Phys. Rev. Lett. 100 (2008) 166101.
[39] J.A. Stroscio, R.J. Celotta, Controlling the dynamics of a single atom in lateral atom manipulation, Science 306 (2004) 242–247.
[40] V. Simic-Milosevic, J. Meyer, K. Morgenstern, Chirality change of chloronitrobenzene on Au(1 1 1) induced by inelastic electron tunneling, Angew. Chem., Int. Ed. 48 (2009) 4061–4064.
[41] T. Kumagai, F. Hanke, S. Gawinkowski, J. Sharp, K. Kotsis, J. Waluk, M. Persson, L. Grill, Thermally and vibrationally induced tautomerization of single porphycene molecules on a Cu(1 1 0) surface, Phys. Rev. Lett. 111 (2013) 733–740.
[42] T. Frederiksen, M. Paulsson, H. Ueba, Theory of action spectroscopy for single molecule reactions induced by vibrational excitations with STM, Phys. Rev. B 89 (2014) 035427.
[43] Y. Kim, T. Komeda, M. Kawai, Single-molecule reaction and characterization by vibrational excitation, Phys. Rev. Lett. 89 (2002) 126104.
[44] M. Ohara, Y. Kim, M. Kawai, Electric field response of a vibrationally excited molecule in an STM junction, Phys. Rev. B 78 (2008) 201405.
[45] K. Motobayashi, C. Matsumoto, Y. Kim, M. Kawai, Vibrational study of water dimers on Pt(1 1 1) using a scanning tunneling microscope, Surf. Sci. 602 (2008) 3136–3139.
[46] K. Motobayashi, L. Árnadóttir, C. Matsumoto, E.M. Stuve, H. Jónsson, Y. Kim, M. Kawai, Adsorption of water dimer on platinum (1 1 1): Identification of the –OH···Pt hydrogen bond, ACS Nano 8 (2014) 11583–11590.
[47] T. Kumagai, S. Hatta, H. Okuyama, T. Aruga, Adsorbed states and scanning tunneling microscopy induced migration of acetylene on Cu(1 1 0), J. Chem. Phys. 126 (2007) 234708.
[48] K. Morgenstern, H. Gawronski, T. Mehlhorn, K.H. Rieder, Local investigation of electron-induced processes in water–metal systems, J. Mod. Opt 51 (2004) 2813–2819.
[49] H.L. Tierney, A.E. Baber, A.D. Jewell, E.V. Iski, M.B. Boucher, E.C.H. Sykes, Mode-selective electrical excitation of a molecular rotor, Chem. Eur. J. 15 (2009) 9678–9680.
[50] S. Katano, Y. Kim, Y. Kagata, M. Kawai, Vibration-assisted rotation and deprotonation of a single formic acid molecule adsorbed on Ni(1 1 0) studied by scanning tunneling microscopy, J. Phys. Chem. C 113 (2009) 19277–19280.
[51] H.-J. Shin, J. Jung, K. Motobayashi, S. Yanagisawa, Y. Morikawa, Y. Kim, M. Kawai, State-selective dissociation of a single water molecule on an ultrathin MgO film, Nat. Mater. 9 (2010) 442–447.
[52] Y. Kim, T. Komeda, M. Kawai, Single-molecule surface reaction by tunneling electrons, Surf. Sci. 502 (2002) 7–11.
[53] T. Komeda, Y. Kim, Y. Fujita, Y. Sainoo, M. Kawai, Local chemical reaction of benzene on Cu(1 1 0) via STM-induced excitation, J. Chem. Phys. 120 (2004). 5347-5342.
[54] Y. Sainoo, Y. Kim, T. Komeda, M. Kawai, Inelastic tunneling spectroscopy using scanning tunneling microscopy on trans-2-butene molecule: Spectroscopy and mapping of vibrational feature, J. Chem. Phys. 120 (2004) 7249–7251.
[55] M. Ohara, Y. Kim, M. Kawai, Scanning tunneling microscope imaging of $(CH_3S)_2$ on Cu(1 1 1), Langmuir 21 (2005) 4779–4781.
[56] M. Ohara, Y. Kim, M. Kawai, Controlling the reaction and motion of a single molecule by vibrational excitation, Chem. Phys. Lett. 426 (2006) 357–360.
[57] M. Ohara, Y. Kim, M. Kawai, Tunneling-electron-induced hopping of methylthiolate on Cu(1 1 1), Jpn. J. Appl. Phys. 45 (2006) 2022–2025.
[58] K. Motobayashi, Y. Kim, R. Arafune, M. Ohara, H. Ueba, M. Kawai, Dissociation pathways of a single dimethyl disulfide on Cu(1 1 1): Reaction induced by simultaneous excitation of two vibrational modes, J. Chem. Phys. 140 (2014) 194705.
[59] H. Ueba, Analysis of lateral hopping of a single CO molecule on Pd(1 1 0), Phys. Rev. B 86 (2012) 035440.
[60] S. Katano, S. Ichihara, H. Ogasawara, H.S. Kato, T. Komeda, M. Kawai, K. Domen, Adsorption structure of 1,3-butadiene on Pd(1 1 0), Surf. Sci. 502–503 (2002) 164–168.
[61] S.W. Hla, K.H. Rieder, STM control of chemical reactions: Single-molecule synthesis, Annu. Rev. Phys. Chem. 54 (2003) 307–330.
[62] W. Ho, Inducing and viewing bond selected chemistry with tunneling electrons, Acc. Chem. Res. 31 (1998) 567–573.
[63] H.W. Kim, M. Han, H.J. Shin, S. Lim, Y. Oh, K. Tamada, M. Hara, Y. Kim, M. Kawai, Y. Kuk, Control of molecular rotors by selection of anchoring sites, Phys. Rev. Lett. 106 (2011) 146101.
[64] J.-H. Kim, J. Jung, K. Tahara, Y. Tobe, Y. Kim, M. Kawai, Direct observation of adsorption geometry for the van der waals adsorption of a single π-conjugated hydrocarbon molecule on Au(1 1 1), J. Chem. Phys. 140 (2014) 074709.
[65] T. Komeda, Y. Kim, M. Kawai, Lateral motion of adsorbate induced by vibrational mode excitation with inelastic tunneling electron, Surf. Sci. 502 (2002) 12–17.
[66] T. Okada, Y. Kim, Y. Sainoo, T. Komeda, M. Trenary, M. Kawai, Coexistence and interconversion of di-σ and π-bonded ethylene on the Pt(1 1 1) and Pd(1 1 0) surfaces, J. Phys. Chem. Lett. 2 (2011) 2263–2266.

[67] C. Matsumoto, Y. Kim, T. Okawa, Y. Sainoo, M. Kawai, Low-temperature STM investigation of acetylene on Pd(1 1 1), Surf. Sci. 587 (2005) 19–24.
[68] Y. Sainoo, Y. Kim, H. Fukidome, T. Komeda, M. Kawai, H. Shigekawa, Characteristic configuration of *cis*-2-butene molecule on Pd(1 1 0) determined by scanning tunneling microscopy, Jpn. J. Appl. Phys. 41 (2002) 4976–4979.
[69] S. Pan, Q. Fu, T. Huang, A. Zhao, B. Wang, Y. Luo, J. Yang, J. Hou, Design and control of electron transport properties of single molecules, Proc. Nat. Acad. Sci. 106 (2009) 15259–15263.
[70] R. Arafune, H.-J. Shin, J. Jung, E. Minamitani, N. Takagi, Y. Kim, M. Kawai, Combined scanning tunneling microscopy and high-resolution electron energy loss spectroscopy study on the adsorption state of CO on Ag(0 0 1), Langmuir 28 (2012) 13249–13252.
[71] K.J. Franke, J.I. Pascual, Effects of electron-vibration coupling in transport through single molecules, J. Phys. Cond. Mat. 24 (2012) 394002.
[72] J. Gaudioso, W. Ho, Single-molecule vibrations, conformational changes, and electronic conductivity of five-membered heterocycles, J. Am. Chem. Soc. 123 (2001) 10095–10098.
[73] J. Gaudioso, H.J. Lee, W. Ho, Vibrational analysis of single molecule chemistry: Ethylene dehydrogenation on Ni(1 1 0), J. Am. Chem. Soc. 121 (1999) 8479–8485.
[74] A.S. Hallback, N. Oncel, J. Huskens, H.J.W. Zandvliet, B. Poelsema, Inelastic electron tunneling spectroscopy on decanethiol at elevated temoeratures, Nano Lett. 4 (2004) 2393–2395.
[75] S. Katano, Y. Kim, M. Hori, M. Trenary, M. Kawai, Reversible control of hydrogenation of a single molecule, Science 316 (2007) 1883–1886.
[76] L.J. Lauhon, W. Ho, Single-molecule vibrational spectroscopy and microscopy: CO on Cu(0 0 1) and Cu(1 1 0), Phys. Rev. B 60 (1999) R8525–R8528.
[77] L.J. Lauhon, W. Ho, Direct observation of the quantum tunneling of single hydrogen atoms with a scanning tunneling microscope, Phys. Rev. Lett. 85 (2000) 4566–4569.
[78] L.J. Lauhon, W. Ho, The initiation and characterization of single bimolecular reactions with a scanning tunneling microscope, Faraday Discuss. 117 (2000) 249–255.
[79] L.J. Lauhon, W. Ho, Single-molecule chemistry and vibrational spectroscopy: Pyridine and benzene on Cu(0 0 1), J. Phys. Chem. A 104 (2000) 2463–2467.
[80] L.J. Lauhon, W. Ho, Effects of temperature and other experimental variables on single molecule vibrational spectroscopy with the scanning tunneling microscope, Rev. Sci. Inst. 72 (2001) 216–223.
[81] N. Okabayashi, Y. Konda, T. Komeda, Inelastic electron tunneling spectroscopy of an alkanethiol self-assembled monolayer using scanning tunneling microscopy, Phys. Rev. Lett. 100 (2008) 217801.
[82] J.I. Pascual, J.J. Jackiw, Z. Song, P.S. Weiss, H. Conrad, H.P. Rust, Adsorbate-substrate vibrational modes of benzene on Ag(1 1 0) resolved with scanning tunneling spectroscopy, Phys. Rev. Lett. 86 (2001) 1050–1053.
[83] B.C. Stipe, M.A. Rezaei, W. Ho, A variable-temperature scanning tunneling microscope capable of single-molecule vibrational spectroscopy, Rev. Sci. Inst. 70 (1999) 137–143.
[84] L. Vitali, M.A. Schneider, K. Kern, L. Wirtz, A. Rubio, Phonon and plasmon excitation in inelastic electron tunneling spectroscopy of graphite, Phys. Rev. B 69 (2004) 121414(R).
[85] D. Wegner, R. Yamachika, X.W. Zhang, Y.Y. Wang, M.F. Crommie, N. Lorente, Adsorption site determination of a molecular monolayer via inelastic tunneling, Nano Lett. 13 (2013) 2346–2350.
[86] B.C. Stipe, M.A. Rezaei, W. Ho, Single-molecule vibrational spectroscopy and microscopy, Science 280 (1998) 1732–1735.
[87] J.W. Medlin, M.D. Allendorf, Theoretical study of the adsorption of acetylene on the (1 1 1) surfaces of Pd, Pt, Ni, and Rh, J. Phys. Chem. B 107 (2003) 217–223.
[88] J.C. Dunphy, M. Rose, S. Behler, D.F. Ogletree, M. Salmeron, P. Sautet, Acetylene structure and dynamics on Pd(1 1 1), Phys. Rev. B 57 (1998) R12705–R12708.
[89] H. Hoffmann, F. Zaera, R.M. Ormerod, R.M. Lambert, J.M. Yao, D.K. Saldin, L.P. Wang, D.W. Bennett, W.T. Tysoe, A near-edge X-ray absorption fine-structure and photoelectron spectroscopic study of the structure of acetylene on Pd(1 1 1) at low-temperature, Surf. Sci. 268 (1992) 1–10.
[90] J. Gaudioso, L.J. Lauhon, W. Ho, Vibrationally mediated negative differential resistance in a single molecule, Phys. Rev. Lett. 85 (2000) 1918–1921.
[91] S.R. Burema, K. Seufert, W. Auwaerter, J.V. Barth, M.L. Bocquet, Probing nitrosyl ligation of surface-confined metalloporphyrins by inelastic electron tunneling spectroscopy, ACS Nano 7 (2013) 5273–5281.
[92] K. Motobayashi, C. Matsumoto, Y. Kim, M. Kawai, Surface dynamics of water monomers and dimers on Pt(1 1 1) surface, J. Surf. Sci. Soc. Jpn. 28 (2007) 354–360.
[93] H. Gawronski, K. Morgenstern, K.H. Rieder, Electronic excitation of ice monomers on Au(1 1 1) by scanning tunneling microscopy – Vibrational spectra and induced processes, Euro. Phys. J.D 35 (2005) 349–353.
[94] A. Michaelides, K. Morgenstern, Ice nanoclusters at hydrophobic metal surfaces, Nat. Mater. 6 (2007) 597–601.
[95] K. Morgenstern, J. Nieminen, Intermolecular bond length of ice on Ag(1 1 1), Phys. Rev. Lett. 88 (2002) 066102.
[96] K. Morgenstern, J. Nieminen, Imaging water on Ag(1 1 1): Field induced reorientation and contrast inversion, J. Chem. Phys. 120 (2004) 10786–10791.
[97] K. Morgenstern, K.H. Rieder, Formation of the cyclic ice hexamer via excitation of vibrational molecular modes by the scanning tunneling microscope, J. Chem. Phys. 116 (2002) 5746–5752.
[98] A. Mugarza, T. Shimizu, O.D. Frank, M. Salmeron, Chemical reactions of water molecules on Ru(0 0 0 1) induced by selective excitation of vibrational modes, Surf. Sci. 603 (2009) 2030–2036.
[99] T. Mitsui, M.K. Rose, E. Fomin, D.F. Ogletree, M. Salmeron, Water diffusion and clustering on Pd(1 1 1), Science 297 (2002) 1850–1852.
[100] L. Árnadóttir, E.M. Stuve, H. Jónsson, Adsorption of water monomer and clusters on platinum(1 1 1) terrace and related steps and kinks II. Surface diffusion, Surf. Sci. 606 (2012) 233–238.
[101] L. Árnadóttir, E.M. Stuve, H. Jónsson, Adsorption of water monomer and clusters on platinum(1 1 1) terrace and related steps and kinks: I. configurations, energies, and hydrogen bonding, Surf. Sci. 604 (2010) 1978–1986.

[102] S. Meng, E.G. Wang, S. Gao, Water adsorption on metal surfaces: A general picture from density functional theory studies, Phys. Rev. B 69 (2004) 195404.
[103] S. Meng, L.F. Xu, E.G. Wang, S. Gao, Vibrational recognition of hydrogen-bonded water networks on a metal surface, Phy. Rev. Lett. 89 (2002) 176104.
[104] K. Jacobi, K. Bedurftig, Y. Wang, G. Ertl, From monomers to ice – New vibrational characteristics of H_2O adsorbed on Pt(1 1 1), Surf. Sci. 472 (2001) 9–20.
[105] M. Nakamura, Y. Shingaya, M. Ito, The vibrational spectra of water cluster molecules on Pt(1 1 1) surface at 20 K, Chem. Phys. Lett. 309 (1999) 123–128.
[106] H. Ogasawara, J. Yoshinobu, M. Kawai, Clustering behavior of water (D_2O) on Pt(1 1 1), J. Chem. Phys. 111 (1999) 7003–7009.
[107] H. Ibach, S. Lehwald, The bonding of water molecules to platinum surfaces, Surf. Sci. 91 (1980) 187–197.
[108] S. Haq, C. Clay, G.R. Darling, G. Zimbitas, A. Hodgson, Growth of intact water ice on Ru(0 0 0 1) between 140 and 160 K: Experiment and density-functional theory calculations, Phys. Rev. B 73 (2006) 115414.
[109] P.A. Thiel, R.A. DePaola, F.M. Hoffmann, The vibrational spectra of chemisorbed molecular clusters: H_2O on Ru(0 0 1), J. Chem. Phys. 80 (1984) 5326–5331.
[110] S.G. Tikhodeev, H. Ueba, Relation between inelastic electron tunneling and vibrational excitation of single adsorbates on metal surfaces, Phys. Rev. B 70 (2004) 125414.
[111] S.G. Tikhodeev, H. Ueba, How vibrationally assisted tunneling with STM affects the motions and reactions of single adsorbates, Phys. Rev. Lett. 102 (2009) 246101.
[112] B.N.J. Persson, A. Baratoff, Inelastic electron tunneling from a metal tip: The contribution from resonant processes, Phys. Rev. Lett. 59 (1987) 339–342.
[113] S.W. Gao, M. Persson, B.I. Lundqvist, Theory of atom transfer with a scanning tunneling microscope, Phys. Rev. B 55 (1997) 4825–4836.
[114] G.P. Salam, M. Persson, R. Palmer, Possibility of coherent multiple excitation in atom transfer with a scanning tunneling microscope, Phys. Rev. B 49 (1994) 10655–10662.
[115] R.E. Walkup, D.M. Newns, P. Avouris, Role of multiple inelastic transition in atom transfer with the scanning tunneling microscope, Phys. Rev. B 48 (1993) 1858–1861.
[116] K. Liu, S. Gao, Excitation of frustrated translation and nonadiabatic adatom hopping inducedby inelastic tunneling, Phys. Rev. Lett. 95 (2005) 226102.
[117] H. Ueba, T. Mii, N. Lorente, B.N.J. Persson, Adsorbate motions induced by inelastic-tunneling current: Theoretical scenarios of two-electron processes, J. Chem. Phys. 123 (2005) 084707.
[118] D.M. Eigler, E.K. Schweizer, Positioning single atoms with a scanning tunnelling microscope, Nature 344 (1990) 524–526.
[119] H. Ueba, Vibrational lineshapes of adsorbates on solid surfaces, Prog. Surf. Sci. 22 (1986) 181–321.
[120] B.N.J. Persson, R. Ryberg, Vibrational phase relaxation at surfaces: CO on Ni(1 1 1), Phys. Rev. Lett. 54 (1985) 2119–2122.
[121] F.M. Hoffman, B.N.J. Persson, Vibrational dephasing of terminally bonded CO on Ru(0 0 1), Phys. Rev. B 34 (1986) 4354–4357.
[122] R. Ryberg, Vibrational line shape of chemisorbed CO, Phys. Rev. B 32 (1985) 2671–2673.
[123] B.N.J. Persson, M. Persson, Vibrational lifetime for CO adsorbed on Cu(1 0 0), Solid State Commun. 36 (1980) 175–179.
[124] A.M. Bradshaw, F.M. Hoffman, The chemisorption of carbon monoxide on palladium single crystal surfaces: IR spectroscopic evidence for localised site adsorption, Surf. Sci. 72 (1978) 513.
[125] V. Dose, Topics in inverse photoemission, J. Vac. Sci. Technol. A 5 (1987) 2032–2037.
[126] B.N.J. Persson, H. Ueba, Theory of inelastic tunneling induced motion of adsorbates on metal surfaces, Surf. Sci. 502-503 (2002) 18–25.
[127] M. Trenary, K.J. Uram, F. Bozso, J.T. Yates Jr., Temperature dependence of the vibrational lineshape of CO chemisorbed on the Ni(1 1 1) surface, Surf. Sci. 146 (1984) 269–280.
[128] T.A. Germer, J.C. Stephenson, E.J. Heilweil, R.R. Cavanagh, Picosecond time-resolved adsorbate response to substrate heating: Spectroscopy and dynamics of CO/Cu(1 0 0), J. Chem. Phys. 101 (1994) 1704–1716.
[129] J. Ellis, J.P. Toennies, G. Witte, Helium atom scattering study of the frustrated translation mode of CO adsorbed on the Cu(0 0 1) surface, J. Chem. Phys. 102 (1995) 5059–5070.
[130] B.G. Briner, M. Doering, H.P. Rust, A.M. Bradshaw, Microscopic molecular diffusion enhanced by adsorbate interactions, Science 278 (1997) 257–260.
[131] N. Lorente, J.I. Pascual, H. Ueba, Two-electron processes of desorption of a single ammonia molecule from Cu(1 0 0), Surf. Sci. 593 (2005) 122–132.
[132] P.A. Sloan, R.E. Palmer, Two-electron dissociation of single molecules by atomic manipulation at room temperature, Nature 434 (2005) 367–371.
[133] R.G. Nuzzo, B.P. Zegarski, L.H. Dubois, Fundamental studies of the chemisorption of organosulfur compounds on gold(1 1 1). Implications for molecular self-assembly on gold surfaces, J. Am. Chem. Soc. 109 (1987) 733–740.
[134] B.A. Sexton, G.L. Nyberg, A vibrational and tds study of sulfur adsorbates on Cu(1 0 0): Evidence for CH_3S species, Surf. Sci. 165 (1986) 251–267.
[135] J. Shchadilova, M. Paulsson, S.G. Thikhodeev, H. Ueba, Rotation of a single acetylene molecule on Cu(0 0 1) by tunneling electrons in STM, Phys. Rev. Lett. 111 (2013) 186102.
[136] J. Shchadilova, M. Paulsson, S.G. Thikhodeev, H. Ueba, Isotope effect in acetylene C_2H_2 and C_2D_2 rotations on Cu(0 0 1), Phys. Rev. B 89 (2014) 165418.
[137] B. Persson, P. Jacobs, Infrared spectroscopy of overtones and combination bands, J. Chem. Phys. 109 (1998) 8641–8651.
[138] L.G. Wang, E.Y. Tsymbal, S.S. Jaswal, First-principles study of adsorption of methanethiol on Co(0 0 0 1), Phys. Rev. B 70 (2004) 075410.
[139] S.A. Sardar, J.A. Syed, E. Ikenaga, S. Yagi, T. Sekitani, S. Wada, M. Taniguchi, K. Tanaka, Orientation and charge transfer upon adsorption of ethanethiol on Cu(1 1 1) surface at 85 K, Nucl. Instrum. Methods. B 199 (2003) 240–243.
[140] G. Henrik, C. Alessandro, A. Wanda, Thiols and disulfides on the Au(1 1 1) surface: The headgroup-gold interaction, J. Am. Chem. Soc. 122 (2000) 3839–3842.